DESIGN, SYNTHESIS, AND APPLICATION OF NOVEL Π-CONJUGATED MATERIALS - PART II

EDITED BY: Haichang Zhang, Taotao Ai and Qixin Zhou
PUBLISHED IN: Frontiers in Chemistry

frontiers Research Topics

ISSN 1664-8714
ISBN 978-2-88971-611-1
DOI 10.3389/978-2-88971-611-1

About Frontiers

Frontiers is more than just an open-access publisher of scholarly articles: it is a pioneering approach to the world of academia, radically improving the way scholarly research is managed. The grand vision of Frontiers is a world where all people have an equal opportunity to seek, share and generate knowledge. Frontiers provides immediate and permanent online open access to all its publications, but this alone is not enough to realize our grand goals.

Frontiers Journal Series

The Frontiers Journal Series is a multi-tier and interdisciplinary set of open-access, online journals, promising a paradigm shift from the current review, selection and dissemination processes in academic publishing. All Frontiers journals are driven by researchers for researchers; therefore, they constitute a service to the scholarly community. At the same time, the Frontiers Journal Series operates on a revolutionary invention, the tiered publishing system, initially addressing specific communities of scholars, and gradually climbing up to broader public understanding, thus serving the interests of the lay society, too.

Dedication to Quality

Each Frontiers article is a landmark of the highest quality, thanks to genuinely collaborative interactions between authors and review editors, who include some of the world's best academicians. Research must be certified by peers before entering a stream of knowledge that may eventually reach the public - and shape society; therefore, Frontiers only applies the most rigorous and unbiased reviews.
Frontiers revolutionizes research publishing by freely delivering the most outstanding research, evaluated with no bias from both the academic and social point of view. By applying the most advanced information technologies, Frontiers is catapulting scholarly publishing into a new generation.

What are Frontiers Research Topics?

Frontiers Research Topics are very popular trademarks of the Frontiers Journals Series: they are collections of at least ten articles, all centered on a particular subject. With their unique mix of varied contributions from Original Research to Review Articles, Frontiers Research Topics unify the most influential researchers, the latest key findings and historical advances in a hot research area! Find out more on how to host your own Frontiers Research Topic or contribute to one as an author by contacting the Frontiers Editorial Office: frontiersin.org/about/contact

DESIGN, SYNTHESIS, AND APPLICATION OF NOVEL π-CONJUGATED MATERIALS - PART II

Topic Editors:
Haichang Zhang, Qingdao University of Science and Technology, China
Taotao Ai, Shaanxi University of Technology, China
Qixin Zhou, University of Akron, United States

Citation: Zhang, H., Ai, T., Zhou, Q., eds. (2021). Design, Synthesis, and Application of Novel π-Conjugated Materials - Part II.
Lausanne: Frontiers Media SA. doi: 10.3389/978-2-88971-611-1

Table of Contents

frontiers in Chemistry

EDITORIAL
published: 23 September 2021
doi: 10.3389/fchem.2021.771438

Editorial: Design, Synthesis, and Application of Novel π-Conjugated Materials—Part II

Zhicheng Dai[1], *Taotao Ai*[2], *Qixin Zhou*[3] *and Haichang Zhang*[1]*

[1]Key Laboratory of Rubber-Plastics of Ministry of Education/Shandong Province (QUST), School of Polymer Science &Engineering, Qingdao University of Science and Technology, Qingdao, China, [2]School of Material Science and Engineering, Shaanxi University of Technology (SNUT), Hanzhong, China, [3]National Center for Education and Research on Corrosion and Materials Performance, Department of Chemical and Biomolecular Engineering, The University of Akron, Akron, OH, United States

Keywords: π-conjugated materials, organic field effect transistors, sensors, organic solar cells, electronics

Editorial on the Research Topic

Design, Synthesis, and Application of Novel π-Conjugated Materials—Part II

During last few years, new π-conjugated materials have received more and more attention in the community due to their potential wide range of applications such as organic field effect transistors (OFETs), solar cells, sensors and so on. Among them, the works with respect to the design and optimization of π-conjugated molecules have been extensively investigated. This research topic includes 10 articles of reviews and original research works, which describe a series of novel π-conjugated materials along with various applications. These articles provide an overview of different types of π-conjugated materials and of how they are designed and characterized, thereby providing an overview of progress and development direction in this field.

Over the last decade, heptazine-based π-conjugated materials, including polymeric graphitic carbon nitride (g-C_3N_4) and corresponding small molecules, have attracted extensive attention by virtue of intriguing optoelectronic and photocatalytic properties in the fields of organic optoelectronics and photocatalysis. From the perspective of organic electroluminescence (EL), Li and co-workers reported an interesting monomeric heptazine derivative (HAP-3DF) which exhibits enhanced EL via n-π* transition character and exciplex-based thermally activated delayed fluorescence (TADF), respectively (Li et al.). The same group subsequently provided an overview of monomeric and polymeric heptazine-based π-conjugated materials for light-emitting. In this review, the metal ion-containing, polymeric g-C_3N_4-based, monomeric heptazine-based light-emitting materials and devices are systematically summarized, which is not only beneficial for the future molecular design of high-performance luminescent materials, but also for the acceleration of practical applications of heptazine-based materials and devices (Li et al.).

Normally, conjugated materials exhibit strong emission in their solution phase, but showing weak or quenched luminescence in the solid phase due to the aggregation. Ma et al. synthesized the molecules that contain tetrastyrene and benzimidazole structures to obtain molecules (TPEBZMZ) with strong aggregation induced luminescence (AIE) effect. The fluorescent nanofiber membrane, prepared by electrospinning TPEBZMZ and polylactic acid (PLA) blend solution, showed excellent and reversible acid-induced discoloration. This work provides not only a novel AIE material, but also a simple strategy to design the stimulus responsive fluorescent film sensor (Ma et al.).

As an interesting electron donor-acceptor material, diketopyrrolopyrrole (DPP)-based donor-acceptor conjugated materials have a very bright prospect in the application of electronic devices, typically in OFET due to their high charge transfer mobility. Zhou et al. reviewed the DPP, iso-DPP and their derivatives-based materials in OFETs, and mentioned that the hole transfer mobility based

OPEN ACCESS

Edited and reviewed by:
Iwao Ojima,
Stony Brook University, Stony Brook, United States

***Correspondence:**
Haichang Zhang
haichangzhang@hotmail.com

Specialty section:
This article was submitted to Biophysics, a section of the journal Frontiers in Molecular Biosciences

Received: *06 September 2021*
Accepted: *13 September 2021*
Published: *23 September 2021*

Citation:
Dai Z, Ai T, Zhou Q and Zhang H (2021) Editorial: Design, Synthesis, and Application of Novel π-Conjugated Materials—Part II. Front. Chem. 9:771438. doi: 10.3389/fchem.2021.771438

on the DPP polymers is up to 26 cm^2 V^{-1} s^{-1}. To obtain high-performance DPP-based semiconductor materials, the research direction should focus on not only the modification of the chemical structures on planar materials backbone and large π-convergence system, but also the molecules packing such as strong π-π stacking and aggregation, short molecular distance etc. (Zhou et al.). Bao's group reviewed hydrogen-bonded materials in OFETs. The authors reviewed a series of small molecules and polymers with hydrogen-bonding association in the application of OFETs, indicating that hydrogen-bonds could not only enable the molecular reassembly to obtain a more ordered crystalline structure and improved π - π stacking, but also reduce the distance of the neighboring molecules and thus increase the molecular packing density. These behaviors could significantly enhance the charge transfer mobility (Shi et al.). Lu et al. also reviewed the conjugated materials in OFETs. and other applications such as organic solar cells (OSCs), sensors, and coating. This article pointed out that there are still a big room for the scientists to explore the highly selective and sensitive sensors. Conjugated polymer coating with multi-functions is also promising and interesting. In addition, the development of novel materials in OSCs with a broad range of light absorption and high charge mobility is still the research trend in the field (Lu et al.).

OSCs, as high-quality next-generation energy transfer devices, have attracted extensive attention by researchers. Among them, fullerene acceptors are being replaced by non-fullerene acceptors because of their weak absorption and limited structural modification. Lin et al. synthesized a non-fullerene electron-acceptor cyclized by selenium branched chain based on ring fusion perylene diimide (PDI) tripolymer, and obtained a device with V_{OC} up to 1.12 V. Although the maximum power conversion efficiency (PCE) in this work is only 1.6%, it still provides a feasible idea for seleniding other compounds to improve the performance of OSCs in the future (Lin et al.). Another type of potential photovoltaic device is perovskite solar cells (PSCs). Hole transfer layer (HTL) plays a crucial role in achieving high performance of PSCs. However, the most used HTLs require the dopant to enhance the PCEs of PSCs due to their inherent low conductivity, leading to the decrease of the stability of the PSCs. Thus, the development of dopant-free hole transfer materials (HTM) is one main research trend. Deng et al. reviewed a series of dopant-free HTMs and pointed out that the molecular design concept for high-performance dopant-free HTMs is enlarging the π-conjugation system, increasing the planarity of molecular backbone, and introducing the functional atoms/groups to achieve interfacial interaction between the HTM layer and the perovskite layer, and, which results in self-assembly within the HTMs (Deng et al.).

A suitable amount of fluoride anion is beneficial for our daily life, but excessive fluoride ion is harmful for human health and chemical engineering as well. Therefore, the detection of fluorine ions in organic media is an important research topic. Deng et al. designed n-tertbutyldimethylsyl substituted diodocarbazole (CA-TBMDS) as a colorimetric sensor for fluoride anion sensors in organic solution. The study showed that CA-TBMDS is a highly sensitive and selective for fluoride anion with a color change from colorless to yellow. The color change could be attributed to the principle of intermolecular proton transfer between the amide units and the fluoride ion. This work pointed out that N-TBMDS units containing organic dyes can be used to produce fluoride anion sensors (Deng et al.).

π-Conjugated polymers are usually prepared by polymerization. Thus, novel methods for the preparation of conjugated polymers have received considerable attention. Tang et al. reported a new strategy for the preparation of conjugated polymers by rearrangement. As their report shows, by using a simple one-step method, which treated polybutadiene with n-butyllithium and *N,N,N′,N′*-tetramethylethylenediamine, polymers with a large number of conjugated double bonds were prepared. This contribution opens a new pathway to the synthesis of π-conjugated polymers (Tang et al.).

In this Research Topic, five research articles and five review articles regarding π-conjugated materials have been collected, which hint that the molecular chemical structures indeed play a key role in the performance of their applications. In future, it is believed that more materials with π - combination will be used in a wide range of application areas as the key design idea. Therefore, the design and improvement of π-conjugated materials will be a very promising research direction and will make a significant impact on the development of clean energy and environmental protection.

AUTHOR CONTRIBUTIONS

ZD prepared the manuscript. TA, QZ, and HZ revised the manuscript and are topic editors of this Research Topic. All authors contributed to the article and approved the submitted version.

ACKNOWLEDGMENTS

The authors acknowledged the support from Natural Science Foundation of China, under Grant 21805151, Natural Science Foundation of Shandong Province, China, under Grant ZR2018MB024, Young Taishan Scholars under Grant 201909120, and Shaanxi University of Technology (SLGPT2019KF01-01, SLG 1901).

Conflict of Interest: The authors declare that the research was conducted in the absence of any commercial or financial relationships that could be construed as a potential conflict of interest.

Publisher's Note: All claims expressed in this article are solely those of the authors and do not necessarily represent those of their affiliated organizations, or those of the publisher, the editors, and the reviewers. Any product that may be evaluated in this article, or claim that may be made by its manufacturer, is not guaranteed or endorsed by the publisher.

frontiers in Chemistry

MINI REVIEW
published: 18 March 2021
doi: 10.3389/fchem.2021.664504

Dopant-Free π-Conjugated Hole Transport Materials for Highly Stable and Efficient Perovskite Solar Cells

Zhifeng Deng[1,2*†], *Shuaiwei Cui*[3†], *Kaichang Kou*[1], *Dongxu Liang*[3], *Xin Shi*[2] *and Jinhui Liu*[3*]

[1] School of Chemistry and Chemical Engineering, Northwestern Polytechnical University (NWPU), Xi'an, China, [2] National and Local Joint Engineering Laboratory for Slag Comprehensive Utilization and Environmental Technology, School of Materials Science and Engineering, Shaanxi University of Technology, Hanzhong, China, [3] Key Laboratory of Rubber-Plastic of Ministry of Education (QUST), School of Polymer Science and Engineering, Qingdao University of Science and Technology, Qingdao, China

Current high-efficiency hybrid perovskite solar cells (PSCs) have been fabricated with doped hole transfer material (HTM), which has shown short-term stability. Doping applied in HTMs for PSCs can enhance the hole mobility and PSCs' power conversion efficiency, while the stability of PSCs will be significantly decreased due to inherent hygroscopic properties and chemical incompatibility. Development of dopant-free HTM with high hole mobility is a challenge and of utmost importance. In this review, a series of selected and typical π-conjugated dopant-free hole transport materials, mainly regarding small molecules, are reviewed, which could consequently help to further design high-performance dopant-free HTMs. In addition, an outline of the molecular design concept and also the perspective of ideal dopant-free HTMs were explored.

Keywords: π-conjugated materials, perovskite solar cells, hole transfer material, dopant-free, molecular design

OPEN ACCESS

Edited by:
Qixin Zhou,
University of Akron, United States

Reviewed by:
Cheng Zhang,
National Renewable Energy Laboratory (DOE), United States
Qianqian Su,
Shanghai University, China

***Correspondence:**
Zhifeng Deng
dengzf@snut.edu.cn
Jinhui Liu
liujinhui7@163.com

[†]These authors have contributed equally to this work

Specialty section:
This article was submitted to Organic Chemistry, a section of the journal Frontiers in Chemistry

Received: *05 February 2021*
Accepted: *25 February 2021*
Published: *18 March 2021*

Citation:
Deng Z, Cui S, Kou K, Liang D, Shi X and Liu J (2021) Dopant-Free π-Conjugated Hole Transport Materials for Highly Stable and Efficient Perovskite Solar Cells. Front. Chem. 9:664504. doi: 10.3389/fchem.2021.664504

INTRODUCTION

Currently, the state-of-the-art perovskite solar cells with conventional *n-i-p* structures utilize 2,2′,7,7′-tetrakis(*N*, *N*′-di-*p*-methoxyphenlamine)-9,9-spirobifluorene (spiro-OMeTAD) or poly-triarylamine (PTTA) as HTMs. However, the HTMs like spiro-OMeTAD and PTAA suffer from low mobility ($< 1 \times 10^{-5}$ cm^2 V^{-1} s^{-1}) and limited conductivity ($< 3 \times 10^{-7}$ S cm^{-1}) (Vivo et al., 2017). These materials thus need hazardous dopants to increase the hole mobility and conductivity; these can include such dopants as bis(trifluoromethane sulfonyl)imide lithium salt (LiTFSI), which may also facilitate device degradation due to the sophisticated oxidation process associated with undesired ion migration and chemical interaction with underlying perovskite layer (Yu and Sun, 2015; Abi Ghanem et al., 2019). In addition, such dopants would make the device prone to hygroscopicity. Considering their drawbacks, over the last few years, a wide range of novel HTMs have been proposed as alternatives by the state-of-the-art organic π-conjugated small molecule and polymer; however, only a few candidates have reached similar initial performance compared to the state-of-the-art HTMs. Unfortunately, those candidates still require high amounts of dopants to operate (Yu and Sun, 2015; Vivo et al., 2017). Even though a few operational dopant-free materials could be obtained, the power conversion efficiency (PCE) still lacks behind the state-of-the-art HTMs (Huang et al., 2016; Liu et al., 2016; Yun et al., 2016; Zhao et al., 2016; Lee et al., 2017). Normally, HTMs would not require an additional doping process if they exhibit hole mobility up to 10^{-4}-10^{-3} cm^2 V^{-1} s^{-1} and have matched energy levers. Therefore, the development of

high-performance dopant-free HTMs is highly desirable and of utmost importance. Molecular design strategies, such as large π-conjugation and strong π-π stacking (Paek et al., 2017), strong planarity (Yun et al., 2016), surface passivation (Cao et al., 2015), introducing functional groups, and novel chemical structures, have been considered to be the most feasible and effective methods mainly used for designing dopant-free HTMs that possess better intermolecular interactions to ensure sufficient hole mobility. In this article, dopant-free π-conjugated small molecules applied to PSCs are reviewed.

LARGE π-CONJUGATION AND STRONG π-π STACKING

Dopant-free HTMs are divided into small molecules and polymers. Compared to polymers, small organic molecular HTMs have received great attention due to their high efficiency and simple synthetic schemes (Zhang et al., 2017a). Simultaneously, they were also shown to have better intra-molecular hole transfer mobility due to better packing. In general, the molecular structure of organic HTMs consists of peripheral donors and central cores, such as pyrene (Ge et al., 2018), fluorene (Rakstys et al., 2017b), carbazole (Chen et al., 2017), benzothiophene (Zimmermann et al., 2017), and indacenodithienothiophene (Liu et al., 2017). The studies on dopant-free organic HTM are quite rare, among which most reported molecules contain thiophene or thiophene derivatives as the donor units or π-conjugated bridge. Very recently, K. Nazeeruddin and co-authors using rigid quinolizino acridine (FA), which is widely used in molecular semiconductors due to its planarity and strong π-π stacking, as the central donor core, tri-thiophene as the π-conjugated bridge, and malenonitrile as the strongest electron acceptor to stabilize the highest occupied molecular orbital (HOMO) energy level, which built a branch oligomer (S1, **Figure 1**) and showed PCE of 18.9% and a maximum power output that was collected after 1300 h that remained at 65% of its initial value (Paek et al., 2017). In addition, this group introduced thiophene or tri-thiophene as branches into the same core and synthesized two oligomers (S2 and S3, **Figure 1**), which were also used as HTMs to fabricate PSCs (Rakstys et al., 2017a). The results showed that π-extension would significantly enhance the PCE of the PSCs from 8.88 to 19.03%.

STRONG PLANARITY

Except for π-conjugation extension, the planarity of a molecular backbone is crucial for the molecular design concept of high-performance dopant-free HTMs. J. Son and co-authors introduced fluorine atoms to the molecules for adjusting the planarity of the backbone and the molecular packing through sulfur–fluorine interactions, which significantly increased the hole mobility and the PCE from 8.95% (S4) to 14.45% (S5) (Yun et al., 2016). Very recently, through a comprehensive study on the deliberate molecular design and modifications of electron donors, correlations between the planarity of HTMs backbone and performance of PSC were reported by Liang's group (Li et al., 2020). In this work, the dithieno[3,2-b:2′,3′-d]pyrrole (DTP) both end substituted by the twisted triphenylamine as the donor (S6) or the capped-by-planar-*N*-phenyl-carbazole donor were synthesized (S7). We used two small molecules, S6 and S7, as dopant-free HTMs to fabricate PSCs, which showed PCEs with 11.59% (S6) and 18.29% (S7). The chemical structure between triphenylamine and the *N*-phenyl-carazole are quite similar except for an additional chemical bond connecting between the two phenyl rings of the triphenylamine; however, the PCE of the S7-based device showed a value almost 60% higher than the one based on S6. The significantly different performance between these two small molecule-based PSCs could be ascribed to S7 with an improved planarity backbone, resulting in a good hole transfer ability.

SURFACE PASSIVATION (INTERFACIAL INTERACTION)

In a photovoltaic device, after light absorption, the generated charge carriers (electron/hole) need to be transported through the perovskite layer and collected at the adjacent charge selective interfaces (Zhang et al., 2017b). Each of these steps plays a key role in the high performance of PSCs. Among them, the quite important (and mostly neglected) part is the hole transfer between the interface of HTM and the perovskite layer. To the best of our knowledge, most reported articles focus on the modification of the HTM's HOMO/LUMO energy levels but not on the inter-layer interaction (Yu and Sun, 2015; Vivo et al., 2017). Compatible HOMO/LUMO energy levels for HTMs will be beneficial for the hole transfer and to block the electron transfer from the perovskite layer to the HTM layer to enable the maximum achievable open-circuit voltage. The good HTM should not only have a compatible HOMO energy level but should also provide intimate inter-layer interaction since the interface interaction would help to rapidly extract holes from the perovskite layer and transfer them to the HTM layer, resulting in a low energy loss and reduced recombination of charge carriers at the interface. Zheng's group reported that a thiolated nanographene perthiolated trisulfur-annulated hexa-peri-hexabenzocoronene (S8, **Figure 2**), as the HTM in the pristine form in PSCs (Cao et al., 2015). The thiol groups at the periphery form Pb-S coordination-bonds at the interface between perovskite and HTM, which was investigated by the infrared spectra. The tight binding of S8 helps to rapidly extract charge from perovskite, resulting in a low energy loss at the interface and PCE of 12.8%. The performance is readily improved by doping with graphene sheets into tri-sulfurannulated hexa-*peri*-hexabenzocoronene (TSHBC), which formed a novel functionalized nanographene that could enhance the hole transporting property within HTM. In addition, M. Zhan and co-workers reported on the introduction of an interaction layer between the perovskite and HTM layers, which could act as Lewis bases and interact with Pb atoms to form trap states that greatly passivate the defects on the surface of the perovskite layer (Zhang et al., 2017b). This technique could

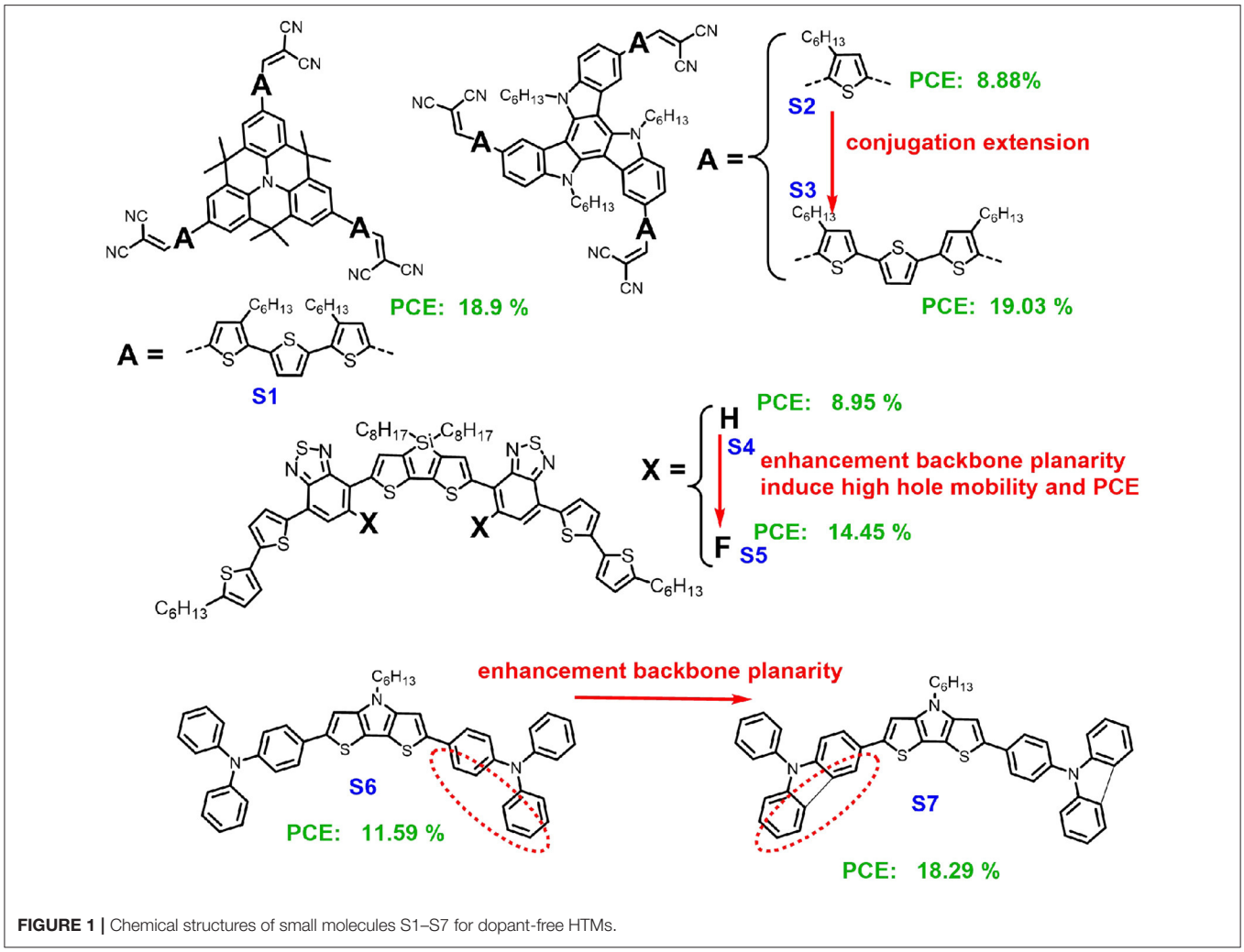

FIGURE 1 | Chemical structures of small molecules S1–S7 for dopant-free HTMs.

significantly enhance the efficiency and stability of the PSCs. Except for sulfur atoms, silicon and nitrogen atoms can also provide lone pair electrons to form Pb-N or Pb-Si coordination-bonds through the formation of Lewis adduct between the under-coordinated Pb atoms at the HTM-perovskite interface. A deeper understanding of the relationship between Pb-S/Pb-N/Pb-S interaction at perovskite/HTM interface and the PSC's performance should be established in the near future.

INTRODUCING FUNCTIONAL GROUP

Research into organic electronics revealed that not only the composition of the organic material but also subtle changes in the material structure (the way how the molecules are stacked) can noticeably alter its bulk properties (Yao et al., 2016). One of the reasons is that the charge transport in conjugated materials is strongly affected by their structures. For totally disordered organic small molecular films, charge mobility is low, while mobility significantly increases if the materials exhibit self-assembling properties that can be exploited to generate ordered structures (Zhang et al., 2018, 2020). Jian et al. designed and synthesized tetrathia-fulvalene derivative (S9, **Figure 2**) and used it as dopant-free HTM, which showed a PCE of 11.03% in 2014, fill factor (FF) of 64%, and open-circuit voltage (V_{oc}) of 0.86 V (Liu et al., 2014). A few years later, Islam's group introduced two amide units into these small molecules (S10) (Kaneko et al., 2019). In S10, intermolecular hydrogen bonds could be formed between amino and the carbonyl groups of the neighboring two molecules in the solid states. Using this small molecule to fabricate the PSCs, a PCE of 14.5% with the V_{oc} of 1.11 V and the FF of 66% were achieved. The increased PSCs performance could be ascribed to the following facts: (i) hydrogen bonding formation between the adjacent molecules, which could improve the inter-molecular hole transfer mobility; and (ii) the exiting multi-nitrogen and oxygen atoms could form surface passivation between the HTMs layer and the perovskite layer, which is beneficial for the hole transfer between the two layers.

MATERIALS WITH NOVEL CHEMICAL STRUCTURES

For high-performance dopant-free HTMs for PSCs, the development of novel chemical structures are important. For commercial applications, it is a challenge to find suitable and

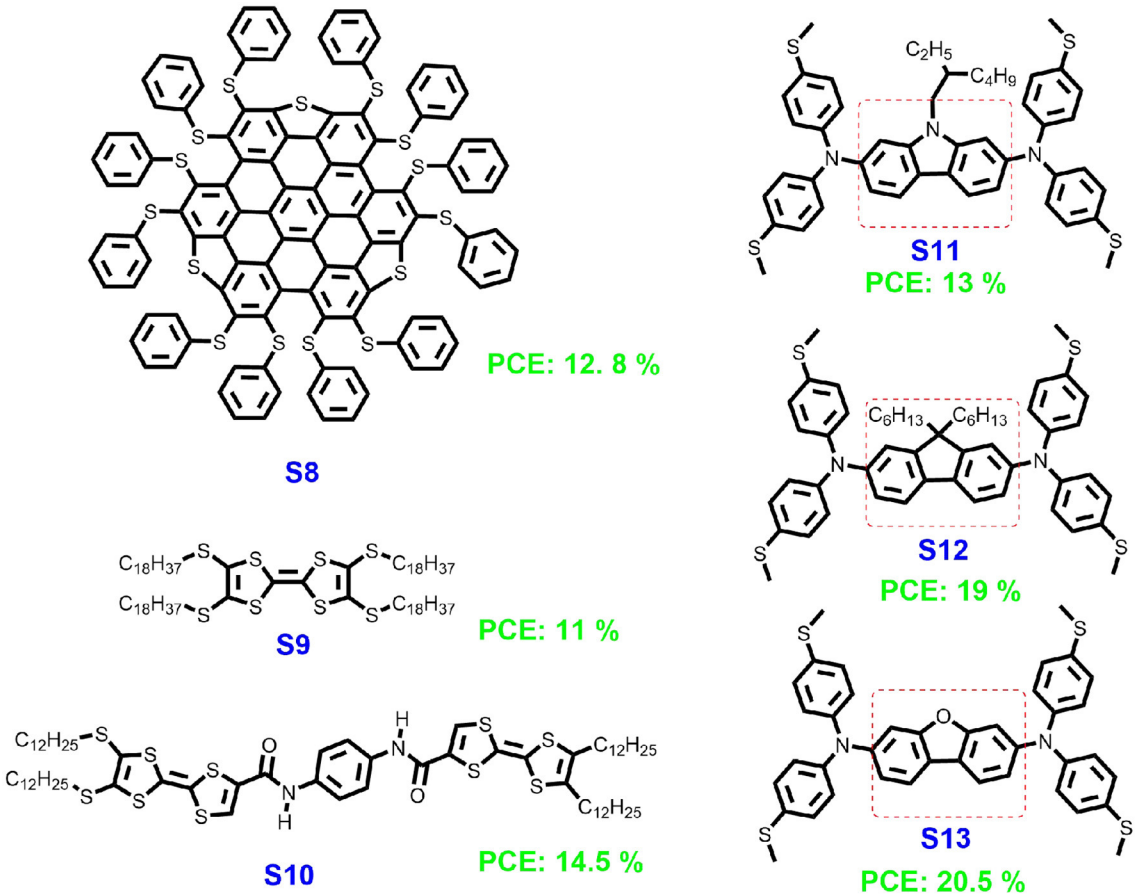

FIGURE 2 | Chemical structures of small molecules S8–S13 for dopant-free HTMs.

low-cost HTMs in PSCs. In 2017, Ding's group designed a novel HTM based on carbazole and *N*, *N*-di-*p*-methylthiophenylamine, which is named S11 (**Figure 2**) (Xu et al., 2017). The dopant-free S11-based planar *p-i-n* perovskite solar cells exhibit a high PCE of 13.05% with a V_{oc} of 1.03 V and FF of 58.23%. Later, the same group modified the structure using 9,9-dihexyl-*9H*-fluorene instead of the carbazole core obtained S12 (Zhang et al., 2019). Using S12 to fabricated the PSCs showed significantly improved performance with a higher PCE of 19.06%, V_{oc} of 1.07 V, and FF of 79.27%. In 2020, the authors further optimized the HTMs structures and changed the core into dibenzo[b,d]furan, resulting in S13. The performance of the PSC-based S13 even further improved with a PCE up to 20.51%, V_{oc} of 1.07 V, and FF of 80.48% (Quan et al., 2020). This investigation indicates that the molecular design is quite important for high-performance HTMs, and developing novel structures is thus crucial.

CONCLUSIONS AND OUTLOOK

Research regarding HTMs for PSCs is crucial and could significantly improve the performance of perovskite solar cell devices in terms of power conversion efficiency, open-circuit voltage, fill factor, etc. Furthermore, due to the high conductivity and hole transfer mobility, HTMs do not need dopant in the HTM layer. The cost of the HTMs is thus decreased; meanwhile, the lifetimes of the PSCs are extended. This review revealed that the ideal HTMs of small molecules could be achieved with high conductivity and hole transfer mobility with low cost and suitable energy levels. To obtain such ideal dopant-free HTMs, several molecular design concepts are summarized in this review, such as enlarging the π-conjugation system, increasing the planarity of molecular backbone, introducing the functional atoms/groups to achieve interface interaction between the HTMs layer and the perovskite layer, and, resulting in self-assembly within the HTMs layer, the development molecules with novel chemical structures. HTMs play a key role in the high performance of PSCs. Future research should focus on the combination of part or all of the abovementioned design concepts in a single molecule to develop desirable HTMs.

AUTHOR CONTRIBUTIONS

ZD and SC prepared the manuscript. DL and XS helped to prepare the references and revise the manuscript. KK revised the manuscript. ZD and JL supervised the whole work. All authors discussed and commented on the paper.

FUNDING

This study was financially supported by Research Projects of Shaanxi University of Technology (SLGPT2019KF01-01, SLG1901).

SUPPLEMENTARY MATERIAL

The Supplementary Material for this article can be found online at: https://www.frontiersin.org/articles/10.3389/fchem.2021.664504/full#supplementary-material

REFERENCES

Abi Ghanem, M., Liang, X., Lydon, B., Potocsnak, L., et al. (2019). Wrinkles: wrinkles riding waves in soft layered materials. *Adv. Mater. Interfaces* 6:1970004. doi: 10.1002/admi.201970004

Cao, J., Liu, Y.-M., Jing, X. J., Yin, J., Li, J., Xu, B., et al. (2015). Well-defined thiolated nanographene as hole-transporting material for efficient and stable perovskite solar cells. *J. Am. Chem. Soc.* 137, 10914–10917. doi: 10.1021/jacs.5b06493

Chen, Z. L., Li, H., Zheng, X. L., Zhang, Q., Li, Z. F., et al. (2017). Low-cost carbazole-based hole-transport material for highly efficient perovskite solar cells. *ChemSusChem* 10, 3111–3117. doi: 10.1002/cssc.201700678

Ge, Q.-Q., Shao, J.-Y., Ding, J., Deng, L.-Y., and Zhou, W.-K. (2018). A two-dimensional hole-transporting material for high-performance perovskite solar cells with 20% average efficiency. *Angew. Chem.* 130, 11125–11131. doi: 10.1002/ange.201806392

Huang, C. Y., Fu, W. F., Li, C.-Z., Zhang, Z. Q., Qiu, W. M., Shi, M. M., et al. (2016). Dopant-free hole-transporting material with a C_{3h} symmetrical truxene core for highly efficient perovskite solar cells. *J. Am. Chem. Soc.* 138, 2528–2531. doi: 10.1021/jacs.6b00039

Kaneko, R., Chowdhury, T. H., Sugawa, K., Lee, J.-J., Otsuki, J., and Islam, A. (2019). Electro-active nanofibers of a tetrathiafulvalene derivative with amide hydrogen bonds as a dopant-free hole transport material for perovskite solar cells. *Solar Energy* 194, 248–253. doi: 10.1016/j.solener.2019.10.078

Lee, J., Byranvand, M. M., Kang, G., Son, S. Y., Song, S., Kim, G.-W., et al. (2017). Green-solvent-processable, dopant-free hole-transporting materials for robust and efficient perovskite solar cells. *J. Am. Chem. Soc.* 139, 12175–12181. doi: 10.1021/jacs.7b04949

Li, M. Y., Wu, J. H., Wang, G. G., Wu, B. X., Sun, Z., et al. (2020). The donor-dependent methoxy effects on the performance of hole-transporting materials for perovskite solar cells. *J. Energy Chem.* 47, 10–17. doi: 10.1016/j.jechem.2019.11.017

Liu, J., Wu, Y., Qin, C., Yang, X., Yasuda, T., Islam, A., et al. (2014). Dopant-free hole-transporting material for efficient and stable perovskite solar cells. *Energy Environ. Sci.* 7, 2963–2967. doi: 10.1039/C4EE01589D

Liu, X. Y., Zheng, X. L., Wang, Y. L., Chen, Z. L., Yao, F., et al. (2017). Dopant-free hole-transport materials based on methoxytriphenylamine-substituted indacenodithienothiophene for solution-processed perovskite solar cells. *ChemSusChem* 10, 2833–2838. doi: 10.1002/cssc.201700197

Liu, Y. S., Hong, Z. R., Chen, Q., Chen, H. J., Chuang,W.-H., Yang, Y. M., et al. (2016). Perovskite solar cells employing dopant-free organic hole transport materials with tunable energy levels. *Adv. Mater.* 28, 440–446. doi: 10.1002/adma.201504293

Paek, S., Qin, P., Lee, Y. H., Cho, K. T., Gao, P., Grancini, G., et al. (2017). Dopant-free hole-transporting materials for stable and fficient perovskite solar cells. *Adv. Mater.* 29:1606555. doi: 10.1002/adma.201606555

Quan, S., Jing, Z., Chen, Q. Y., Wang, Y. K., Zhou, Y., Song, B., et al. (2020). High-efficiency planar *p-i-n* perovskite solar cells based on dopant-free dibenzo[b,d]furan-centred linear hole transporting material. *J. Power Sources* 449:227488. doi: 10.1016/j.jpowsour.2019.227488

Rakstys, K., Paek, S., Gao, P., Gratia, P., Marszlek, T., et al. (2017a). Molecular engineering of face-on oriented dopant-free hole transporting material for perovskite solar cells with 19% PCE. *J. Mater. Chem. A.* 5, 7811–7815. doi: 10.1039/C7TA01718A

Rakstys, K., Paek, S., Grancini, G., Gao, P., Jankauskas, V., Asiri, A. M., et al. (2017b). Low-cost perovskite solar cells employing dimethoxydiphenylamine-substituted bistricyclic aromatic enes as hole transporting materials. *ChemSusChem* 10, 3825–3832. doi: 10.1002/cssc.201700974

Vivo, P., Salunke, J. K., and Priimagi, A. (2017). Hole-transporting materials for printable perovskite solar cells. *Materials* 10:1087. doi: 10.3390/ma10091087

Xu, L., Huang, P., Zhang, J., Jia, X., Ma, Z., Sun, Y., et al. (2017). *N,N*-Di-para-methylthiophenylamine-substituted (2-ethylhexyl)-9H-carbazole: a simple, dopant-free hole-transporting material for planar perovskite solar cells. *J. Phys. Chem. C.* 121, 21821–21826. doi: 10.1021/acs.jpcc.7b04469

Yao, J., Yu, C., Liu, Z., Luo, H., Yang, Y., Zhang, G., et al. (2016). Significant improvement of semiconducting performance of the diketopyrrolopyrrole-quaterthiophene conjugated polymer through side-chain engineering via hydrogen-bonding. *J. Am. Chem. Soc.* 138, 173–185. doi: 10.1021/jacs.5b09737

Yu, Z., and Sun, L. (2015). Recent progress on hole-transporting materials for emerging organometal halide perovskite solar Cells. *Adv. Energy Mater.* 5:1500213. doi: 10.1002/aenm.201500213

Yun, J. H., Park, S., Heo, J. H., Yoon, S., Kang, J., et al. (2016). Enhancement of charge transport properties of small molecule semiconductors by controlling fluorine substitution and effects on photovoltaic properties of organic solar cells and perovskite solar cells. *Chem. Sci.* 7, 6649–6661. doi: 10.1039/C6SC02448C

Zhang, H. C., Deng, R. N., Wang, J., Li, X., Chen, Y.-M., Liu, K. W., et al. (2017a). Crystalline organic pigment-based field-effect transistors. *ACS Appl. Mater. Interfaces* 9, 21891–21899. doi: 10.1021/acsami.7b03170

Zhang, H. C., Li, R., Deng, Z. F., Cui, S. W., Wang, Y. H., Zheng, M., et al. (2020). π-Conjugated oligomers based on aminobenzodifuranone and diketopyrrolopyrrole. *Dyes Pigm.* 181:108552. doi: 10.1016/j.dyepig.2020.108552

Zhang, H. C., Liu, K. W., Wu, K. Y., Chen, Y. M., Deng, R. N., Li, X., et al. (2018). Hydrogen-bonding-mediated solid-state self-assembled isoepindolidiones (isoEpi) crystal for organic field-effect transistor. *J. Phys. Chem. C.* 122, 5888–5895. doi: 10.1021/acs.jpcc.7b11992

Zhang, J., Sun, Q., Chen, Q., Wang, Y., Zhou, Y., Song, B., et al. (2019). High efficiency planar p-i-n perovskite solar cells using low-cost fluorene-based hole transporting material. *Adv. Funct. Mater.* 29:1900484. doi: 10.1002/adfm.201900484

Zhang, M., Wang, J., Li, L., Zheng, G., Liu, K., Qin, M., et al. (2017b). High-mobility p-type organic semiconducting interlayer enhancing efficiency and stability of perovskite solar cells. *Adv. Sci.* 4:1700025. doi: 10.1002/advs.201700025

Zhao, X., Zhang, F., Yi, C., Bi, D., Bi, X., Wei, P., et al. (2016). A novel one-step synthesized and dopant-free hole transport material for efficient and stable perovskite solar cells. *J. Mater. Chem. A.* 4, 16300–16334. doi: 10.1039/C6TA05254A

Zimmermann, I., Urieta-Mora, J., Gratia, P., Aragó, J., Grancini, G., Molina-Ontoria, A., et al. (2017). High-efficiency perovskite solar cells using molecularly engineered, thiophene-rich, hole-transporting materials: influence of alkyl chain length on power conversion efficiency. *Adv. Energy Mater.* 7:1601674. doi: 10.1002/aenm.201601674

Conflict of Interest: The authors declare that the research was conducted in the absence of any commercial or financial relationships that could be construed as a potential conflict of interest.

The handling Editor declared a past co-authorship with one of the authors ZD.

frontiers in Chemistry

PERSPECTIVE
published: 01 April 2021
doi: 10.3389/fchem.2021.665877

Rearrangement Strategy for the Preparation of Polymers With π-Conjugated Structures

Jian Tang, Tinghao Xie, Jieting Geng, Jing Hua* and Zhaobo Wang**

Key Laboratory of Rubber-Plastics, Ministry of Education, Shandong Education, Shandong Provincial Key Laboratory of Rubber-plastics, Qingdao University of Science and Technology, Qingdao, China

π-Conjugated polymers are usually prepared by polymerization only. In this perspective article, typical synthesis methods of conjugated polymers are briefly summarized, and a novel strategy for preparing conjugated polymers by rearrangement is proposed. During the metalation process, many conjugated structures were generated in polybutadiene by double bond migration. The effects of reaction time, temperature, and catalyst dosage on the product structure were investigated. Moreover, the structure of the products was confirmed by FTIR, ^{1}H NMR, and 2D HSQC NMR spectra. Thus, a possible reaction mechanism was proposed, in which polybutadiene generates allylic carbanions in the presence of n-butyllithium, and then the double bonds migrate through the carbanions rearrangement to generate many conjugated structures in the backbone chain. The method shows promise in facile and low-cost synthesis of conjugated polymers without the need for precious metal catalysts.

Keywords: conjugated polymers, n-butyllithium, rearrangement, carbanion, polybutadiene

OPEN ACCESS

Edited by:
Taotao Ai,
Shaanxi University of Technology, China

Reviewed by:
Chunlin Xiao,
Osaka University, Japan
Kai Liu,
Chinese Academy of Sciences, China

****Correspondence:***
Tinghao Xie
xietinghao0312@163.com
Jing Hua
huajing72@qust.edu.cn
Zhaobo Wang
wangzhb.cn@gmail.com

Specialty section:
This article was submitted to Organic Chemistry, a section of the journal Frontiers in Chemistry

Received: *09 February 2021*
Accepted: *01 March 2021*
Published: *01 April 2021*

Citation:
Tang J, Xie T, Geng J, Hua J and Wang Z (2021) Rearrangement Strategy for the Preparation of Polymers With π-Conjugated Structures. Front. Chem. 9:665877. doi: 10.3389/fchem.2021.665877

INTRODUCTION

π-conjugated polymers are polymers containing conjugated structures in the backbone chain. The chemical and physical properties of π-conjugated polymers vary drastically with their structure. The application of these diverse π-conjugated polymers represents a potentially fertile field for chemistry and materials research (Dai et al., 2020; Saito et al., 2020). Recently, there is an increasing interest in conjugated polymers, and their applications are becoming more widespread, such as intrinsically conducting polymers (Aydemir et al., 2016), solar cells (Zhang et al., 2019; Liu et al., 2020), and organic light emitting diodes (OLEDs) (Lozano-Hernández et al., 2020; Milster et al., 2020). Besides, conjugated double bonds have more excellent reactivity compared to isolated double bonds, so conjugated polymers are widely used as substrates to prepare high-performance materials through chemical modification. For instance, conjugated polymers can be modified by cycloaddition reactions to prepare a variety of functional polymers (Yuksekdag et al., 2017), and they can also be used as macromonomers to prepare polymers with complex topologies (Makovetskii et al., 2006; Deepak and Gauthier, 2019), which often have excellent hydrodynamic properties.

Generally, conjugated polymers are prepared mainly by means of polymerization, including coordination polymerization and condensation polymerization. As early as

1958, Natta and co-workers reported the synthesis of polyacetylene using Ti/Al catalysts, which was a method based on coordination polymerization (Saxman et al., 1985). In 2000, Shirakawa et al. awarded the Nobel Prize in Chemistry for their studies in conductive polymers, particularly the doped polyacetylene, thus triggering a boom in the study of conducting polymers based on coordination polymerization (Shirakawa, 2001). In recent years, the application of conjugated polymers in emerging fields such as solar cells and OLEDs has received much attention from researchers. Most of the novel π-conjugated materials used in these fields are synthesized by condensation polymerization, especially Suzuki coupling polymerization (Guo et al., 2013).

The development of novel methods for the synthesis of conjugated polymers has also been a hot topic in this field. Over the years, various palladium- and nickel-catalyzed cross-coupling reactions have been developed, allowing couplings of aryl halides with organometallic aryl derivatives, which provides us with a versatile tool for the preparation of conjugated polymers (Baker et al., 2018). More recently, direct arylation polymerization (DArP) has attracted much attention for its efficiency and environmental friendliness. In DArP, the preparation of monomers is usually facile, no organostannane or organoboron monomers are required, and the by-products are less toxic, in line with the requirements of green chemistry (Bura et al., 2016).

From the above examples, it can be seen that the development of convenient, low-cost and environmentally friendly methods for the synthesis of conjugated polymers is one of the goals pursued by researchers in this field. Besides, the lack of alternative synthesis methods has more or less plagued chemists in the design and preparation of advanced conjugated polymers. Herein, we describe a novel strategy for the preparation of conjugated polymers. We found that the double bonds in polydienes were rearranged in the presence of alkyllithium (Tang et al., 2021). In this work, we have studied this phenomenon in detail and developed a new method for the synthesis of conjugated polymers from non-conjugated (isolated) polymers by a rearrangement strategy. This method is easy to operate, all the substrates are commercially available, and no precious metal catalysts are employed.

REARRANGEMENT STRATEGY FOR PREPARING CONJUGATED POLYMERS

This work was prompted by the unexpected finding of C=C bond rearrangement and migration of polybutadiene in the presence of n-butyllithium (n-BuLi) and N,N,N′,N′-tetramethylethylenediamine (TMEDA) (Tang et al., 2021). Polybutadiene was dissolved in n-hexane and heated in the presence of butyllithium/TMEDA to prepare samples for analysis. Details of the experimental procedure can be found in the **Supplementary Material**. The products of rearrangement of polybutadiene were analyzed by FTIR and NMR spectroscopy.

Spectroscopic studies of the products confirm the presence of a large number of conjugated double bonds in the n-BuLi-treated polybutadiene. In the FTIR spectrum of the treated polybutadiene (**Figure 1A**), The peak at 1,655 cm^{-1} assigned to the C=C stretching vibration gradually shifted to 1,611 cm^{-1} as the reaction time increases. Such a significant redshift is attributed to the averaging of the electron density due to the formation of the conjugated double bonds. In addition, the broad signal at 5.7 ppm in the ^{1}H NMR spectrum of the treated polybutadiene in **Figure 1B** is assigned to protons in the conjugated structures, which shifted to lower fields compared to protons in the unconjugated structure (5.4 ppm). The stacking of multiple conjugated structures leads to the further dispersion of the electron cloud, which can explain the weak signals appearing at lower fields (5.8–6.5 ppm). The continuous conjugated structures obtained by rearrangement are similar to that of polyacetylene. These signals in the low field are consistent with the pioneers' reports about NMR spectra of polyacetylene (Buskuhl et al., 2009). Moreover, the 2D HSQC spectrum shown in **Figure 1C** confirms the plausibility of the above assignment. The cross-correlation peak I indicates that the signal at 5.7 ppm (^{1}H) is highly correlated with the signal at 131.8 ppm (^{13}C), and both the signals at 131.8 ppm in the ^{13}C NMR spectrum and 5.7 ppm in the ^{1}H NMR spectrum are from carbons or protons of the conjugated structures.

From the above FTIR spectra as well as NMR spectral evidence, it can be deduced that conjugated double bond appeared in polybutadiene after treated with n-BuLi/TMEDA. Thus, we propose a possible reaction mechanism based on the characterization of the product structure. As shown in **Figure 1D**, the first step of the process is called the lithium-hydrogen exchange reaction or lithiation reaction. The n-BuLi abstracts a proton from polybutadiene and then forms the allylic carbanion intermediate **1a**. Next, the carbanion **1a** undergoes a rearrangement process to form intermediate **2**. As we can see, the proton sandwiched between the two C=C bonds in intermediate **2** is more acidic because the two double bonds disperse the electron density. This speculation was supported by density functional theory (DFT) calculations. Considering that the polymer contains too many atoms, making it difficult to calculate, we designed an oligomer containing only a few structural units as a model, thus simplifying the calculation. The DFT calculations were implemented by ORCA 4.2.1 program package (Neese, 2011). The electrostatic potential (ESP) analysis was performed with the Multiwfn 3.7 program (Lu and Chen, 2012). **Figure 1E** shows the ESP colored van der Waals surface for the model of intermediate 2. The blue region in this figure has a positive ESP, which is more likely to be attacked by a negatively charged Lewis base such as n-BuLi (Liu et al., 2021). As shown in this figure, the maximum electrostatic potential energy is found near the region sandwiched by two C=C bonds (Maximum value = 9.74 kcal/mol, all extreme values and their distribution are given in the **Supplementary Material**). Therefore, the protons in this area are more likely to be abstracted by alkyllithium, forming a new allylic carbanion **2a**. As with the transition process from

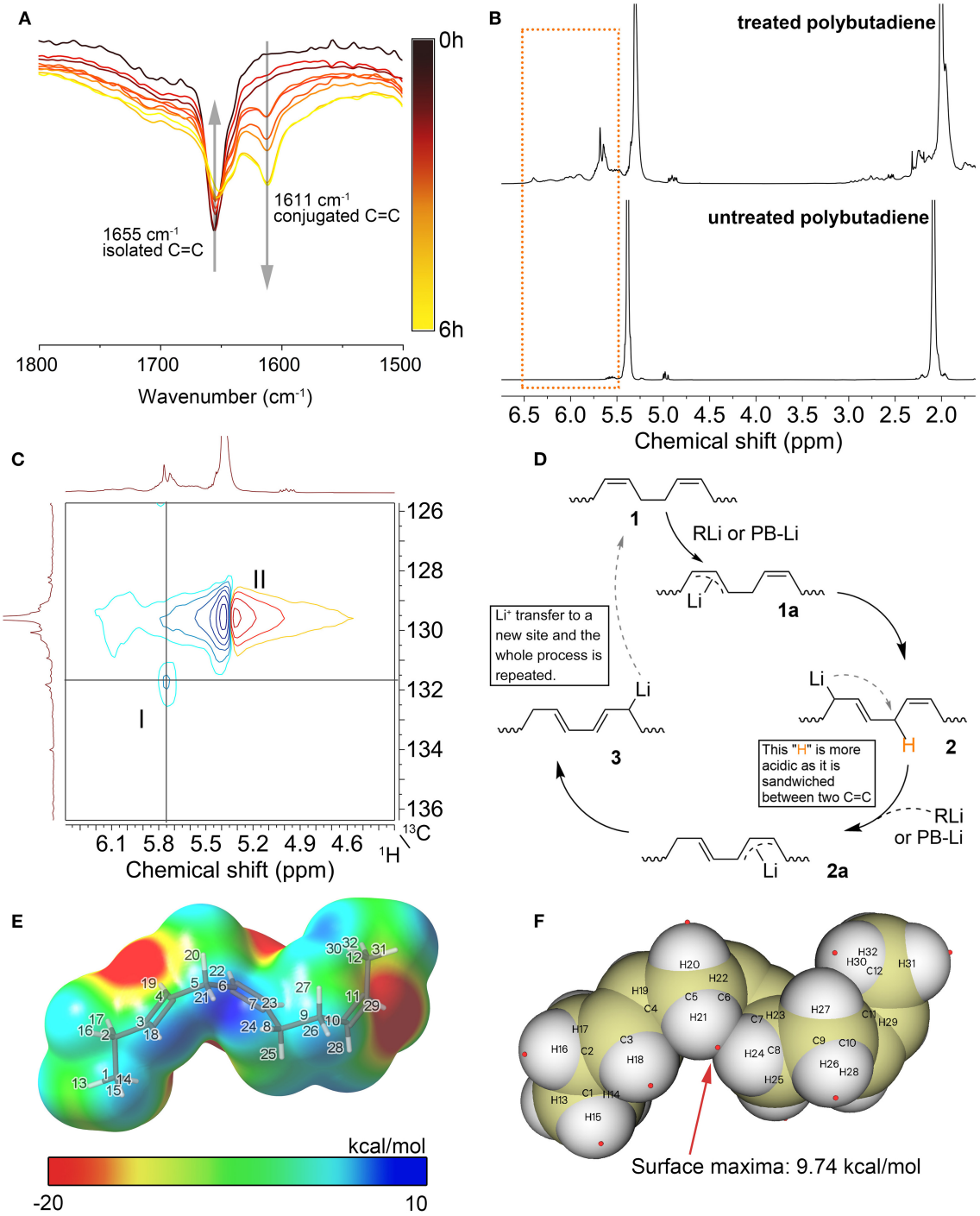

FIGURE 1 | (A) FTIR spectra of treated polybutadiene with different reaction times. **(B)** ^{1}H NMR spectra for PB and its rearrangement product. Reaction condition: 1 h, 80°C, in n-hexane, TMEDA/n-BuLi = 1:1, the molar ratio of n-BuLi to C=C is 1:1. **(C)** 2D ^{1}H-^{13}C HSQC NMR of treated polybutadiene. The reaction condition is the same as before. **(D)** Proposed reaction mechanism. **(E)** ESP mapped van der Waals surface for the model of key intermediate. **(F)** Distribution of ESP maxima (red spheres) on the van der Waals surface of the model. Preparation and analysis procedures for samples in this figure are given in **Supplementary Material**.

1a to **2**, intermediate **2a** tends to resonate into the more stable structure **3** because the conjugated structure has the lowest energy. This process is repeated throughout the polymer chain until most of the isolated double bonds are converted into conjugated double bonds. Notably, n-BuLi is not the only lithium species that can extract protons from the polymer. The lithiated

TABLE 1 | Optimization of reaction conditions[a].

Entry	Time	T	[Li]/[PB][b]	C. content[c]
1	0 min	/	/	0%
2	5 min	80°C	1	11.9%
3	15 min	80°C	1	31.4%
4	30 min	80°C	1	35.2%
5	60 min	80°C	1	40.2%
6	90 min	80°C	1	43.9%
7	120 min	80°C	1	44.8%
8	240 min	80°C	1	56.8%
9	360 min	80°C	1	68.9%
10	60 min	80°C	0.1	9.6%
11	60 min	80°C	0.3	16.9%
12	60 min	80°C	0.5	23.9%
13	60 min	0°C	1	trace
14	60 min	30°C	1	5.6%
15	60 min	60°C	1	20.0%

[a]*Reaction condition: in n-hexane, TMEDA/n-BuLi = 1:1. The samples preparation procedures are given in the* ***Supplementary Material****.* [b]*The molar ratio of n-BuLi to C=C bond.* [c]*C. content: conjugated double bond content, i.e., the molar proportion of conjugated C=C bonds to all C=C bonds. It was determined by* ^{1}*H NMR.*

polybutadiene (PB-Li) can also work as a Lewis base to extract protons from the polymer chain. This process is quite like a chain transfer process, where lithium atoms are transferred from a site to another so that lithium can be recycled in this process.

Moreover, a series of rearrangement reactions were carried out at different reaction temperatures, times, and catalyst dosages to optimize the reaction conditions. As shown in entries 1–9 in **Table 1**, the proportion of conjugated double bonds to the total double bonds in the products increased with increasing reaction time. The reaction is a relatively slow process, so the content of conjugated double bonds in the product can be regulated by controlling the reaction time. As with most reactions, the dosage of catalyst directly affects the conversion. When the dosage of n-BuLi was 10% double bond equivalent, the percentage of conjugated double bonds in the product was only 9.6% (The molar ratio of conjugate double bonds to all double bonds, same below) at 60 min of reaction, while the percentage of conjugated double bonds in the product was 16.9, 23.9, and 40.2% when the dosage of n-BuLi was 30, 50, and 100% double bond equivalent. Besides, the temperature also strongly affected the reaction. Almost no conjugated double bonds were detected in the products when the reaction was carried out at 0°C for 60 min. At a reaction temperature of 30°C, the percentage of conjugated double bonds in the resulting polymers was only 5.6%, whereas approaching 20.0% at 60°C. Consequently, we can regulate the amount of conjugated double bonds freely by controlling the conditions such as temperature, reaction time, and catalyst dosage.

CONCLUSIONS

The n-BuLi/TMEDA system can induce double bond migration in polybutadiene, which results in the generation of π-conjugated structures. The kinetic study of the reaction shows that the rearrangement process occurs gradually, so the content of conjugated double bonds in the products can be regulated by controlling temperature, reaction time, and catalyst dosage. Furthermore, based on spectroscopic evidence, the reaction mechanism was described as a process in which carbanion rearrangement leads to the conversion of the double bond to a more stable conjugated structure.

Since the resulting polymer does not contain aromatic rings, it is not suitable as a conductive polymer or for making optoelectronic devices. However, the conjugated double bonds give it excellent reactivity, so it can be used as a substrate to prepare various functional materials by chemical modification. For example, it can be used as a backbone to prepare comb polymer by grafting polymerization. It can also be chemically modified to prepare functional polymer materials with various functional groups. We have to admit that this strategy has some shortcomings yet, such as narrow substrate scope and low stereoselectivity, which may limit its application at this stage. However, this method does not involve precious metal catalysts such as palladium, and all substrates are low-cost commercially available reagents, which is in line with the concept of sustainable development. This idea of preparing conjugated polymers from ready-made polymers is promising, and we hope that this work provides new ideas for the research of π-conjugated polymer synthesis.

DATA AVAILABILITY STATEMENT

The original contributions generated for the study are included in the article/**Supplementary Material**, further inquiries can be directed to the corresponding author/s.

AUTHOR CONTRIBUTIONS

JT and TX prepared materials and carried out experiments. JG helped to characterize materials. JH and ZW supervised the work. All authors contributed to revising the manuscript and approved the final version.

FUNDING

This study was financially supported by the Natural Science Foundation of Shandong Province (contract Grant No. ZR201910260069).

SUPPLEMENTARY MATERIAL

The Supplementary Material for this article can be found online at: https://www.frontiersin.org/articles/10.3389/fchem.2021.665877/full#supplementary-material

REFERENCES

Aydemir, N., Malmstrom, J., and Travas-Sejdic, J. (2016). Conducting polymer based electrochemical biosensors. *Phys. Chem. Chem. Phys.* 18, 8264–8277. doi: 10.1039/C5CP06830D

Baker, M. A., Tsai, C. H., and Noonan, K. J. T. (2018). Diversifying cross-coupling strategies, catalysts and monomers for the controlled synthesis of conjugated polymers. *Chemistry* 24, 13078–13088. doi: 10.1002/chem.201706102

Bura, T., Blaskovits, J. T., and Leclerc, M. (2016). Direct (Hetero)arylation polymerization: trends and perspectives. *J. Am. Chem. Soc.* 138, 10056–10071. doi: 10.1021/jacs.6b06237

Buskuhl, H., Freitas, R. A., Monache, F. D., Barison, A., Campos, F. R., Corilo, Y. E., et al. (2009). A new polyacetylene from vernonia scorpioides (Lam.) Pers. *(Asteraceae)* and its *in vitro* antitumoral activity. *J. Brazil. Chem. Soc.* 20, 1327–1333. doi: 10.1590/S0103-50532009000700018

Dai, Z., Ai, T., Zhou, Q., and Zhang, H. (2020). Editorial: Design, synthesis, and application of novel pi-conjugated materials. *Front. Chem.* 8:634698. doi: 10.3389/fchem.2020.634698

Deepak, V. D., and Gauthier, M. (2019). Synthesis of isoprenic polybutadiene macromonomers for the preparation of branched polybutadiene. *Eur. Polym. J.* 113, 133–141. doi: 10.1016/j.eurpolymj.2019.01.041

Guo, X., Baumgarten, M., and Müllen, K. (2013). Designing π-conjugated polymers for organic electronics. *Prog. Polym. Sci.* 38, 1832–1908. doi: 10.1016/j.progpolymsci.2013.09.005

Liu, J., Wang, E., and Zhao, K. (2020). Editorial: polymer solar cells: molecular design and microstructure control. *Front. Chem.* 8:697. doi: 10.3389/fchem.2020.00697

Liu, Z., Lu, T., and Chen, Q. (2021). Intermolecular interaction characteristics of the all-carboatomic ring, cyclo[18]carbon: focusing on molecular adsorption and stacking. *Carbon N. Y.* 171, 514–523. doi: 10.1016/j.carbon.2020.09.048

Lozano-Hernández, L. A., Maldonado, J. L., Hernández-Cruz, O., Nicasio-Collazo, J., Rodríguez, M., Barbosa-García, O., et al. (2020). Structurally simple OLEDs based on a new fluorinated poly(oxindolylidenearylene). *Dyes Pigm.* 173:107989. doi: 10.1016/j.dyepig.2019.107989

Lu, T., and Chen, F. (2012). Multiwfn: a multifunctional wavefunction analyzer. *J. Comput. Chem.* 33, 580–592. doi: 10.1002/jcc.22885

Makovetskii, K., Yakovlev, V., Golenko, T., and Bondarenko, G. (2006). Preparation of branched cis-1, 4-polybutadiene in the presence of a neodymium catalyst. *Polymer Sci. Series B* 48, 61–65. doi: 10.1134/S1560090406030018

Milster, S., Grünbaum, T., Bange, S., Kurrmann, S., Kraus, H., Stoltzfus, D. M., et al. (2020). Perdeuterated conjugated polymers for ultralow-frequency magnetic resonance of OLEDs. *Angewand. Chem.* 132, 9474–9478. doi: 10.1002/ange.202002477

Neese, F. (2011). The ORCA program system. *WIREs Comput. Mol. Sci.* 2, 73–78. doi: 10.1002/wcms.81

Saito, M., Ohkita, H., and Osaka, I. (2020). π-Conjugated polymers and molecules enabling small photon energy loss simultaneously with high efficiency in organic photovoltaics. *J. Mater. Chem. A* 8, 20213–20237. doi: 10.1039/D0TA05108J

Saxman, A. M., Liepins, R., and Aldissi, M. (1985). Polyacetylene: its synthesis, doping and structure. *Prog. Polym. Sci.* 11, 57–89. doi: 10.1016/0079-6700(85)90008-5

Shirakawa, H. (2001). Nobel lecture: the discovery of polyacetylene film—the dawning of an era of conducting polymers. *Rev. Mod. Phys.* 73, 713–718. doi: 10.1103/RevModPhys.73.713

Tang, J., Xie, T., Yuan, Y., Hua, J., Zhuang, T., Luo, Y., et al. (2021). Degradation of polydienes induced by alkyllithium: characterization and reaction mechanism. *Macromolecules* 54, 1147–1158. doi: 10.1021/acs.macromol.0c01934

Yuksekdag, Y. N., Gevrek, T. N., and Sanyal, A. (2017). Diels-alder clickable polymer brushes: a versatile catalyst-free conjugation platform. *ACS Macro. Lett.* 6, 415–420. doi: 10.1021/acsmacrolett.7b00041

Zhang, H., Liu, M., Yang, W., Judin, L., Hukka, T. I., Priimagi, A., et al. (2019). Thionation enhances the performance of polymeric dopant-free hole-transporting materials for perovskite solar cells. *Adv. Mater. Interf.* 6:1901036. doi: 10.1002/admi.201901036

Conflict of Interest: The authors declare that the research was conducted in the absence of any commercial or financial relationships that could be construed as a potential conflict of interest.

frontiers in Chemistry

MINI REVIEW
published: 14 April 2021
doi: 10.3389/fchem.2021.671294

Diketopyrrolopyrrole Based Organic Semiconductor Materials for Field-Effect Transistors

Xiangyu Zou[1†], *Shuaiwei Cui*[2†], *Junqiang Li*[3], *Xueling Wei*[1*] and *Meng Zheng*[2,3*]

[1] National and Local Joint Engineering Laboratory for Slag Comprehensive Utilization and Environmental Technology, School of Materials Science and Engineering, Shaanxi University of Technology (SNUT), Hanzhong, China, [2] Key Laboratory of Rubber–Plastic of Ministry of Education (QUST), School of Polymer Science and Engineering, Qingdao University of Science and Technology, Qingdao, China, [3] Qingdao Haiwan Science and Technology Industry Research Institute Co., Ltd., Qingdao, China

Over the past several decades, organic conjugated materials as semiconductors in organic field effect transistors (OFETs) have attracted more and more attention from the scientific community due to their intriguing properties of mechanical flexibility and solution processability. However, the device fabrication technique, design, and synthesis of novel organic semiconductor materials with high charge carrier mobility is crucial for the development of high-performance OFETs. In the past few years, more and more novel materials were designed and tested in the OFETs. Among which, diketopyrrolopyrrole (DPP) and its derivatives, as the electron acceptors to build donor-acceptor (D-A) typed materials, are the perspective. In this article, recently reported molecules regarding the DPP and its derivatives for OFETs application are reviewed. In addition, the relationship between the chemical structures and the performance of the device are discussed. Furthermore, an outlook of DPP-based materials in OFETs with a future design concept and the development trend are provided.

Keywords: DPP, organic semiconductor materials, organic field effect transistors, D-A typed materials, molecular design concept

OPEN ACCESS

Edited by:
Qixin Zhou,
University of Akron, United States

Reviewed by:
Jianfeng Hou,
Luliang University, China
Hongtao Shen,
Northeastern University at Qinhuangdao, China

***Correspondence:**
Xueling Wei
weixling0808@163.com
Meng Zheng
zhengmeng.555@hotmail.com

†These authors have contributed equally to this work

Specialty section:
This article was submitted to Organic Chemistry, a section of the journal Frontiers in Chemistry

Received: *23 February 2021*
Accepted: *16 March 2021*
Published: *14 April 2021*

Citation:
Zou X, Cui S, Li J, Wei X and Zheng M (2021) Diketopyrrolopyrrole Based Organic Semiconductor Materials for Field-Effect Transistors. Front. Chem. 9:671294. doi: 10.3389/fchem.2021.671294

INTRODUCTION

During the past decade, organic semiconducting materials including π-conjugated small molecules and polymers have attracted increasing attention due to their potential applications in organic electronic devices such as organic field-effect transistors (OFETs) and organic photovoltaics (OPVs) (Zhao et al., 2016; Huang et al., 2017). Compared to traditional Si- and GaAs-based technologies, organic semiconductors offer unique features, such as their mechanical flexibility, variable optical band gaps, and low-temperature large-area solution processability. The transistor is the fundamental building block of modern electronic devices and is used to amplify and switch electronic signals (Guo X. G. et al., 2014). To fabricate high-performance OFETs, charge transfer mobility (μ), threshold voltage, and current on/off ration are the three key factors. Among these three factors, high charge carrier mobility is the most important and a challenging, since the existing organic semiconductor's charge transfer mobilities are far behind compared to the inorganic Si-based ones, resulting in it not meeting the commercial demand (Qiu et al., 2020). Except the device fabrication technique, the chemical structures of the organic semiconductors play a key role for improvement of the charge carrier's mobility.

This could be ascribed that in the OFETs, charge carriers need to be frequently transferred between individual molecules and within molecules in order to transport from one electrode the another (Zhang et al., 2017a, 2020). The chemical structures of the organic materials are easily tunable with diverse core/backbone architectures, which can fulfill better solid-state packing, thin-film morphology, overlap of the molecules, π-π stacking and the crystalline, resulting in improvement to the inter-charge transfer mobility. In addition, novel organic molecules with large π-conjugation system, good planarity, and strong donor-acceptor groups are beneficial for the intra-charge transfer (Guo X. G. et al., 2014).

The charge is divided into electron and hole, based on whether the OFETs are distinguished into p-type (hole transfer type), n-type (electron transfer type), and ambipolar type (electron and hole transfer type). Currentlys, the n-type and ambipolar type OFETs have received more attention from the scientific society, because the existing highest electron mobility and the stability of the OFETs are much lower than the reported highest hole mobility. Research revealed that the design and synthesis of novel organic semiconductor materials with high charge carrier mobility is crucial for the development of high-performance OFETs. In the past few years, more and more novel materials were designed and tested in the OFETs. Among which, diketopyrrolopyrrole (DPP) and their derivatives, as the electron acceptors to build donor-acceptor typed materials, are the perspective (Donaghey et al., 2013; Lin et al., 2018; Lee et al., 2019). In this article, recently reported molecules regarding to the DPP for OFETs application are reviewed. In addition, the relationship between the chemical structures and the performance of the device are also discussed. Finally, we provide our perspective to address the existing critical points of high-performance OFETs and the molecular design concept regarding the DPP derivatives, by outlining potential evolution trends. We hope that this work will promote new insights and further research studies to boost the development of OFETs for the next-generation applications.

DPP-BASED CONJUGATED MATERIALS

DPP-based molecules were often constructed by a core containing two amine units and carbonyl groups with bicyclo, and end flanked by the aromatic groups. The core endowed the DPP derivatives with strong electron deficiency properties, which can be used to build donor-acceptor system molecules. In addition, once the aromatic groups were flanked with small units, the conjugated backbone of the DPP exhibited highly planar which endowed the high intra-charge transfer mobility (Bao et al., 2020). DPP-based materials have often exhibited extraordinarily strong π-π interaction and aggregation properties between the neighboring DPP moieties, resulting in the materials having beneficial properties for inter-charge transfer mobility. Hence DPP and its derivatives-based materials were widely studied and used in build high-performance OFETs (Qu and Tian, 2012).

DPP

Since the first DPP-based materials application in OFETs were reported by Bürgi et al. with a hole mobility (μ_h) of 0.1 $cm^2\ V^{-1}\ s^{-1}$ and electron mobility (μ_e) of 0.09 $cm^2\ V^{-1}\ s^{-1}$ (Lukas et al., 2008), the DPP derivatives received more and more attention from chemists as one of the most promising building blocks in organic semiconductors. Recently, Zhang's group reported the hydrogen bonded DPP based small molecules with a hole mobility of 0.26 $cm^2\ V^{-1}\ s^{-1}$ (Zhang et al., 2017a) and the polymer with a hole mobility up to 1.02 $cm^2\ V^{-1}\ s^{-1}$ (Zhang et al., 2019) (**Figures 1A,B**). Kang et al. using DPP as the acceptor to synthesize D-A type polymers with the μ_h up to 12 $cm^2\ V^{-1}\ s^{-1}$ (Kang et al., 2013) (**Figure 1C**). Until now, the best DPP-based OFET was reported by Luo et al. Through intruding tetramethylammonium iodide into the DPP polymer, good ordered lamellar packing of the alkyl side chains and inter-chain π-π interactions film were formed, meanwhile the μ_h was up to 26 $cm^2\ V^{-1}\ s^{-1}$ and μ_e up to 4.4 $cm^2\ V^{-1}\ s^{-1}$ (Luo et al., 2016) (**Figure 1D**). This work reveals that the DPP chromophore is a potential building blocks in the semiconductors materials.

In 2016, Bao's group introduced 2,6-pyridine dicarboxamide with non-conjugated alkyl units into the DPP-based polymer backbone, with the interaction between the C=O group and N-H group in the adjacent molecules, which could form hydrogen bonding between the neighboring molecules. These kinds of polymers showed not only high hole transfer mobility (1.32 $cm^2\ V^{-1}\ s^{-1}$), but also exhibited self-healable properties (Oh et al., 2016) (**Figure 1E**). Almost at the same time, Yao and co-authors, introducing urea-containing alkyl chains into the DPP based polymers, developed hydrogen bonded polymers with a hole mobility up to 13.1 $cm^2\ V^{-1}\ s^{-1}$ (Yao et al., 2015) (**Figure 1F**). These works indicate that hydrogen bonding association could significantly improve the DPP-based charge transfer mobility.

The flanked aromatic group attached to the DPP core are crucial for the design DPP-based molecules. The most reported flanked units are the thiophene units. Besides that, other groups were also introduced as the flanked units attached to the DPP core to build novel chromophore, such as the naphthalene (Liu et al., 2018), furanyl (Sonar et al., 2012), thiazole (Li et al., 2014), pyrrinde (Li et al., 2017), thienothiophene (Jiang et al., 2017), and so on (**Figure 1G**). These new materials also showed good performance in the OFETs.

isoDPP

IsoDPP is a regioisomer of DPP, the chemical structure of which is similar to the DPP with a switching position of the carbonyl group and the nitrogen atom (**Figure 2A**). Compared to the DPP-based semiconductors, the isoDPP-based one received less attention, though it has as much potential as the DPP-based ones. IsoDPP was firstly developed roughly 30 years ago in one step from pluvinic acid (Rochat et al., 1985; Deng et al., 2019). The first isoDPP-based polymers were synthesized by Tieke's group in 2011 (Welterlich et al., 2012), while the first isoDPP-based polymer in OFETs were tested by Facchetti's group in 2013 (Lu et al., 2013). The polymers were constructed by the donor-acceptor system, isoDPP units as the acceptor and the dithieno[3,2-b:2′,3′-d]silole units as the donor, which

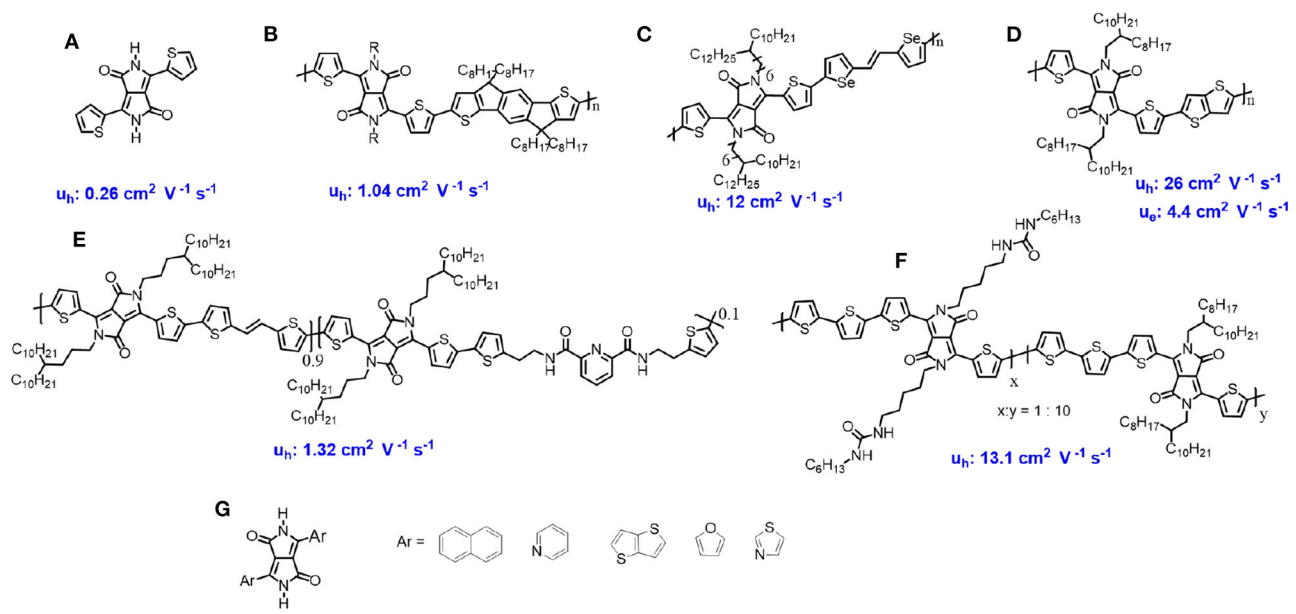

FIGURE 1 | Chemical structures of DPP-based materials for OFET and their charge transfer mobility.

showed p-type behavior with a hole mobility of 0.03 cm^2 V^{-1} s^{-1} (**Figure 2B**). In 2018, Zhang et al. reported similar polymers with the same polymer backbone but different alkyl-chain. This polymer showed a hole mobility of 0.09 (Zhang et al., 2018) (**Figure 2C**). The high hole mobility could be ascribed to the high molecular weight, which is beneficial for the charge transfer within the single polymer backbone. In addition, the author reported that through one-step thionation reaction using Lawesson's reagent, oxygen–sulfur exchange in the isoDPP core happened, resulting in a new chromophore isoDTPP. The isoDTPP based polymers showed hole mobility up to 0.49 cm^2 V $^{-1}$ s $^{-1}$, which is almost five times larger compared to the isoDPP-based one, and the electron mobility to 0.29 cm^2 V $^{-1}$ s $^{-1}$. This indicates that the isoDTPP is a promising building block for high performance organic semiconductors[1]. Recently, Guo et al. reported a copolymer containing isoDPP and DPP in the polymer backbone to construct acceptor-acceptor system polymers (Guo X. et al., 2014) (**Figure 2D**). This polymer showed ambipolar behavior with balanced holes and electrons mobilities around 0.02 cm^2 V^{-1} s^{-1}. The charge carrier mobility of this polymer exhibited around two to three orders of magnitude higher than the reported DPP-based "homo" -polymer (Zoombelt et al., 2010). This could be ascribed to the fact that the isoDPP polymers showed good order and quite close packing distance of 0.38 nm in the solid state, which is beneficial for the charge carrier transport between the neighboring molecules.

Not like the DPP-based materials, the isoDPP-based materials were only designed by two types, such as phenyl-flanked and the thiophene-flanked isoDPP. Gendron et al. (2014) and Zhang et al. (2013) prepared the single crystal of these two different small molecules, which showed that the core of isoDPP was fully coplanar as DPP. The studies showed that using a thiophene ring instead of a phenyl ring attached the isoDPP core could significantly improve the planarity of the conjugated isoDPP backbone. In addition, the thiophene units exhibits stronger donor units than the benzene groups, which could form the donor-acceptor system between the thiophene and the isoDPP core. A high planar conjugation backbone and stronger donor-acceptor system is beneficial for the intra-charge transfer, thus the thiophene-flanked isoDPP has more potential. IsoDPP chromophore as a novel building block has potential in semiconductors materials, though it has not received the desired attention. Future research regarding to the isoDPP-based materials should be focused on adjusting the flanked groups (Zhao et al., 2019), improving the planarity materials conjugated backbone (Zhang et al., 2016; Li et al., 2021), introducing functions units into the core (Oh et al., 2016), and so on.

DPP-Based Derivatives

In the past few years, various kinds of DPP-based derivatives were widely developed and used as the organic semiconductors in OFETs. In 2020, Shi et al. designed a novel building block, denoted as a half-fused DPP, in which one of the flanking thiophene units is fused to the DPP core *via* a carbon-carbon double bond at the N-position (Shi et al., 2020). In this work, through Stille coupling, donor-acceptor polymer, the difluorothiophene as donor, and the half-fused DPP as acceptor, was synthesized with a molecular number weight of 24.4 kDa (**Figure 2E**). The obtained polymer exhibited ambipolar behavior with μ_h of 2.23 and μ_e of 1.08 cm^2 V^{-1} s^{-1}, while the non-fused DPP based polymer with similar chemical structures showed quite low charge carrier mobility with μ_h of 0.78 and μ_e of 0.24 cm^2 V^{-1} s^{-1}. The significant improvement charge carrier

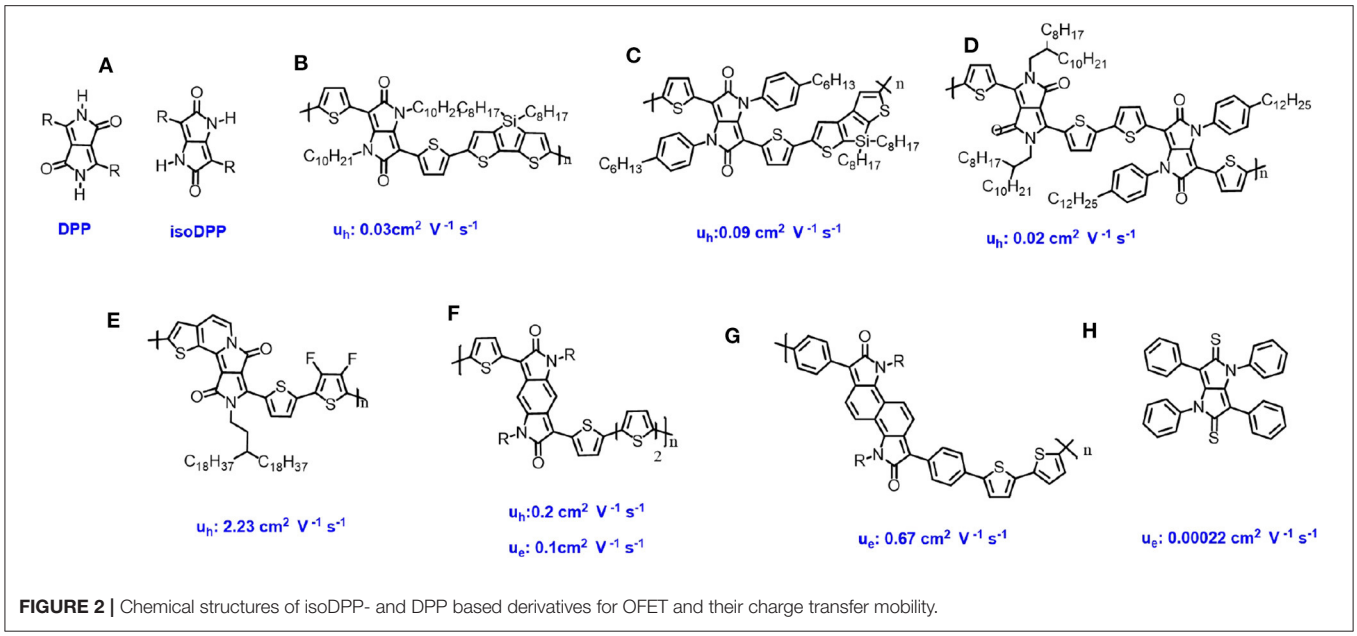

FIGURE 2 | Chemical structures of isoDPP- and DPP based derivatives for OFET and their charge transfer mobility.

mobility should be ascribed that: the high planar backbone, monosubstituted alkyl chain, instead disubstituted alkyl chains reducing the steric crowding, a short π-π stacking distance and lower LUMO energy levels. This research reversed that the planarity of the polymer backbone is crucial for high performance organic semiconductors.

Enlarging the π-conjugation system of isoDPP core results in benzodipyrrolidone (BDP) and naphtodipyrrolidone (NDP). Compared to the isoDPP, the BDP, and NDP showed similar chemical structures except the core are tri- and tera-cyclic (Deng et al., 2019). Rumer et al. reported BDP based polymers with ambipolar behavior with μ_h and μ_e of 0.2 and 0.1 cm^2 V^{-1} s^{-1}, respectively (Rumer et al., 2013) (**Figure 2F**), while a similar polymer consisting of NDP based polymer exhibited n-type behavior with μ_e of 0.67 cm^2 V^{-1} s^{-1} (Zhang et al., 2017b) (**Figure 2G**). The different properties of these semiconductors could be due to the fact that the π-conjugation extension could not only enlarge the charge transfer pathway, but also adjust the frontier molecular orbitals.

Upon thiolation reaction, the carbonyl of the DPP core could be easily transferred into thiocarbonyl resulting DTPP (Gendron et al., 2017). The DTPP based small molecules showed p-type behavior with hole mobility around 2.2×10^{-4} cm^2 V^{-1} s^{-1} (**Figure 2H**). The low mobility could be ascribed to the simple structures, in which the DTPP core is flanked with a benzene ring. To further optimize these molecules, other donor units, such as thiophene, thienothiophene, and so on, instead of the benzene ring, could be used.

CONCLUSION AND OUTLOOK

Until now, DPP chromophore and its derivatives, as one of the most popular acceptor units, were widely used in construction donor-acceptor materials, which showed high charge transfer mobility in the OFETs. However, the isoDPP-based ones received less attention though they are promising. In this article, DPP-based materials, including DPP, isoDPP, and DPP-based derivatives, as the semiconductor in OFETs were reviewed. Though DPP-based materials were promising in OFETs, great opportunities and challenges still remain in the development of DPP-based semiconductors with high charge carrier mobility, typically for the ambipolar type OFETs. To obtain high-performance DPP-based semiconductor materials, the highlighted development comes from the following factors: planar materials backbone, large π-conjugation system, highly crystalline, strong π-π stacking and aggregation, short molecular distance, and so on. Recently research reversed the idea that DPP chromophore is a promising unit to build high-performance semiconductor materials. Further optimizing its structures, typically the isoDPP-based materials, are always challenging and urgently necessary.

AUTHOR CONTRIBUTIONS

XZ and SC prepared the manuscript. JL revised the manuscript. XW and MZ supervised the whole work. All authors discussed and commented on the paper.

FUNDING

This study was financially supported by National Natural Science Foundation of China (No. 51504147), Special Scientific Research Planned Projects of Education Department of Shaanxi Provincial (No. 15JK1165), and Research Projects of Shaanxi University of Technology (No. SLGKY2007).

REFERENCES

Bao, W. W., Li, R., Dai, Z. C., Tang, J., Shi, X., Geng, J. T., et al. (2020). Diketopyrrolopyrrole (dpp)-based materials and its applications: a review. *Front. Chem.* 8:679. doi: 10.3389/fchem.2020.00679

Deng, Z. F., Ai, T. T., Li, R., Yuan, W., Zhang, K., Du, H. L., et al. (2019). Conjugated polymers containing building blocks 1,3,4,6-tetraarylpyrrolo[3,2-b]pyrrole-2,5-dione (IsoDPP), benzodipyrrolidone (BDP) or naphthodipyrrolidone (NDP): a review. *Polymers* 11:1683. doi: 10.3390/polym11101683

Donaghey, J. E., Sohn, E. H., Ashraf, R. S., Anthopouios, T. D., Watkins, S. E., Song, K., et al. (2013). Pyrroloindacenodithiophene polymers: the effect of molecular structure on OFET performance. *Polym. Chem.* 4, 3537–3544. doi: 10.1039/c3py00335c

Gendron, D., Gann, E., Pattison, K., Maasoumi, F., Mcneill, C.R., Watkins, S.E., et al. (2014). Synthesis and properties ofpyrrolo[3,2-b]pyrrole-1,4-diones (isoDPP) derivatives. *J. Mater. Chem. C* 2, 4276–4288. doi: 10.1039/c4tc00427b

Gendron, D., Maasoumi, F., Armin, A., Pattison, K., Burn, P. L., Meredith, P., et al. (2017). A thiocarbonyl-containing small molecule for optoelectronics. *RSC Adv.* 7, 10316–10322. doi: 10.1039/C7RA00693D

Guo, X., Puniredd, S. R., He, B., Marszalek, T., Baumgarten, M., Pisula, W., et al. (2014). Combination of two diketopyrrolopyrrole isomers in one polymer for ambipolar transport. *Chem. Mater.* 26, 3595–3598. doi: 10.1021/cm5017245

Guo, X. G., Facchetti, A., and Marks, T. J. (2014). Imide- and amide-functionalized polymer semiconductors. *Chem. Rev.* 114, 8943–9021. doi: 10.1021/cr500225d

Huang, Y. L., Chen, H., Yang, J. W., Tian, W. L., and Wang, W. Z. (2017). 3D-Printed OFETs of the 1,4-bis(3-phenylquinoxalin-2-yl)benzene-based polymer semiconductors. *Polym. Chem.* 8, 4878–4886. doi: 10.1039/C7PY00810D

Jiang, Z. Y., Ni, Z. J., Wang, H. L., Wang, Z., Zhang, J. Q., Qiu, G., et al. (2017). Versatile asymmetric thiophene/benzothiophene flanked diketopyrrolopyrrole polymers with ambipolar properties for ofets and oscs. *Polym. Chem.* 8, 5603–5610. doi: 10.1039/C7PY00940B

Kang, I., Yun, H.-J., Chung, D. S., Kwon, S.-K., and Kim, Y.-H. (2013). Record high hole mobility in polymer semiconductors *via* side-chain engineering. *J. Am. Chem. Soc.* 135, 14896–14899. doi: 10.1021/ja405112s

Lee, S. M., Lee, H. R., Dutta, G. K., Lee, J. H., Oh, J. H., and Yang, C. (2019). Furan-flanked diketopyrrolopyrrole-based chalcogenophene copolymers with siloxane hybrid side chain for organic field-effect transistors. *Polym. Chem.* 10, 2854–2862. doi: 10.1039/C9PY00448C

Li, R., Dai, Z., Zheng, M., Wang, C., Deng, Z., Zhuang, T., et al. (2021). Benzo/Naphthodifuranone-based polymers: effect of perpendicular-extended main chain π-conjugation on organic field-effect transistor performances. *Macromol. Rapid Commun.* 2000703. doi: 10.1002/marc.202000703

Li, W. W., Roelofs, W. S. C., Turbiez, M., Wienk, M. M., and Janssen, R. A. J. (2014). Polymer solar cells with diketopyrrolopyrrole conjugated polymers as the electron donor and electron acceptor. *Adv. Mater.* 26, 3304–3309. doi: 10.1002/adma.201305910

Li, Z. J., Xu, X. F., Zhang, W., Genene, Z., Mammo, W., Yartsev, A., et al. (2017). High photovoltage all-polymer solar cells based on a diketopyrrolopyrrole-isoindigo acceptor polymer. *J. Mater. Chem. A* 5, 11693–11700. doi: 10.1039/C6TA09379E

Lin, F.-J., Lin, S.-D., Chin, C.-H., Chuang, W.-T., and Hsu, C.-S. (2018). Novel onjugated polymers based on bis-dithieno[3,2-*b*;2',3'-*d*]pyrrole vinylene donor and diketopyrrolopyrrole acceptor: side chain engineering in organic field effect transistors. *Polym. Chem.* 9, 28–37. doi: 10.1039/C7PY01340J

Liu, Q., Sun, H. B., Blaikie, C., Caporale, C., Manzhos, S., Feron, K., et al. (2018). Correction: Naphthalene flanked diketopyrrolopyrrole based organic semiconductors for high performance organic field effect transistors. *NewJ. Chem.* 42, 12374–12385. doi: 10.1039/C8NJ01453A

Lu, S. F., Drees, M., Yao,Y., Boudinet, D., Yan, H., Pan, H. L., et al. (2013). 3,6-Dithiophen-2-yl-diketopyrrolo[3,2-b]pyrrole (isoDPPT) as an acceptor building block for organic opto-electronics. *Macromolecules* 46, 3895–3906. doi: 10.1021/ma400568b

Lukas, B., Mathieu, T., Reto, P., Frank, B., Hans-Jörg, K., and Carsten, W. (2008). High-mobility ambipolar near-infrared light-emitting polymer field-effect transistors. *Adv. Mater.* 20, 2217–2224. doi: 10.1002/adma.200702775

Luo, H. W., Yu, C. M., Liu, Z. T., Zhang, G. X., Geng, H., Yi, Y. P., et al. (2016). Remarkable enhancement of charge carrier mobility of conjugated polymer field-effect transistors upon incorporating an ionic additive. *Sci. Adv.* 2:e1600076. doi: 10.1126/sciadv.1600076

Oh, J. Y., Rondeau-Gagné, S., Chiu, Y.-C., Chortos, A., Lissel, F., Wang, G.-J. N., et al. (2016). Intrinsically stretchable and healable semiconducting polymer for organic transistors. *Nature* 539, 411–415. doi: 10.1038/nature20102

Qiu, D. D., Adil, M. A., Lu, K., and Wei, Z. X. (2020). The crystallinity control of polymer donor materials for high-performance organic solar cells. *Front. Chem.* 8:603134. doi: 10.3389/fchem.2020.603134

Qu, S. Y., and Tian, H. (2012). Diketopyrrolopyrrole (dpp)-based materials for organic photovoltaics. *Chem. Commun.* 48, 3039–3051. doi: 10.1039/c2cc17886a

Rochat, A. C., Iqbal, A., Pfenninger, J., and Casser, L. (1985). *Process for Dyeing a High Molecular Organic Material, Polycyclic Compounds and Their Preparation*. European Patent.

Rumer, J. W., Levick, M., Dai, S.-Y., Rossbauer, S., Huang, Z., Binik, L., et al. (2013). BPTs: thiophene-flanked benzodipyrrolidone conjugated polymers for ambipolar organic transistors. *Chem. Commun.* 49, 4465–4467. doi: 10.1039/c3cc40811f

Shi, D. D., Liu, Z. T., Ma, J., Zhao, Z. Y., Tan, L. X., Lin, G. B., et al. (2020). Half-fused diketopyrrolopyrrole-based conjugated donor-acceptor polymer for ambipolar field-e?ect transistors. *Adv. Funct. Mater.* 30:1910235. doi: 10.1002/adfm.201910235

Sonar, P., Foong, T. R. B., Singh, S. P., Li, Y. N., and Dodabalapur, A. (2012). A furan-containing conjugated polymer for high mobility ambipolar organic thin film transistors. *Chem. Commun.* 48, 8383–8385. doi: 10.1039/c2cc33093h

Welterlich, I., Charov, O., and Tieke, B. (2012). Deeply colored polymers containing 1,3,4,6-tetraarylpyrrolo[3,2-b]pyrrole-2,5-dione (IsoDPP) units in the main chain. *Macromolecules* 45, 4511–4519. doi: 10.1021/ma300483u

Yao, J. J., Yu, C. M., Liu, Z. T., Luo, H. W., Yang, Y., Zhang, G. X., et al. (2015). Significant improvement of semiconducting performance of the diketopyrrolopyrrole-quaterthiophene conjugated polymer through side-chain engineering *via* hydrogen-bonding. *J. Am. Chem. Soc.* 138, 173–185. doi: 10.1021/jacs.5b09737

Zhang, H.C., Welterlich, I., Neudoerfl, J.-M., Tieke, B., Yang, C., Chen, X., et al. (2013). Synthesisandcharacterization of 1,3,4,6-tetraarylpyrrolo[3,2-b]-pyrrole-2,5-dione (isoDPP)-based donor-acceptor polymers with low band gap. *Polym. Chem.* 4, 4682–4689. doi: 10.1039/c3py00570d

Zhang, H. C., Deng, R. N., Wang, J., Li, X., Chen, Y.-M., Liu, K. W., et al. (2017a). Crystalline organic pigment-based field-effect transistors. *ACS Appl. Mater. Interfaces.* 9, 21891–21899. doi: 10.1021/acsami.7b03170

Zhang, H. C., Li, R., Deng, Z. F., Cui, S. W., Wang, Y. H., and Zheng, M. M. (2020). π-conjugated oligomers based on aminobenzodifuranone and diketopyrrolopyrrole. *Dyes Pigments.* 181:108552. doi: 10.1016/j.dyepig.2020.108552

Zhang, H. C., Liu, M., Yang, W. J., Judin, L., Hukka, T., Priimagi, A., et al. (2019). Thionation enhances the performance of polymeric dopant-free hole-transporting materials for perovskite solar cells. *Adv. Mater. Interfaces.* 20:1901036. doi: 10.1002/admi.201901036

Zhang, H. C., Yang, K., Zhang, K., Zhang, Z. Z., Sun, Q. K., and Yang, W. J. (2018). Thionating iso-diketopyrrolopyrrole-based polymers: From p-type to ambipolar field effect transistors with enhanced charge mobility. *Polym. Chem.* 9, 1807–1814. doi: 10.1039/C8PY00292D

Zhang, H. C., Zhang, S., Mao, Y. F., Liu, K. W., Chen, Y.-M., Jiang, Z., et al. (2017b). Naphthodipyrrolidone (NDP) based conjugated polymers with high electron mobility and ambipolar transport properties. *Polym. Chem.* 8, 3255–3260. doi: 10.1039/C7PY00616K

Zhang, W. F., Zheng, N. H., Wei, C. Y., Huang, J. Y., Gao, D., Shi, K., et al. (2016). Vinylidenedithiophenmethyleneoxindole: a centrosymmetric building block for donor-acceptor

copolymers. *Polym. Chem.* 7, 1413–1421. doi: 10.1039/C5PY01500F

Zhao, C. W., Guo, Y. T., Zhang, Y. F., Yan, N. F., You, S. Y., and Li, W. W. (2019). Diketopyrrolopyrrole-based conjugated materials for non-fullerene organic solar cells. *J. Mater. Chem. A* 7, 10174–. doi: 10.1039/C9TA01976F

Zhao, N., Ai, N., Cai, M., Wang, X., Pei, J., and Wan, X. X. (2016). Thiophene-fused isoindigo based conjugated polymers for ambipolar organic field-effect transistors. *Polym. Chem.* 7, 235–243. doi: 10.1039/C5PY01488C

Zoombelt, A. P., Mathijssen, S. G. J., Turbiez, M. G. R., Wienk, M. M., and Janssen, R. A. J. (2010). Small band gap polymers based on diketopyrrolopyrrole. *J. Mater. Chem.* 20, 2240–2247. doi: 10.1039/b919066j

Conflict of Interest: JL and MZ who were employed by company Qingdao Haiwan Science and Technology Industry Research Institute Co., Ltd.

The remaining authors declare that the research was conducted in the absence of any commercial or financial relationships that could be construed as a potential conflict of interest.

frontiers in Chemistry

ORIGINAL RESEARCH
published: 12 May 2021
doi: 10.3389/fchem.2021.681994

Truxene Functionalized Star-Shaped Non-fullerene Acceptor With Selenium-Annulated Perylene Diimides for Efficient Organic Solar Cells

Kaiwen Lin[1,2]*, *Boming Xie*[2], *Zhenfeng Wang*[2], *Qingwu Yin*[2], *Yuehui Wang*[1], *Chunhui Duan*[2]*, *Fei Huang*[2]* and *Yong Cao*[2]

[1] Department of Materials and Food, Zhongshan Institute, University of Electronic Science and Technology of China, Zhongshan, China, [2] State Key Laboratory of Luminescent Materials and Devices, Institute of Polymer Optoelectronic Materials and Devices, South China University of Technology, Guangzhou, China

OPEN ACCESS

Edited by:
Haichang Zhang,
Qingdao University of Science and Technology, China

Reviewed by:
Shuai Chen,
Jiangxi Science and Technology Normal University, China
Ming Wang,
Donghua University, China

***Correspondence:**
Kaiwen Lin
kevinlin1990@163.com
Chunhui Duan
duanchunhui@scut.edu.cn
Fei Huang
msfhuang@scut.edu.cn

Specialty section:
This article was submitted to Organic Chemistry, a section of the journal Frontiers in Chemistry

Received: *17 March 2021*
Accepted: *01 April 2021*
Published: *12 May 2021*

Citation:
Lin K, Xie B, Wang Z, Yin Q, Wang Y, Duan C, Huang F and Cao Y (2021) Truxene Functionalized Star-Shaped Non-fullerene Acceptor With Selenium-Annulated Perylene Diimides for Efficient Organic Solar Cells. Front. Chem. 9:681994. doi: 10.3389/fchem.2021.681994

An electron acceptor with a truxene core and ring-fusion perylene diimide (PDI) tripolymer annulated by selenium (Se) branch, named as FTr-3PDI-Se, is designed and synthesized. FTr-3PDI-Se exhibits large conjugated planar conformation, strong absorption spectra in the regions of 300–400 and 450–550 nm, the deep HOMO energy level of 6.10 eV, and high decomposition temperature above 400°C. The FTr-3PDI-Se: PBDB-T-2Cl based device achieved a disappointing power conversion efficiency (PCE) of 1.6% together with a high V_{OC} of 1.12 V. The low PCE was due to the large aggregates of blend film, the imbalanced hole/electron transport and low PL quenching efficiencies. The high V_{OC} can be attributed to the high-lying LUMO level of FTr-3PDI-Se and the low-lying HOMO level of PBDB-T-2Cl. Our research presents an interesting and effective molecule-designing method to develop non-fullerene acceptor.

Keywords: organic solar cells, non-fullerene acceptor, truxene, perylene diimides, selenium

INTRODUCTION

Organic solar cells (OSCs) have attracted boundless interest over the past few decades owing to the advantages of light weight, low cost, wide source, and large-scale roll-to-roll printing process (Kang et al., 2016; Hou et al., 2018). Recently, the fullerene acceptors, due to their numerous of disadvantages of weak absorption, limited structural modifications and electronic energy levels non-tunability, were marginalized by non-fullerene acceptors (NFAs) (Cheng et al., 2018; Yan et al., 2018). Significant progress in NFAs-based OSCs has been achieved with power conversion efficiency (PCE) over 18% (Lin et al., 2020; Liu Q. et al., 2020; Zhan et al., 2021). Among the widely reported NFAs, fused-ring electron acceptors (FREAs) and perylene diimide derivatives (PDIs) are the two main study directions.

Because of the strong electron affinity, high absorption coefficient and electron mobility, as well as energy-level tunability, PDIs are widely developed (Zhan et al., 2011; Li and Wonneberger, 2012; Liu et al., 2016; Sun et al., 2016; Feng et al., 2018; Agnieszka and Frank, 2019; Li M. Y. et al., 2020). The large conjugated skeleton of PDI exhibits strong aggregation tendency, which may result in self-trapping of light excitons and afterwards generate fast bimolecular recombination of charge

carriers, limiting the high performance of OSCs (Sharenko et al., 2013; Liu S. Y. et al., 2015). The researcher verified that changing the planarity of the PDIs is the popular methods to avoid this strong aggregation (Zhong et al., 2014, 2016; Lin et al., 2016; Zhang et al., 2016; Duan et al., 2017a; Liu X. et al., 2017; Liu et al., 2018). For example, various 3D electron acceptors with the central aromatic core (atom) and twisted PDI trimers or tetramer were investigated (Liu Y. H. et al., 2015; Lee et al., 2016; Zhan et al., 2017; Zhang A. D. et al., 2017; Lin et al., 2018a; Liu W. X. et al., 2020). A twisted configuration of PDIs is confirmed effectively to avoid large aggregation. However, the single bonding connection between central core and PDIs would weaken charge mobility due to an excessive twist geometry, giving a low OSCs performance. Therefore, the proper twisted non-planar structures, i.e., good balance of desirable film morphology with proper domain size and sufficient charge transport ability seems to be the key point for developing high-performance PDI electron acceptors (Lin et al., 2018a).

Interestingly, oxidative ring-fusion between the central aromatic core and the PDI branches was verified to be an effective strategy to achieve an exquisite balance aforesaid for high OSCs performance (Hartnett et al., 2016; Meng et al., 2016a, 2017; Zhong et al., 2016; Wang et al., 2017; Zhang J. Q. et al., 2017; Lin et al., 2018a; Chen et al., 2020). The fused PDI NFAs all exhibited better planarity than non-fused counterparts, since the aromatic core and PDI branches were locked by the adjacent benzene. Meanwhile, the fused PDI NFAs showed stronger intermolecular π-π stacking and higher electron mobility (Lin et al., 2018a). Moreover, these fused PDI NFAs generated proper phase separation with proper domain size and high domain purity when blended with donors (Chen et al., 2018; Hu et al., 2018; Wu et al., 2019). Therefore, the fused PDI NFAs displayed better OSCs properties compared with unfused ones (Li et al., 2016; Meng et al., 2016a, 2017; Liu X. F. et al., 2017; Wang et al., 2017; Zhang J. Q. et al., 2017; Lin et al., 2018a; Yin et al., 2019; Carlotti et al., 2020).

Recently, several studies showed that five-membered heteroatom-annulated (nitrogen/chalcogen-fused in bay regions) of PDIs has been regarded as the most effective molecular design strategy to achieve high performance OSCs (Sun et al., 2015; Meng et al., 2016a; Cann et al., 2017). The five-membered heteroatom-annulated PDI NFAs reinforced intra- and intermolecular interactions, leading to high electron mobility, which achieved improved PCEs. Among the varied nitrogen/chalcogen, the selenium atom (Se), since its enormous and loose electron cloud, is much easier to realize orbital overlap between the adjacent PDI NFAs, afterwards enhance the charge carrier mobility (Meng et al., 2016b; Li et al.,

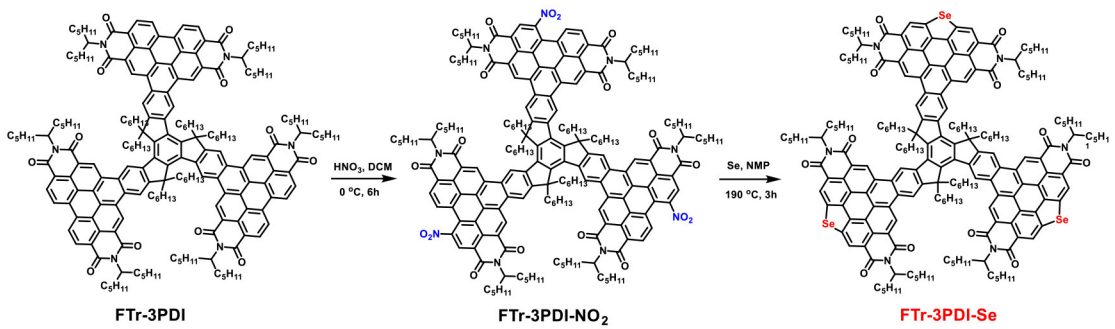

SCHEME 1 | Chemical structure and synthetic routes of FTr-3PDI-Se.

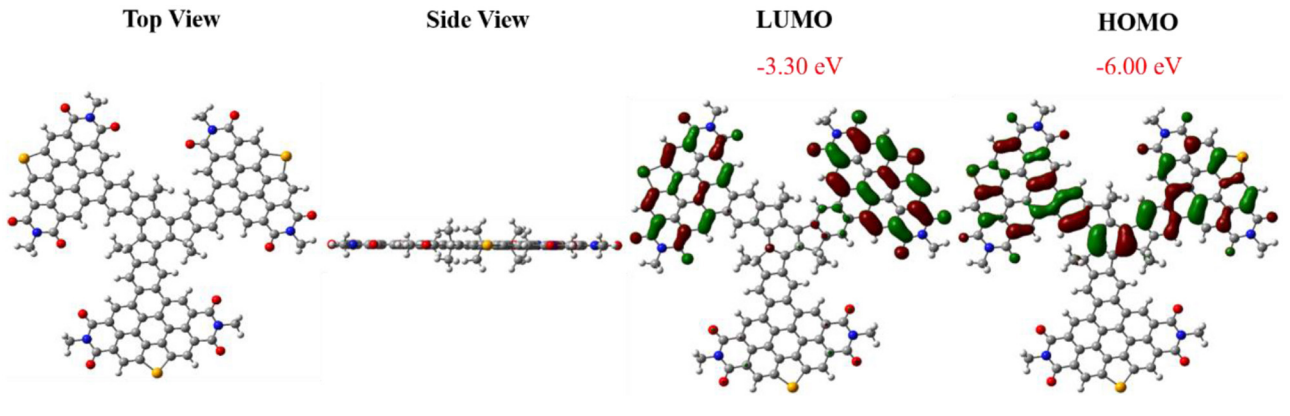

FIGURE 1 | Views of the optimized geometries of FTr-3PDI-Se, and the LUMO/HOMO electron distribution obtained using DFT calculations at the B3LYP/6-31G(d) level.

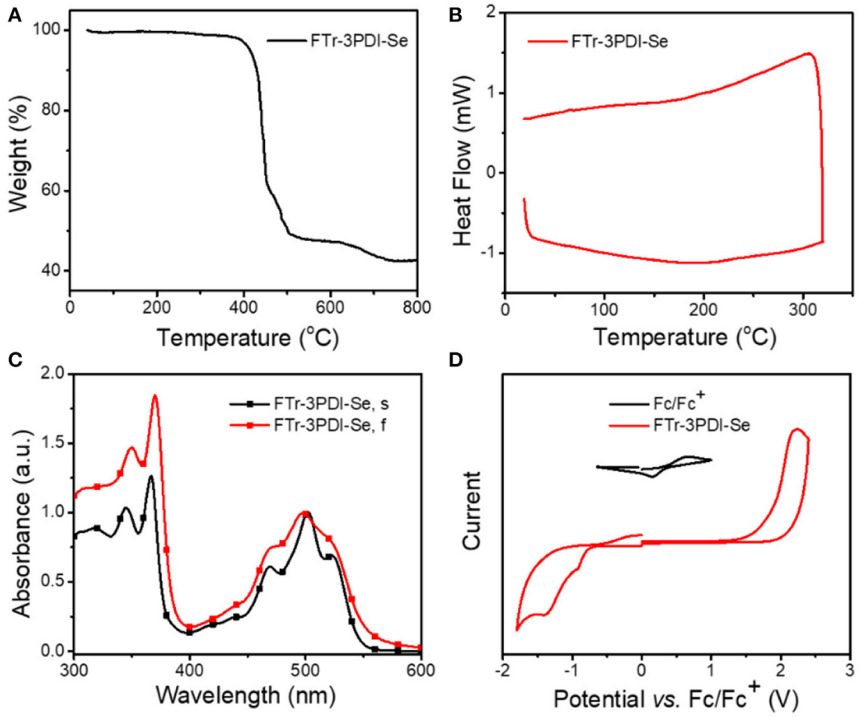

FIGURE 2 | (A) TGA of FTr-3PDI-Se; **(B)** DSC of FTr-3PDI-Se; **(C)** normalized UV–vis absorption spectra of FTr-3PDI-Se in $CHCl_3$ solution (FTr-3PDI-Se, s) and in film (FTr-3PDI-Se, f); **(D)** CV curves of FTr-3PDI-Se.

2018; Luo et al., 2018; Li G. et al., 2020; Yang et al., 2020). Moreover, due to the natural easy-polarizing characteristic of the Se atom, the Se-annulated PDIs exhibit the stronger intra- and intermolecular interactions, which also confirmed the important application foreground of Se-annulation PDIs in non-fullerene OSCs (Duan et al., 2017b; Yin et al., 2018; Li et al., 2019; Luo et al., 2019; Qureshi et al., 2020; Wang et al., 2020).

Truxene has been demonstrated as a promising skeleton to construct high performance NFAs (Nielsen et al., 2013, 2014; Lin et al., 2018b; Wu et al., 2018). Inspired by the above achievements of Se-annulated PDIs, herein, we report the design and synthesis of truxene functionalized star-shaped NFAs with fused selenium-annulated PDIs, named FTr-3PDI-Se (**Scheme 1**). The devices based on poly[(2,6-(4,8-bis(5-(2-ethylhexyl-3-chloro)thiophen-2-yl)-benzo[1,2-b:4,5-b']dithiophene))-alt-(5,5-(1',3'-di-2-thienyl-5',7'-bis(2-ethylhexyl)benzo[1',2'-c:4',5'-c']dithiophene-4,8-dione)] (PBDB-T-2Cl): FTr-3PDI-Se exhibited a PCE of 1.6% with a high open-circuit voltage (V_{oc}) of 1.12 V. The FTr-3PDI-Se exhibited large conjugated planar skeleton that can effectively promote the blend films to form large aggregates, which may lead to bimolecular recombination, limiting the OSCs performance.

RESULT AND DISCUSSION

Material Synthesis and Characterization

The synthetic routes of FTr-3PDI-Se was presented in **Scheme 1** and the detailed synthetic procedure was provided in the Supporting Information. Compounds FTr-3PDI was synthesized according to the reported method (Lin et al., 2018a). FTr-3PDI-NO_2 was prepared with a high yield of 95% using the fuming HNO_3. Finally, the three fused selenium-annulated PDIs branches based on truxene, FTr-3PDI-Se, was synthesized by reductive cyclization reaction with Se powder. The as-synthesized FTr-3PDI-NO_2 and FTr-3PDI-Se were fully characterized by ^{1}H NMR, ^{13}C NMR, and MALDI-TOF mass spectrometry (**Supplementary Figures 1–6**). Although large conjugated planar conformation, FTr-3PDI-Se electron acceptor displays moderate solubility in section of organic solvents such as chloroform, toluene, and chlorobenzene at room temperature. We ascribe it to the six hexyl chains of the truxene core.

Theoretical Calculations

The geometry and electron distribution of FTr-3PDI-Se was presented by employing the density functional theory (DFT) method at the B3LYP/6-31G(d,p) level in the Gaussian 09 software, where the long alkyl chain (–C_6H_{13} of the truxene core and –C_5H_{11} of the PDIs branches) was simplified to methyl groups (**Figure 1**). Obviously, FTr-3PDI-Se exhibits an overall planarity structure from the top view and side view. According to the optimized geometry, the highest occupied molecular orbital (HOMO) and lowest unoccupied molecular orbital (LUMO) electron distribution were calculated. The LUMO is distributed on two fused selenium-annulated PDIs sub-group. The HOMO is localized on one two fused selenium-annulated PDIs and truxene. The different wave function distributions between HOMO and LUMO are attributed to the degenerate orbital/multiple

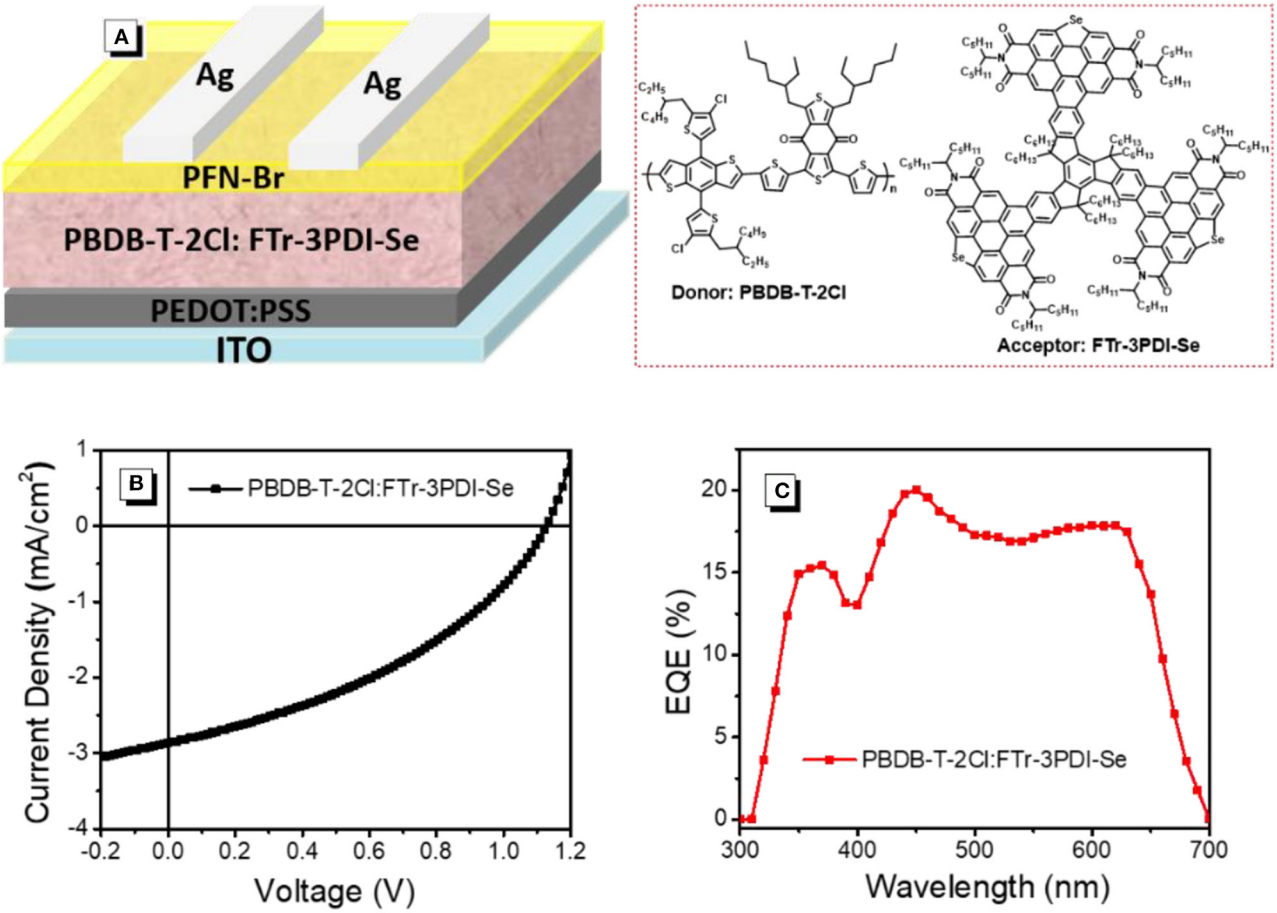

FIGURE 3 | (A) The device structure; **(B)** current densityevoltage (*J-V*) characteristics; **(C)** external quantum efficiency (EQE) spectra of PBDB-T-2Cl: FTr-3PDI-Se solar cells.

resonance configurations of the three fused selenium-annulated PDI groups. Furthermore, the calculated LUMO and HOMO levels were −3.30 and −6.00 eV.

Thermodynamic, Optical, and Electrochemical Properties

Thermogravimetric analysis (TGA) measurement (**Figure 2A**) demonstrated that FTr-3PDI-Se showed outstanding thermal stability along with a high decomposition temperature (T_d, 5%weight loss) exceeding 400°C under nitrogen atmosphere, benefiting from large conjugated planar conformation. Afterwards, differential scanning calorimetry (DSC) was performed without obvious endo- and exothermal peaks from room temperature to 320°C in the second heating cycle (**Figure 2B**). The spectrum of FTr-3PDI-Se in chloroform solution showed two sets of absorption bands in the range of 300–600 nm. The short wavelength region displayed a maximal sharp peak of 360 nm with two broad shoulder peak, while the longer wavelength region exhibited the maximal peak of 500 nm with two broad shoulder peak as well (**Figure 2C**). FTr-3PDI-Se in thin film showed similar absorption spectra outline to their solution ones, indicating that the intermolecular aggregation is effective suppressed. Meanwhile, FTr-3PDI-Se demonstrated a slightly large optical bandgap of 2.24 eV with optical absorption onsets 555 nm ($E_g^{opt} = 1240/\lambda_{onset}$ eV). The absorption profiles of FTr-3PDI-Se is complementary to the strong absorption of PDBT-T-2Cl donor, which was exhibited in **Supplementary Figure 7**. The electrochemical property of FTr-3PDI-Se in chloroform solution was investigated by CV, as shown in **Figure 2D**. The half-wave potential of Fc/Fc^+ was measured to be 0.40 V, and the energy levels of HOMO and LUMO were estimated from the onset oxidation (E_{ox}^{onset}) and reduction (E_{red}^{onset}) potentials by equations: $E_{HOMO} = -e(E_{ox}^{onset} - E_{Fc/Fc+} + 4.8)$ and $E_{LUMO} = -e(E_{red}^{onset} - E_{Fc/Fc+} + 4.8)$, respectively (Li et al., 1999). The HOMO/LUMO levels are −6.10/−3.65 eV. The slightly high-lying LUMO level cooperate with low-lying HOMO level of donor will contribute to achieve a high V_{oc}. Meanwhile, the down-shifted HOMO level maintain the excellent chemical durability, and is favorable for hole transfer from excited acceptor to donor in OSCs (Duan et al., 2016, 2017b; 2018; Jia et al. 2017).

Photovoltaic Properties

The OSCs devices were prepared and measured with a conventional device structure of ITO (indiumtin oxide)/PEDOT:PSS (poly(3,4-ethylenedioxythiophene):poly (styrenesulfonate))/PBDB-T-2Cl: FTr-3PDI-Se/PFN-Br (poly[(9,9-bis(3'-((N,N-dimethyl)-N-ethylammonium)-propyl)-2,7-fluorene)-alt-2,7-(9,9-dioctylfluorene)])/Ag (**Figure 3A**). PDBT-T-2Cl was picked as the medium-bandgap donor to matched FTr-3PDI-Se acceptor benefiting from their complementary absorption and appropriate energy levels. The devices were fabricated and evaluated in terms of donor/acceptor weight ratios, solvent additives, and thermal annealing. All the device parameters under the mentioned above conditions are listed in **Supplementary Tables 1–3**. The optimal devices fabrication is that chlorobenzene as the main processing solvent with 1% chloronaphthalene solvent additives, and the annealing temperature is 120°C. The total concentration of PDBT-T-2Cl and FTr-3PDI-Se was optimized to be 20 mg mL^{-1} with the donor:acceptor weight ratio of 1.5:1. The optimized device parameters are summarized in **Table 1**, and the corresponding *J–V* curves are shown in **Figure 3B**. The optimized OSC device based on PBDB-T-2Cl: FTr-3PDI-Se exhibited a PCE of 1.6% with a high V_{oc} of 1.12 V, but a relatively poor short-circuit current density (J_{sc}) of 3.6 mA cm^{-2} and a fill factor (FF) of 38.9%. The high V_{oc} is consistent with the high-lying LUMO level of FTr-3PDI-Se and low-lying HOMO level of PDBT-T-2Cl.

The external quantum efficiency (EQE) spectra of PBDB-T-2Cl: FTr-3PDI-Se films were collected from the above optimized devices and displayed in **Figure 3C**. The calculated J_{sc} of 3.5 mA cm^{-2} from the EQE spectra was consistent with the measured J_{sc} (**Table 1**). The continuous EQE responses between 300 and 700 nm for the PBDB-T-2Cl: FTr-3PDI-Se based device results from the complementary absorption of PBDB-T-2Cl: FTr-3PDI-Se blend film (**Supplementary Figure**).

TABLE 1 | Photovoltaic parameters of OSCs based on PBDB-T-2Cl: FTr-3PDI-Se under AM1.5G illumination at 100 mW cm^{-2}.

Acceptor devices	V_{oc} (V)	J_{sc} (mA cm^{-2})	J^{a}_{cal} (mA cm^{-2})	FF	PCE (%)
PBDB-T-2Cl: FTr-3PDI-Se	1.12	3.6	3.5	0.39	1.6

[a] *Calculated from EQE intetrations.*

Charge Transport and Recombination

The charge transport were acquired by single-carrier devices with a device structure of ITO/ZnO/PBDB-T-2Cl: FTr-3PDI-Se/Ca/Al for electron only devices and ITO/PEDOT:PSS/PBDB-T-2Cl: FTr-3PDI-Se/MoO_3/Ag for hole only devices, respectively (**Supplementary Figure 8**). The hole mobilities (μ_h) of PBDB-T-2Cl: FTr-3PDI-Se blend film was estimated to be 4.5×10^{-6} cm^2 V^{-1} s^{-1}. In contrast, the electron mobility (μ_e) was measured to be 2.2×10^{-4} cm^2 V^{-1} s^{-1}, which are two orders of magnitude higher than μ_h. The low hole mobility and highly imbalanced μ_e/μ_h seriously suppress the charge transport and give rise to more bimolecular recombination, which in turn acquire low FF and J_{sc}.

The photoluminescence (PL) quenching experiments were proceeded to study the charge transfer efficiency. As shown in **Supplementary Figure 9**, the PL quenching efficiencies of PBDB-T-2Cl: FTr-3PDI-Se blend films are 83.3 and 47.7% as compared to the neat PBDB-T-2Cl and FTr-3PDI-Se films, respectively, suggesting a moderate exciton dissociation efficiency.

Morphology

The surface morphology of PBDB-T-2Cl: FTr-3PDI-Se blend films were investigated using atomic force microscopy (AFM). The film exhibited obvious phase separation with nanofibrillar structures (**Figure 4**), forming a relative coarse surface with a RMS surface roughness of 3.97 nm. The large planar conformation of FTr-3PDI-Se, can effectively promote the blend films to form large aggregates.

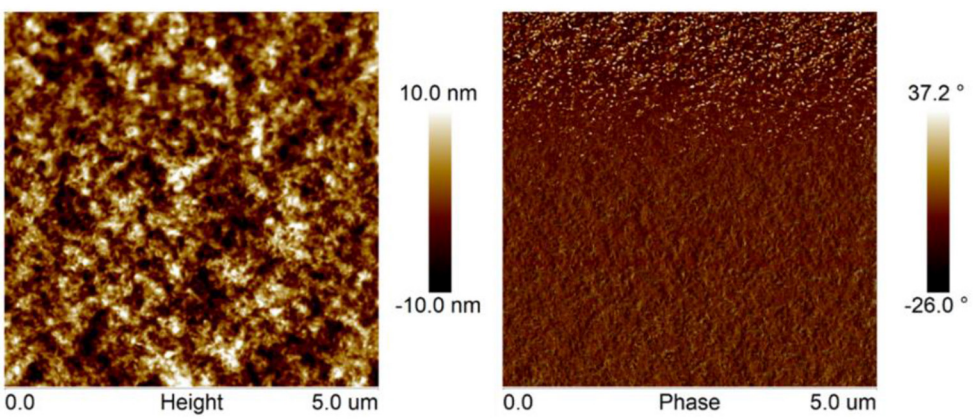

FIGURE 4 | AFM height and phase images of PBDB-T-2Cl: FTr-3PDI-Se blend films.

CONCLUSION

In summary, FTr-3PDI-Se was synthesized and employed as electron acceptors for organic solar cells. The optimized devices based on PBDB-T-2Cl: FTr-3PDI-Se displayed a PCE of 1.6%, which was attributed to the following reasons. The conjugated planar conformation of FTr-3PDI-Se, verified by the DFT quantum calculation, can effectively promote the blend films to form large aggregates, which impeded the charge transport. Meanwhile, the imbalanced hole/electron transport and low PL quenching efficiencies seriously obstruct the charge transport and reduce exciton dissociation efficiency. Obviously, this research missed the balance between the highly twisted non-planar structures and coplanar conformation. Taking the excellent advantages into consideration and discard the disadvantages, we expect that the combination of the fused selenium-annulated PDIs with other conformation cores will create more promising and practical acceptors.

DATA AVAILABILITY STATEMENT

The original contributions presented in the study are included in the article/**Supplementary Material**, further inquiries can be directed to the corresponding authors.

AUTHOR CONTRIBUTIONS

KL and FH: designed experiments. KL, QY, ZW, BX, and YW: carried out experiments. KL, YC, and CD: analyzed experimental results. KL and CD: wrote the manuscript. All authors contributed to the article and approved the submitted version.

FUNDING

We are grateful to the Guangdong Innovative and Entrepreneurial Research Team Program (2019ZT08L075), Guangdong Flexible Electronic Materials and Devices Innovative Team, Guangdong Province Colleges and Universities Young Innovative Talents Project (2019KQNCX190, 2019KTSCX210), and Ph.D. Early Development Program of University of Electronic Science and Technology of China Zhongshan Institute (419YKQN16) for their financial support of this study.

SUPPLEMENTARY MATERIAL

The Supplementary Material for this article can be found online at: https://www.frontiersin.org/articles/10.3389/fchem.2021.681994/full#supplementary-material

REFERENCES

Agnieszka, N. K., and Frank, W. (2019). Progress in the synthesis of perylene bisimide dyes. *Org. Chem. Front*. 6, 1272–1318. doi: 10.1039/C8QO01368C

Cann, J., Dayneko, S., Sun, J.-P., Hendsbee, A. D., Hill, I. G., and Welch, G. C. (2017). N-Annulated perylene diimide dimers: acetylene linkers as a strategy for controlling structural conformation and the impact on physical, electronic, optical, and photovoltaic properties. *J. Mater. Chem. C* 5, 2074–2083. doi: 10.1039/C6TC05107C

Carlotti, B., Madu, I. K., Kim, H., Cai, Z. X., Jiang, H. J., Muthike, A. K., et al. (2020). Activating intramolecular singlet exciton fission by altering p-bridge flexibility in perylene diimide trimers for organic solar cells. *Chem. Sci*. 11, 8757–8770. doi: 10.1039/D0SC03271A

Chen, F., Ding, G. D., Tang, A. L., Xiao, B., Li, J. F., and Zhou, E. J. (2018). A perylenediimide dimer containing an asymmetric p-bridge and its fused derivative for fullerene-free organic solar cells. *J. Mater. Chem. C* 6, 2580–2587. doi: 10.1039/C8TC00089A

Chen, H. Q., Wang, L., Sun, H., Liu, Q., Tan, X., Sang, S. L., et al. (2020). PDI-based heteroacenes as acceptors for fullerene-free solar cells: importance of their twisted geometry. *New J. Chem*. 44, 13093–13099. doi: 10.1039/D0NJ01733G

Cheng, P., Li, G., Zhan, X. W., and Yang, Y. (2018). Next-generation organic photovoltaics based on non-fullerene acceptors. *Nat. Photon*. 12, 131–142. doi: 10.1038/s41566-018-0104-9

Duan, C.H., Willems, R. E. M., Franeker, J. J., Bruijnaers, B. J., Wienk. M. M., and Janssen. R. A. J. (2016). Effect of side chain length on the charge transport, morphology, and photovoltaic performance of conjugated polymers in bulk heterojunction solar cells. *J. Mater. Chem*. A, 4, 1855–1866. doi: 10.1039/c5ta09483f

Duan, C. H., Guzám, D., Colberts, F. J. M., Janssen, R. A. J., and Torres, T. (2018). Subnaphthalocyanines as electron acceptors in polymer solar cells: improving device performance by modifying peripheral and axial substituents. *Chem. Eur. J*. 24, 1–6. doi: 10.1002/chem.201800596

Duan, Y. W., Xu, X. P., Li, Y., Li, Z. J., and Peng, Q. (2017b). Chalcogen-atom-annulated perylene diimide trimers for highly efficient nonfullerene polymer solar cells. *Macromol. Rapid Commun*. 38:1700405. doi: 10.1002/marc.201700405

Duan, Y. W., Xu, X. P., Yan, H., Wu, W. L., Li, Z. J., and Peng, Q. (2017a). Pronounced effects of a triazine core on photovoltaic performance-efficient organic solar cells enabled by a PDI trimer-based small molecular acceptor. *Adv. Mater*. 29:1605115. doi: 10.1002/adma.201605115

Feng, J. J., Jiang, W., and Wang, Z. H. (2018). Synthesis and application of rylene imide dyes as organic semiconducting materials. *Chem. Asian J*. 13, 20–30. doi: 10.1002/asia.201701424

Hartnett, P. E., Matte, H. S. S. R., Eastham, N. D., Jackson, N. E., Wasielewski, M. R., Marks, T. J., et al. (2016). Ring-fusion as a perylenediimide dimer design concept for high-performance non-fullerene organic photovoltaic acceptors. *Chem. Sci*. 7, 3543–3555. doi: 10.1039/C5SC04956C

Hou, J. H., Inganäs, O., Friend, R. H., and Gao, F. (2018). Organic solar cells based on non-fullerene acceptors. *Nat. Mater*. 17, 119–128. doi: 10.1038/nmat5063

Hu, H. W., Li, Y. K., Zhang, J. Q., Peng, Z. X., Ma, L., Xin, J. M., et al. (2018). Effect of ring-fusion on miscibility and domain purity: key factors determining the performance of PDI-based nonfullerene organic solar cells. *Adv. Energy Mater*. 8:1800234. doi: 10.1002/aenm.201800234

Jia, J. C., Zheng, N. N., Wang, Z. F., Huang, Y. P., Duan, C. H., Huang, F., et al. (2017). The effect of endcapping groups in A-D-A type non-fullerene acceptors on device performance of organic solar cells. *Sci. China Chem*. 60, 1458–1467. doi: 10.1007/s11426-017-9102-1

Kang, H., Kim, G., Kim, J., Kwon, S., Kim, H., and Lee, K. (2016). Bulk-heterojunction organic solar cells: five core technologies for their commercialization. *Adv. Mater*. 28, 7821–7861. doi: 10.1002/adma.201601197

Lee, J., Singh, R., Sin, D. H., Kim, H. G., Song, K. C., and Cho, K. (2016). A nonfullerene small molecule acceptor with 3D interlocking geometry enabling efficient organic solar cells. *Adv. Mater*. 28, 69–76. doi: 10.1002/adma.201504010

Li, C., and Wonneberger, H. (2012). Perylene imides for organic photovoltaics: yesterday, today, and tomorrow. *Adv. Mater*. 24, 613–636. doi: 10.1002/adma.201104447

Li, G., Wang, S. H., Li, D. D., Liu, T., Yan, H., Tang, B., et al. (2020). Chalcogen-fused perylene diimides-based nonfullerene acceptors for high-performance

organic solar cells: insight into the effect of O, S, and Se. *Sol. RRL* 4:1900453. doi: 10.1002/solr.201900453

Li, G., Wang, S. H., Liu, T., Hao, P., Liu, Z. H., et al. (2018). Non-fullerene acceptor engineering with threedimensional thiophene/selenophene-annulated perylene diimides for high performance polymer solar cells. *J. Mater. Chem. C* 6, 12601–12607. doi: 10.1039/C8TC04926B

Li, G., Yang, S. F., Liu, T., Li, J. W., Yang, W. B., Luo, Z. H., et al. (2019). Functionalizing tetraphenylpyrazine with perylene diimides (PDIs) as high-performance nonfullerene acceptors. *J. Mater. Chem. C* 7, 14563–14570. doi: 10.1039/C9TC05643B

Li, M. Y., Yin, H., and Sun, G. Y. (2020). PDI derivatives with functional active position as non-fullerene small molecule acceptors in organic solar cells: from different core linker to various conformation. *Appl. Mater. Today* 21:100799. doi: 10.1016/j.apmt.2020.100799

Li, S. X., Liu, W. Q., Li, C. Z., Liu, F., Chen, H. Z., Russelld, T. P., et al. (2016). A simple perylene diimide derivative with a highly twisted geometry as an electron acceptor for efficient organic solar cells. *J. Mater. Chem. A* 4, 10659–10665. doi: 10.1039/c6ta04232e

Li, Y. F., Cao, Y., Gao, J., Wang, D. L., Yu, G., Heeger, A. J. (1999). Electrochemical properties of luminescent polymers and polymer light-emitting electrochemical cells. *Synth. Met.* 99, 243–248. doi: 10.1016/S0379-6779(99)00007-7

Lin, H. R., Chen, S. S., Hu, H. W., Zhang, L., Ma, T. X., and Yan, H. (2016). Reduced intramolecular twisting improves the performance of 3D molecular acceptors in non-fullerene organic solar cells. *Adv. Mater.* 28, 8546–8551. doi: 10.1002/adma.201600997

Lin, K. W., Wang, S. L., Wang, Z. F., Yin, Q. W., Liu, X., Jia, J. C., et al. (2018a). Electron acceptors with a truxene core and perylene diimide branches for organic solar cells: the effect of ring-fusion. *Front. Chem.* 6:328. doi: 10.3389/fchem.2018.00328

Lin, K. W., Xie, B. M., Wang, Z. F., Duan, C. H., Huang, F., Cao, Y., et al. (2018b). Star-shaped electron acceptors containing a truxene core for non-fullerene solar cells. *Org. Electron.* 52, 42–50. doi: 10.1016/j.orgel.2017.10.009

Lin, Y., Nugraha, M., Firdaus, Y., Scaccabarozzi, A., Anies, F., Emwas, A., et al. (2020). A simple n-dopant derived from diquat boosts the efficiency of organic solar cells to 18.3%. *ACS Energy Lett.* 5, 3663–3671. doi: 10.1021/acsenergylett.0c01949

Liu, Q., Jiang, Y., Jin, K., Qin, J., Xu, J., Li, W., et al. (2020). 18% Efficiency organic solar cells. *Sci. Bull.* 65, 272–275. doi: 10.1016/j.scib.2020.01.001

Liu, S. Y., Wu, C. H., Li, C. Z., Liu, S. Q., Wei, K. H., Chen, H. Z., et al. (2015). A tetraperylene diimides based 3D nonfullerene acceptor for efficient organic photovoltaics. *Adv. Sci.* 2015, 2:1500014. doi: 10.1002/advs.201500014

Liu, W. X., Zhang, C. E., Liu, J. C., and Bo, Z. S. (2020). PDI-based hexapod-shaped nonfullerene acceptors for the high-performance as-cast organic solar cells. *ACS Appl. Mater. Interfaces* 12, 37409–37417. doi: 10.1021/acsami.0c11159

Liu, X., Liu, T., Duan, C. H., Sun, Y. M., Huang, F., Cao, Y., et al. (2017). Non-planar perylenediimide acceptors with different geometrical linker units for efficient nonfullerene organic solar cells. *J. Mater. Chem. A* 5, 1713–1723. doi: 10.1039/C6TA08739F

Liu, X. F., Cai, Y. H., Huang, X. B., Zhang, R. B., and Sun, X. B. (2017). A perylene diimide electron acceptor with a triptycene core for organic solar cells. *J. Mater. Chem. C* 5, 3188–3194. doi: 10.1039/C7TC00378A

Liu, Y. H., Mu, C., Jiang, K., Zhao, J. B., Li, Y. K., Yan, H., et al. (2015). A tetraphenylethylene core-based 3D structure small molecular acceptor enabling efficient non-fullerene organic solar cells. *Adv. Mater.* 27, 1015–1020. doi: 10.1002/adma.201404152

Liu, Z. T., Wu, Y., Zhang, Q., and Gao, X. (2016). Non-fullerene small molecule acceptors based on perylene diimides. *J. Mater. Chem. A* 4, 17604–17622. doi: 10.1039/C6TA06978A

Liu, Z. T., Zhang, L. H., Shao, M., Wu, Y., Zeng, D., Gao, X., et al. (2018). Fine-tuning the quasi-3D geometry: enabling efficient nonfullerene organic solar cells based on perylene diimides. *ACS Appl. Mater. Interfaces* 10, 762–768. doi: 10.1021/acsami.7b16406

Luo, Z. H., Liu, T., Chen, Z. X., Xiao, Y. Q., Yang, C. L., et al. (2019). Isomerization of perylene diimide based acceptors enabling high-performance nonfullerene organic solar cells with excellent fill factor. *Adv. Sci.* 6:1802065. doi: 10.1002/advs.201802065

Luo, Z. H., Liu, T., Cheng, W. L., Wu, K. L., Xie, D. J., Yang, C. L., et al. (2018). A three-dimensional thiophene-annulated perylene bisimide as a fullerene-free acceptor for a high performance polymer solar cell with the highest PCE of 8.28% and a V_{OC} over 1.0 V. *J. Mater. Chem. C* 6, 1136–1142. doi: 10.1039/C7TC05261H

Meng, D., Fu, H. T., Fan, B. B., Li, Y., Sun, Y. M., Wang, Z. H., et al. (2017). Rigid nonfullerene acceptors based on triptycene–perylene dye for organic solar cells. *Chem. Asian J.* 12, 1286–1290. doi: 10.1002/asia.201700440

Meng, D., Fu, H. T., Xiao, C. Y., Meng, X. Y., Sun, Y. M., Wang, Z. H., et al. (2016a). Three-bladed rylene propellers with three-dimensional network assembly for organic electronics. *J. Am. Chem. Soc.* 138, 10184–10190. doi: 10.1021/jacs.6b04368

Meng, D., Sun, D., Zhong, C. M., Sun, Y. M., Wang, Z. H. et al. (2016b). High-performance solution-processed non-fullerene organic solar cells based on selenophene-containing perylene bisimide acceptor. *J. Am. Chem. Soc.* 138, 375–380. doi: 10.1021/jacs.5b11149

Nielsen, C. B., Voroshazi, E., Holliday, S., Cnops, K., Cheyns, D., and McCulloch, I. (2014). Electron-deficient truxenone derivatives and their use in organic photovoltaics. *J. Mater. Chem. A* 2, 12348–12354. doi: 10.1039/C4TA01653J

Nielsen, C. B., Voroshazi, E., Holliday, S., Cnops, K., Randb, B. P., and McCulloch, I. (2013). Efficient truxenone-based acceptors for organic photovoltaics. *J. Mater. Chem. A* 1, 73–76. doi: 10.1039/C2TA00548D

Qureshi, M. B. A., Li, M., Wang, H., Song, J. S., and Bo, Z. S. (2020). Nonfullerene acceptors with an N-annulated perylene core and two perylene diimide units for efficient organic solar cells. *Dyes Pigments* 173:107970. doi: 10.1016/j.dyepig.2019.107970

Sharenko, A., Proctor, C. M., Poll, T. S. V., Henson, Z. B., Nguyen, T.-Q., and Bazan, G. C. (2013). A high-performing solution-processed small molecule: perylene diimide bulk heterojunction solar cell. *Adv. Mater.* 25, 4403–4406. doi: 10.1002/adma.201301167

Sun, D., Meng, D., Cai, Y. H., Huo, L. J., Sun, Y. M., Wang, Z. H., et al. (2015). Non-fullerene-acceptor-based bulk-heterojunction organic solar cells with efficiency over 7%. *J. Am. Chem. Soc.* 137, 11156–11162. doi: 10.1021/jacs.5b06414

Sun, M., Müllen, K., and Yin, M. Z. (2016). Water-soluble perylenediimides: design concepts and biological applications. *Chem. Soc. Rev.* 45, 1513–1528. doi: 10.1039/C5CS00754B

Wang, B., Liu, W. Q., Li, H. B., Mai, J. Q., Li, C. Z., Chen, H. Z., et al. (2017). Electron acceptors with varied linkages between perylene diimide and benzotrithiophene for efficient fullerene-free solar cells. *J. Mater. Chem. A* 5, 9396–9401. doi: 10.1039/C7TA02582C

Wang, K. K., Xia, P., Wang, K. W., You, X. X., Xia, J. L., et al. (2020). π-Extension, selenium incorporation, and trimerization: "three in one" for efficient perylene diimide oligomer-based organic solar cells. *ACS Appl. Mater. Interfaces* 12, 9528–9536. doi: 10.1021/acsami.9b21929

Wu, M. L., Yi, J.-P., Hu, J., Xia, P., Wang, H., Chen, F., et al. (2019). Ring fusion attenuates the device performance: star-shaped long helical perylene diimide based non-fullerene acceptors. *J. Mater. Chem. C* 7, 9564–9572. doi: 10.1039/C9TC02150G

Wu, W. L., Zhang, G. J., Xu, X. P., Wang, S. C., Li, Y., and Peng, Q. (2018). Wide bandgap molecular acceptors with a truxene core for efficient nonfullerene polymer solar cells: linkage position on molecular configuration and photovoltaic properties. *Adv. Funct. Mater.* 28:1707493. doi: 10.1002/adfm.201707493

Yan, C. Q., Barlow, S., Wang, Z. H., Yan, H., Jen, A. K.-Y., Marder,. S. R., et al. (2018). Non-fullerene acceptors for organic solar cells. *Nat. Rev. Mater.* 3:18003. doi: 10.1038/natrevmats.2018.3

Yang, J., Chen, F., Cong, P., Xiao, H. J., Geng, Y. F., et al. (2020). Tuning the optoelectronic properties of vinylene linked perylenediimide dimer by ring annulation at the inside or outside bay positions for fullerene-free organic solar cells. *J. Energy Chem.* 40, 112–119. doi: 10.1016/j.jechem.2019.03.007

Yin, Y. L., Song, J., Guo, F. Y., Sun, Y. M., Zhao, L. C., and Zhang, Y. (2018). Asymmetrical vs. symmetrical selenophene-annulated fused perylenediimide acceptors for efficient non-fullerene polymer solar cells. *ACS Appl. Energy Mater.* 1, 6577–6585. doi: 10.1021/acsaem.8b01484

Yin, Y. L., Zheng, Z., Chen, D. Y., Liu, M., Zhang, J., Guo, F. Y., et al. (2019). Fusion or non-fusion of quasi-two-dimensional fused perylene diimide acceptors: the importance of molecular geometry for fullerene-free organic solar cells. *J. Mater. Chem. A* 7, 27493–27502. doi: 10.1039/C9TA10174H

Zhan, L. L., Li, S. X., Xia, X. X., Li, Y. K., Lu, X. H., Zuo, L. J., et al. (2021). Layer-by-layer processed ternary organic photovoltaics with efficiency over 18%. *Adv. Mater*. 33:2007231. doi: 10.1002/adma.202007231

Zhan, X. J., Xiong, W. T., Gong, Y. B., Liu, T., Xie, Y. J., Peng, Q., et al. (2017). Pyrene-fused perylene diimides: new building blocks to construct non-fullerene acceptors with extremely high open-circuit voltages up to 1.26 V. *Sol. RRL* 1:1700123. doi: 10.1002/solr.201700123

Zhan, X. W., Facchetti, A., Barlow, S., Marks, T. J., Ratner, M. A., Wasielewski, M. R., et al. (2011). Rylene and related diimides for organic electronics. *Adv. Mater*. 23, 268–284. doi: 10.1002/adma.201001402

Zhang, A. D., Li, C., Yang, F., Zhang, J. Q., Wang, Z. H., Wei, Z. X., et al. (2017). An electron acceptor with porphyrin and perylene bisimides for efficient non-fullerene solar cells. *Angew. Chem. Int. Ed*. 56, 2694–2698. doi: 10.1002/anie.201612090

Zhang, J. Q., Li, Y. K., Huang, J. C., Hu, H. W., Zhang, G. Y., Yan, H.e., et al. (2017). Ring-fusion of perylene diimide acceptor enabling efficient nonfullerene organic solar cells with a small voltage loss. *J. Am. Chem. Soc*. 139, 16092–16095. doi: 10.1021/jacs.7b09998

Zhang, X., Yao, J. N., and Zhan, C. L. (2016). Synthesis and photovoltaic properties of low bandgap dimeric perylene diimide based non-fullerene acceptors. *Sci. China Chem*. 59, 209–217. doi: 10.1007/s11426-015-5485-8

Zhong, H. L., Wu, C. H., Li, C. Z., Carpenter, J., Chueh, C.-C., Jen, A. K.-Y., et al. (2016). Rigidifying nonplanar perylene diimides by ring fusion toward geometry-tunable acceptors for high-performance fullerene-free solar cells. *Adv. Mater*. 28, 951–958. doi: 10.1002/adma.201504120

Zhong, Y.u., Trinh, M. T., Xiao, S. X., Ng, F., Zhu, X. Y., Nuckolls, C., et al. (2014). Efficient organic solar cells with helical perylene diimide electron acceptors. *J. Am. Chem. Soc*. 136, 15215–15221. doi: 10.1021/ja5092613

Conflict of Interest: The authors declare that the research was conducted in the absence of any commercial or financial relationships that could be construed as a potential conflict of interest.

frontiers in Chemistry

PERSPECTIVE
published: 13 May 2021
doi: 10.3389/fchem.2021.693813

Enhanced Electroluminescence Based on a π-Conjugated Heptazine Derivative by Exploiting Thermally Activated Delayed Fluorescence

Jie Li[1], *Heqi Gong*[1], *Jincheng Zhang*[1], *Shiyi Zhou*[1], *Li Tao*[1], *Lihua Jiang*[2] *and Qiang Guo*[1]*

[1]College of Optoelectronic Technology, Chengdu University of Information Technology, Chengdu, China, [2]College of Electrical Engineering & New Energy, Hubei Provincial Engineering Technology Research Center for Power Transmission Line, China Three Gorges University, Yichang, China

Heptazine derivatives have attracted much attention over the past decade by virtue of intriguing optical, photocatalytic as well as electronic properties in the fields of hydrogen evolution, organic optoelectronic technologies and so forth. Here, we report a simple π-conjugated heptazine derivative (HAP-3DF) possessing an n→π^* transition character which exhibits enhanced electroluminescence by exploiting thermally activated delayed fluorescence (TADF). Green-emitting HAP-3DF shows relatively low photoluminescence quantum efficiencies (Φ_p) of 0.08 in toluene and 0.16 in doped film with bis(2-(diphenylphosphino)phenyl) ether oxide (DPEPO) as the matrix. Interestingly, the organic light-emitting diode (OLED) incorporating 8 wt% HAP-3DF:DPEPO as an emitting layer achieved a high external quantum efficiency (EQE) of 3.0% in view of the fairly low Φ_p of 0.16, indicating the presence of TADF stemming from n→π^* transitions. As the matrix changing from DPEPO to 1,3-di (9*H*-carbazol-9-yl)benzene (mCP), a much higher Φ_p of 0.56 was found in doped film accompanying yellow emission. More importantly, enhanced electroluminescence was observed from the OLED containing 8 wt% HAP-3DF:mCP as an emitting layer, and a rather high EQE of 10.8% along with a low roll-off was realized, which should be ascribed to the TADF process deriving from exciplex formation.

Keywords: electroluminescence, heptazine, thermally activated delayed fluorescence, organic light-emitting diode, exciplex

OPEN ACCESS

Edited by:
Haichang Zhang,
Qingdao University of Science and Technology, China

Reviewed by:
Wang Yanbin,
Changzhou University, China
Shuanghong Wu,
University of Electronic Science and Technology of China, China

****Correspondence:***
Qiang Guo
qiangguo@cuit.edu.cn

Specialty section:
This article was submitted to Organic Chemistry, a section of the journal Frontiers in Chemistry

Received: *12 April 2021*
Accepted: *03 May 2021*
Published: *13 May 2021*

Citation:
Li J, Gong H, Zhang J, Zhou S, Tao L, Jiang L and Guo Q (2021) Enhanced Electroluminescence Based on a π-Conjugated Heptazine Derivative by Exploiting Thermally Activated Delayed Fluorescence. Front. Chem. 9:693813. doi: 10.3389/fchem.2021.693813

INTRODUCTION

Organic light-emitting diodes (OLEDs) have received numerous attentions and experienced rapid development in the fields of display and lighting in view of extremely fascinating advantages such as flexibility, thinness, fast response (Im et al., 2017; Choi et al., 2018; Fukagawa et al., 2018). In contrast with traditional fluorescent and phosphorescent materials, pure organic luminophores based on thermally activated delayed fluorescence (TADF) exhibit great potential and better performance with both high electroluminescence (EL) efficiency and low cost (Uoyama et al., 2012; Zhang et al., 2014; Hirata et al., 2015; Sohn et al., 2020). The key design strategy of TADF molecules is to realize a small energy gap (ΔE_{ST}) between the lowest excited singlet (S_1) and triplet (T_1) states through an effective separation of electron densities of the highest occupied molecular orbital (HOMO) and the lowest unoccupied molecular orbital (LUMO) with respect to electron-donating and electron-accepting

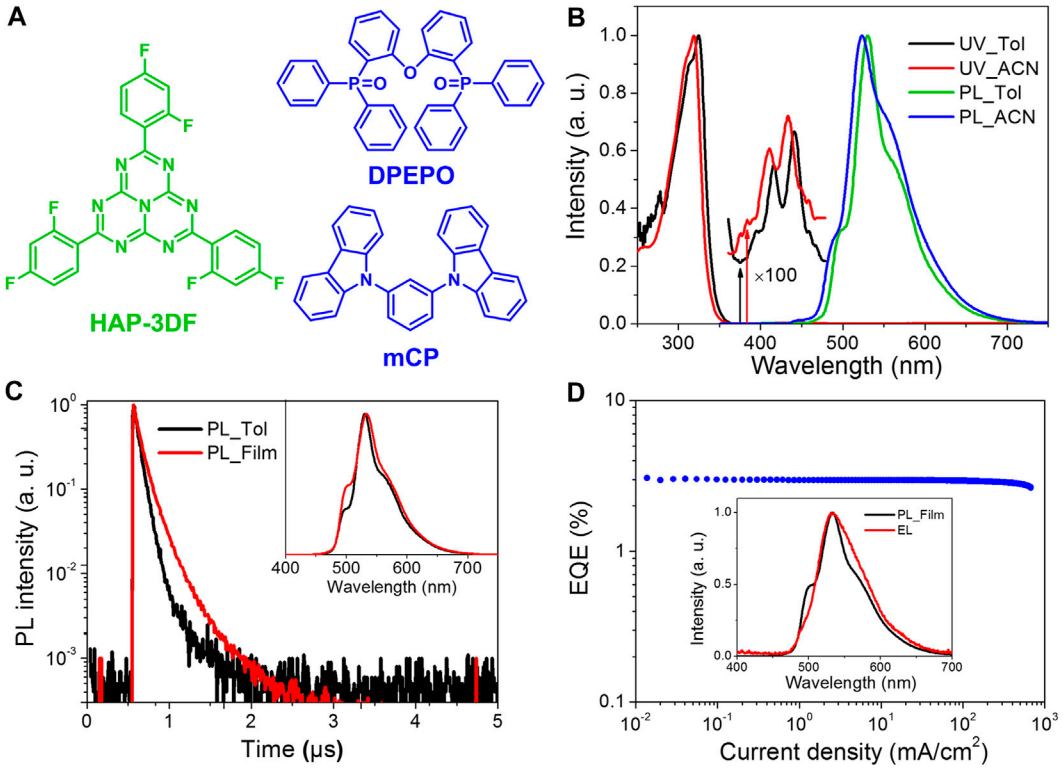

FIGURE 1 | (A) Chemical structures of HAP-3DF, DPEPO and mCP. **(B)** UV and PL spectra of HAP-3DF in toluene (Tol) and acetonitrile (ACN). **(C)** Transient PL decay and PL spectra (Inset) of HAP-3DF in toluene (Tol) and DPEPO film (8 wt%). **(D)** EQE characteristics of the OLED incorporating 8 wt% HAP-3DF:DPEPO. Inset: PL spectrum in 8 wt% HAP-3DF:DPEPO and EL spectrum recorded at a current density of 10 mA cm^{-2}.

moieties, respectively (Lee et al., 2012). Current trends in developing highly efficient TADF emitters are mostly focusing on intramolecular donor-acceptor (D-A) type molecules owing to the accompanying small singlet-triplet splitting during the charge-transfer (CT) transitions (Mehes et al., 2012; Zhang et al., 2012; Tanaka et al., 2013; Kawasumi et al., 2015; Chen et al., 2018; Zeng et al., 2018). Alternatively, small ΔE_{ST} can be realized by exciplex formation *via* intermolecular CT between electron donors and acceptors, or more localized n→π^* transitions involving the lone-pair electrons of heteroatoms and π antibonding molecular orbitals (Goushi et al., 2012; Li et al., 2014; Wu et al., 2019; Jeon and Lee, 2020; Zhao et al., 2020).

In this work, we report a π-conjugated heptazine derivative, 2,5,8-tris(2,4-difluorophenyl)-1,3,4,6,7,9,9b-heptaazaphenalene (HAP-3DF), which exhibits enhanced EL by exploiting n→π^* transitions and exciplex-based TADF, respectively. On the basis of the planar and comparatively rigid heterocyclic system with six C=N bonds surrounding a sp^2-hybridized N atom of the heptazine core, heptazine derivatives have aroused widespread attention over the past decade by virtue of charming optical, photocatalytic as well as electronic properties in the fields of hydrogen evolution, organic optoelectronic technologies and so forth (Ge et al., 2013; Li et al., 2013; Ou et al., 2017; Liu and Ma, 2020). Considering the strong electron-accepting ability of HAP-3DF, bis(2-(diphenylphosphino)phenyl) ether oxide (DPEPO) with two electron-accepting diphenylphosphine oxide groups was chosen as the host material. Encouragingly, the OLED incorporating 8 wt% HAP-3DF:DPEPO as an emitting layer achieved a high maximum external quantum efficiency (EQE) of 3.0% in comparison to the fairly low photoluminescence quantum efficiency (Φ_p) of 0.16, indicating the presence of TADF stemming from n→π^* transitions. To realize exciplex-based TADF, 1,3-di (9*H*-carbazol-9-yl)benzene (mCP) with two electron-donating carbazole moieties was chosen as the electron-donating material for HAP-3DF. More importantly, enhanced EL was observed from the OLED containing 8 wt% HAP-3DF:mCP as an emitting layer, and a rather high EQE of 10.8% along with a low roll-off was realized, which should be assigned to the TADF process deriving from exciplex formation. The chemical structures of HAP-3DF, DPEPO and mCP are depicted in **Figure 1A**.

RESULTS AND DISCUSSION

Details of synthetic routes and quantum chemical calculation of HAP-3DF are described in the **Supplementary Material**. The HOMO and LUMO of HAP-3DF are depicted in **Supplementary Figure S1**. The HOMO is mainly distributed over the sp^2-hybridized N atoms in the heptazine core while the LUMO spreads to the whole π-conjugated system, which is in accordance with the character of n→π^* transition. Based on

the optimized geometry structure, the energies of S_1 and T_1 were calculated to be 2.7753 eV (HOMO→LUMO) and 2.6022 eV (HOMO→LUMO), respectively, indicating that both S_1 and T_1 possess n→π^* transition characteristics. Meanwhile, the ΔE_{ST} is calculated to be as small as 0.1731 eV, implying that n→π^* transition could be an efficient TADF pathway.

To further confirm the n→π^* transition character of HAP-3DF, the ultraviolet–visible absorption (UV) and photoluminescence (PL) spectra were recorded in toluene and a more polar solvent, acetonitrile, respectively (**Figure 1B**). The intense absorption band centered around 320 nm is assigned to π→π^* electronic transition with regard to the π-conjugated system. It is noteworthy that there is an additional low-energy band centered around 450 nm, which should be attributed to the n→π^* transition involving the lone-pair electrons of N heteroatoms and a π antibonding molecular orbital. As expected, both UV and PL spectra of HAP-3DF in acetonitrile showed typical blue shifts compared with that in toluene, indicating typical n→π^* transition characteristics due to the stabilization effect of polar acetonitrile molecules on lone-pair electrons of N atoms (Sidman, 1958; Goodman, 1961). Moreover, both the long-wavelength absorption and emission bands show well-resolved vibronic structures, which should be ascribed to the rigid molecular structure of HAP-3DF. Transient PL decay of HAP-3DF in oxygen-free toluene in the time range of 5 μs is shown in **Figure 1C**, and it presented a prompt fluorescence lifetime of 70 ns and a delayed one of 290 ns The radiative rate constant (k_r) of S_1 can be calculated to be $1.1 \times 106\ s^{-1}$ combining with the corresponding Φ_p of 0.08. The extremely low fluorescence rate and Φ_p are in good agreement with the typical characteristics of n→π^* transitions. Further, transient PL decay and emission spectrum of the 8 wt% HAP-3DF:DPEPO doped film in vacuum were measured (**Figure 1C**), and a more intense delayed component and a higher Φ_p of 0.16 were observed, probably because of the suppressed nonradiative decay due to the rigid and tightly packed environment. Meanwhile, the well-resolved PL spectrum centered at 530 nm is quite similar to that in toluene, indicating that all photons are generated from the same excited singlet state of HAP-3DF in the doped film.

To get better insights into EL characteristics of HAP-3DF, an OLED containing 8 wt% HAP-3DF:DPEPO as an emitting layer was fabricated. The device structure was ITO/α-NPD (35 nm)/TCTA (5 nm)/8 wt% HAP-3DF:DPEPO (15 nm)/DPEPO (5 nm)/TPBI (40 nm)/LiF (0.8 nm)/Al (80 nm), where ITO is indium tin oxide, α-NPD is *N*,*N*′-di (naphthalen-1-yl)-*N*,*N*′-diphenylbenzidine as a hole transport layer, TPBI is 1,3,5-tris(*N*-phenylbenzimidazole-2-yl)benzene as an electron transport layer, and LiF and Al act as the cathode. Thin tris(4-(9H-carbazol-9-yl)phenyl)amine (TCTA) and DPEPO layers were inserted to block electrons from the cathode and holes from the anode, respectively, and simultaneously confine the excitons in the emitting layer. The OLED structure and energy diagram are depicted in **Supplementary Figure S2**. The EL performance are shown in **Figure 1D** and **Supplementary Figures S3, S4**. The EL spectra measured at 1, 10 and 100 mA cm^{-2} are well overlapped with a maximum emission peak of 530 nm, and in good accordance with the PL spectrum of the emitting layer. More importantly, without any light out-coupling enhancement architechure, the OLED showed a comparatively high maximum EQE of 3.0% along with a rather low roll-off considering the fairly low Φ_p of 0.16. The theoretical maximum EQE can be calculated from the following formula, $EQE = \gamma \times \eta_r \times PLQY \times \eta_{out}$, where γ is the electron/hole recombination ratio, η_r is the exciton formation ratio for radiative transitions (η_r = 0.25 for conventional fluorescent emitters), and η_{out} is the light out-coupling efficiency. Accordingly, the theoretical maximum EQE should be limited to 0.8–1.2% assuming that HPM-3DF is a conventional fluorescent molecule with γ = 1.0, η_r = 0.25, PLQY = 0.16 and η_{out} = 0.2–0.3. Thus, the high EL efficiency should be ascribed to the effective TADF process in HAP-3DF based on n→π^* transitions by harvesting radiative singlet excitons upon efficient up-conversion of abundant triplet excitons under electrical excitation.

On the basis of the strong electron-accepting ability of HAP-3DF, exciplex-based TADF could be anticipated by mixing with materials with the electron donating character. The exciplex is an excited complex produced by π→π^* interactions between adjacent conjugated linkers or between a linker and a guest molecule, typically exhibiting broad, featureless luminescence (Allendorf et al., 2009). As is well-known, there is usually an obviously red-shifted and broadened emission spectrum for exciplexes compared with corresponding pure emitters (Goushi et al., 2012; Hung et al., 2013). Herein, as a widely used host material, mCP was chosen as the electron donor on account of the two electron-donating carbazole moieties. An optimized exciplex system of 8 wt% HAP-3DF:mCP was fabricated and characterized. The PL spectra and transient PL decay of 8 wt% HAP-3DF:mCP are presented in **Figure 2A**, respectively. In contrast, the PL spectrum of 8 wt% HAP-3DF:mCP exhibits typical exciplex characteristics with a broad and featureless band centered at 556 nm, which is 26 nm red-shifted compared with that of 8 wt% HAP-3DF:DPEPO. Meanwhile, the full width at half maximum (FWHM) of the exciplex system is 79 nm, which is only 12 nm larger than that of HAP-3DF alone (67 nm), and the narrow FWHM is beneficial to the color purity of OLEDs. Excitingly, the exciplex system shows a remarkably high Φ_p of 0.56, which is much higher than that of 8 wt% HAP-3DF:DPEPO. The narrow FWHM and high Φ_p should be associated with the rigid geometries and tight molecular packing of HAP-3DF and mCP, which can effectively confine molecular motions, suppress the nonradiative transition of singlet and triplet exciplex excitons, and endow the blend film with high PL performance. **Figure 2B** shows the transient PL decay of an 8 wt% HAP-3DF:DPEPO film in vacuum condition at 300 K. Obviously, the transient decay process can be divided into prompt and delayed components. The prompt component with the lifetime of 92 ns should be assigned to conventional fluorescence-based exciplex emission, while the two delayed components with lifetimes of 617 ns and 2.75 μs are generated from the exciplex-based TADF involving an up-conversion process of triplet excitons from T_1 to S_1 (Goushi et al., 2012). To better elucidate the exciplex mechanism, prompt and delayed PL spectra of 8 wt% HAP-3DF:mCP at 300 K were characterized

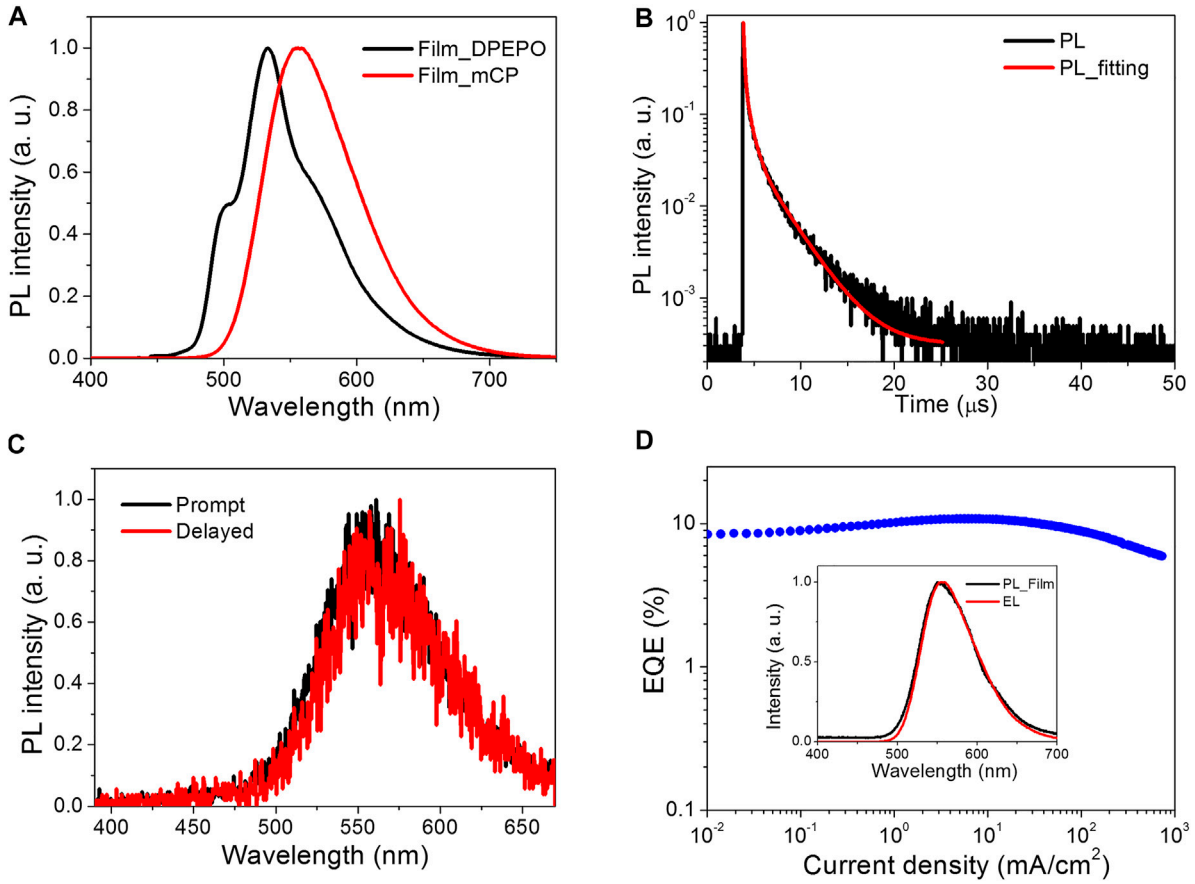

FIGURE 2 | (A) PL spectra of 8 wt% HAP-3DF in DPEPO and mCP. **(B)** Transient PL decay of 8 wt% HAP-3DF:mCP. **(C)** Prompt and delayed PL spectra of 8 wt% HAP-3DF:mCP at 300 K. **(D)** EQE as a function of current density. Inset: PL spectrum in 8 wt% HAP-3DF:mCP and EL spectrum recorded at a current density of 10 mA cm^{-2}.

(**Figure 2C**). The well-overlapped prompt and delayed emission spectra confirm that all photons stemmed from the same excited state. Moreover, 6-dicarbazolo-1,5-pyridine (PYD2) was chosen as another electron-donating material in view of the similar molecular structure with mCP (**Supplementary Figure S5**). The photophysical characteristics of 8 wt% HAP-3DF:PYD2 film at 300 K were measured and shown in **Supplementary Figure S5 and Table S2**. In comparison to the 8 wt% HAP-3DF:mCP exciplex system, the 8 wt% HAP-3DF:PYD2 film shows quite similar PL spectrum, indicating the formation of exciplex between HAP-3DF and PYD2 molecules. Meanwhile, the obvious delayed emission and well-overlapped prompt and delayed components further verify the presence of exciplex formation. Notably, the 8 wt% HAP-3DF:PYD2 exciplex film exhibits a lower Φ_p of 0.39, which might be associated with the subtly changing electron-donating ability of HAP-3DF due to the introduction of pyridine, and the variance of intermolecular interactions between HAP-3DF and PYD2 in comparison to that of HAP-3DF and mCP.

To verify the EL performance of the exciplex system, an OLED based on the 8 wt% HAP-3DF:mCP exciplex system was fabricated with a structure of ITO/α-NPD (35 nm)/TCTA (5 nm)/8 wt% HAP-3DF:mCP (15 nm)/DPEPO (5 nm)/TPBI (40 nm)/LiF (0.8 nm)/Al (80 nm). The OLED structure and energy diagram are depicted in **Supplementary Figure S6**. The EL performance are shown in **Figure 2D** and **Supplementary Figures S7, S8**. The EL spectra measured at 1, 10 and 100 mA cm^{-2} are well overlapped and almost identical to the PL spectrum of an 8 wt% HAP-3DF:mCP blend film. The photon energy of the exciplex was calculated to be 2.5 eV from the onset of the EL spectrum (492 nm), which is consistent with the energy difference between the LUMO of HAP-3DF (−3.4 eV) and HOMO of mCP (−5.9 eV) (**Supplementary Figure S9**). From the current density–voltage–luminance (*J–V–L*) characteristics, the OLED exhibited a considerably high luminance of 18,478 cd m^{-2} at 12.4 V. Encouragingly, a remarkably high EQE of 10.8% was realized along with a rather low roll-off (10.8% at 1000 cd m^{-2}, 9.6% at 5000 cd m^{-2}, 8.5% at 10,000 cd m^{-2}), which significantly exceeds the theoretical maximum EQE (2.8–4.2%) if the 8 wt% HAP-3DF:mCP system is a conventional fluorescent emitter. Overall, the excellent EL

performance is partially attributed to the well-balanced electron and hole fluxes into the emitting zone. Meanwhile, the rigid geometries and tight molecular packing of HAP-3DF and mCP molecules are beneficial to effectively confining molecular motions and suppressing the nonradiative transition of singlet and triplet excitons. More importantly, it should be ascribed to the efficient up-conversion of triplet exciplex excitons from T_1 to S_1 through TADF process which endows the OLED with high EL performance.

CONCLUSION

In summary, we report a π-conjugated heptazine derivative (HAP-3DF) exhibiting enhanced EL by exploiting $n\rightarrow\pi^*$ transition and exciplex-based TADF, respectively. To realize TADF through two different processes, DPEPO with two electron-accepting diphenylphosphine oxide groups and mCP with two electron-donating carbazole moieties, were chosen as the host materials for HAP-3DF. Encouragingly, the OLED incorporating 8 wt% HAP-3DF:DPEPO as an emitting layer achieved a high EQE of 3.0% in comparison to the fairly low Φ_p of 0.16, indicating the presence of efficient TADF stemming from $n\rightarrow\pi^*$ transitions. More importantly, enhanced EL was observed from the OLED containing 8 wt% HAP-3DF:mCP as an emitting layer, and a remarkably high EQE of 10.8% along with a fairly low roll-off (10.8% at 1000 cd m^{-2}, 9.6% at 5000 cd m^{-2}, 8.5% at 10,000 cd m^{-2}) was realized, which should be assigned to the TADF process deriving from exciplex formation. These findings are of fundamental interest for the development of highly efficient OLEDs based on $n\rightarrow\pi^*$ transitions and exciplex systems.

DATA AVAILABILITY STATEMENT

The original contributions presented in the study are included in the article/**Supplementary Material**, further inquiries can be directed to the corresponding author.

AUTHOR CONTRIBUTIONS

JL and QG conceived the research and supervised the whole work. HG, JZ and SZ prepared materials and characterized the photophysical properties. LT contributed to theoretical calculations. LJ contributed to the analysis of luminescence mechanism. All authors contributed to the manuscript revision and approved the submitted version.

FUNDING

This work was financially supported by the National Natural Science Foundation of China (61505015, 21801028, 11704050), Department of Science and Technology of Sichuan Province (2019YJ0358, 2017FZ0085, 2020YFG0038), Education Department of Sichuan Province (18ZB0114, 16ZA0205) and Department of Human Resources and Social Security of Sichuan Province (2019Z226).

SUPPLEMENTARY MATERIAL

The Supplementary Material for this article can be found online at: https://www.frontiersin.org/articles/10.3389/fchem.2021.693813/full#supplementary-material

REFERENCES

Allendorf, M. D., Bauer, C. A., Bhakta, R. K., and Houk, R. J. T. (2009). Luminescent Metal-Organic Frameworks. *Chem. Soc. Rev.* 38, 1330–1352. doi:10.1039/b802352m

Chen, J. X., Wang, K., Zheng, C. J., Zhang, M., Shi, Y. Z., Tao, S. L., et al. (2018). Red Organic Light-Emitting Diode with External Quantum Efficiency beyond 20% Based on a Novel Thermally Activated Delayed Fluorescence Emitter. *Adv. Sci. (Weinh)* 5, 1800436. doi:10.1002/advs.201800436

Choi, M., Park, Y. J., Sharma, B. K., Bae, S.-R., Kim, S. Y., and Ahn, J.-H. (2018). Flexible Active-Matrix Organic Light-Emitting Diode Display Enabled by MoS2thin-Film Transistor. *Sci. Adv.* 4, eaas8721. doi:10.1126/sciadv.aas8721

Fukagawa, H., Sasaki, T., Tsuzuki, T., Nakajima, Y., Takei, T., Motomura, G., et al. (2018). Long-lived Flexible Displays Employing Efficient and Stable Inverted Organic Light-Emitting Diodes. *Adv. Mater.* 30, 1706768. doi:10.1002/Adma.201706768

Ge, L., Han, C., Xiao, X., and Guo, L. (2013). Synthesis and Characterization of Composite Visible Light Active Photocatalysts Mos2-G-C3n4 with Enhanced Hydrogen Evolution Activity. *Int. J. Hydrogen Energ.* 38, 6960–6969. doi:10.1016/j.ijhydene.2013.04.006

Goodman, L. (1961). Transitions in the Azines. *J. Mol. Spectrosc.* 6, 109–137. doi:10.1016/0022-2852(61)90235-1

Goushi, K., Yoshida, K., Sato, K., and Adachi, C. (2012). Organic Light-Emitting Diodes Employing Efficient Reverse Intersystem Crossing for Triplet-To-Singlet State Conversion. *Nat. Photon* 6, 253–258. doi:10.1038/nphoton.2012.31

Hirata, S., Sakai, Y., Masui, K., Tanaka, H., Lee, S. Y., Nomura, H., et al. (2015). Highly Efficient Blue Electroluminescence Based on Thermally Activated Delayed Fluorescence. *Nat. Mater* 14, 330–336. doi:10.1038/Nmat4154

Hung, W.-Y., Fang, G.-C., Chang, Y.-C., Kuo, T.-Y., Chou, P.-T., Lin, S.-W., et al. (2013). Highly Efficient Bilayer Interface Exciplex for Yellow Organic Light-Emitting Diode. *ACS Appl. Mater. Inter.* 5, 6826–6831. doi:10.1021/am402032z

Im, Y., Kim, M., Cho, Y. J., Seo, J.-A., Yook, K. S., and Lee, J. Y. (2017). Molecular Design Strategy of Organic Thermally Activated Delayed Fluorescence Emitters. *Chem. Mater.* 29, 1946–1963. doi:10.1021/acs.chemmater.6b05324

Jeon, S. K., and Lee, J. Y. (2020). Highly Efficient Exciplex Organic Light-Emitting Diodes by Exciplex Dispersion in the Thermally Activated Delayed Fluorescence Host. *Org. Electron.* 76, 105477. doi:10.1016/j.orgel.2019.105477

Kawasumi, K., Wu, T., Zhu, T., Chae, H. S., Van Voorhis, T., Baldo, M. A., et al. (2015). Thermally Activated Delayed Fluorescence Materials Based on Homoconjugation Effect of Donor-Acceptor Triptycenes. *J. Am. Chem. Soc.* 137, 11908–11911. doi:10.1021/jacs.5b07932

Lee, S. Y., Yasuda, T., Nomura, H., and Adachi, C. (2012). High-efficiency Organic Light-Emitting Diodes Utilizing Thermally Activated Delayed Fluorescence from Triazine-Based Donor-Acceptor Hybrid Molecules. *Appl. Phys. Lett.* 101, 093306. doi:10.1063/1.4749285

Li, J., Nakagawa, T., MacDonald, J., Zhang, Q., Nomura, H., Miyazaki, H., et al. (2013). Highly Efficient Organic Light-Emitting Diode Based on a Hidden Thermally Activated Delayed Fluorescence Channel in a Heptazine Derivative. *Adv. Mater.* 25, 3319–3323. doi:10.1002/adma.201300575

Li, J., Zhang, Q., Nomura, H., Miyazaki, H., and Adachi, C. (2014). Thermally Activated Delayed Fluorescence from $3n\pi^*$ to $1n\pi^*$ Up-Conversion and its Application to Organic Light-Emitting Diodes. *Appl. Phys. Lett.* 105, 013301. doi:10.1063/1.4887346

Liu, Y., and Ma, Z. (2020). G-c3n4 Modified by Meso-Tetrahydroxyphenylchlorin for Photocatalytic Hydrogen Evolution under Visible/near-Infrared Light. *Front. Chem.* 8, 605343. doi:10.3389/fchem.2020.605343

Méhes, G., Nomura, H., Zhang, Q., Nakagawa, T., and Adachi, C. (2012). Enhanced Electroluminescence Efficiency in a Spiro-Acridine Derivative through Thermally Activated Delayed Fluorescence. *Angew. Chem. Int. Ed.* 51, 11311–11315. doi:10.1002/anie.201206289

Ou, H., Lin, L., Zheng, Y., Yang, P., Fang, Y., and Wang, X. (2017). Tri-s -Triazine-Based Crystalline Carbon Nitride Nanosheets for an Improved Hydrogen Evolution. *Adv. Mater.* 29, 1700008. doi:10.1002/adma.201700008

Sidman, J. W. (1958). Electronic Transitions Due to Nonbonding Electrons Carbonyl, Aza-Aromatic, and Other Compounds. *Chem. Rev.* 58, 689–713. doi:10.1021/cr50022a004

Sohn, S., Ha, M. W., Park, J., Kim, Y.-H., Ahn, H., Jung, S., et al. (2020). High-efficiency Diphenylpyrimidine Derivatives Blue Thermally Activated Delayed Fluorescence Organic Light-Emitting Diodes. *Front. Chem.* 8, 356. doi:10.3389/fchem.2020.00356

Tanaka, H., Shizu, K., Nakanotani, H., and Adachi, C. (2013). Twisted Intramolecular Charge Transfer State for Long-Wavelength Thermally Activated Delayed Fluorescence. *Chem. Mater.* 25, 3766–3771. doi:10.1021/cm402428a

Uoyama, H., Goushi, K., Shizu, K., Nomura, H., and Adachi, C. (2012). Highly Efficient Organic Light-Emitting Diodes from Delayed Fluorescence. *Nature* 492, 234–238. doi:10.1038/nature11687

Wu, T. L., Liao, S. Y., Huang, P. Y., Hong, Z. S., Huang, M. P., Lin, C. C., et al. (2019). Exciplex Organic Light-Emitting Diodes with Nearly 20% External Quantum Efficiency: Effect of Intermolecular Steric Hindrance between the Donor and Acceptor Pair. *ACS Appl. Mater. Inter.* 11, 19294–19300. doi:10.1021/acsami.9b04365

Zeng, W., Lai, H. Y., Lee, W. K., Jiao, M., Shiu, Y. J., Zhong, C., et al. (2018). Achieving Nearly 30% External Quantum Efficiency for Orange-Red Organic Light Emitting Diodes by Employing Thermally Activated Delayed Fluorescence Emitters Composed of 1,8-Naphthalimide-Acridine Hybrids. *Adv. Mater.* 30, 1704961. doi:10.1002/adma.201704961

Zhang, Q., Li, B., Huang, S., Nomura, H., Tanaka, H., and Adachi, C. (2014). Efficient Blue Organic Light-Emitting Diodes Employing Thermally Activated Delayed Fluorescence. *Nat. Photon* 8, 326–332. doi:10.1038/Nphoton.2014.12

Zhang, Q., Li, J., Shizu, K., Huang, S., Hirata, S., Miyazaki, H., et al. (2012). Design of Efficient Thermally Activated Delayed Fluorescence Materials for Pure Blue Organic Light Emitting Diodes. *J. Am. Chem. Soc.* 134, 14706–14709. doi:10.1021/ja306538w

Zhao, J., Ye, J., Du, X., Zheng, C., He, Z., Yang, H., et al. (2020). Efficient Exciplex-based Green and Near-Infrared Organic Light-Emitting Diodes Employing a Novel Donor-Acceptor Type Donor. *Chem. Asian J.* 15, 4093–4097. doi:10.1002/asia.202001091

Conflict of Interest: The authors declare that the research was conducted in the absence of any commercial or financial relationships that could be construed as a potential conflict of interest.

frontiers in Chemistry

MINI REVIEW
published: 18 June 2021
doi: 10.3389/fchem.2021.717569

Heptazine-Based π-Conjugated Materials for Light-Emitting

Jie Li[1], *Li Tao*[1], *Yanqing Wang*[2], *Yali Yao*[3] *and Qiang Guo*[1]*

[1]College of Optoelectronic Technology, Chengdu University of Information Technology, Chengdu, China, [2]College of Polymer Science and Engineering, Sichuan University, Chengdu, China, [3]School of Physical Education, Chengdu Normal University, Chengdu, China

On the basis of planar and relatively rigid nitrogen-rich heterocyclic system of the heptazine core, heptazine-based π-conjugated materials have aroused widespread attention over the past decade by virtue of the fascinating electronic, optical, thermal, and mechanical properties in the fields of light-emitting, photocatalysis, sensors, environmental remediation, and so forth. However, there are still several obstacles to be solved before practical applications, such as low photoluminescence quantum efficiencies for light-emitting and weak visible absorption for photocatalysis. To further enhance various properties of heptazine-based π-conjugated materials, a series of strategies have been developed, including ingenious molecular design and modification, novel synthetic, and preparation methods. In this review, the significant progress of monomeric and polymeric heptazine-based π-conjugated materials and their applications typically in light-emitting are reviewed, which is beneficial for the acceleration of practical applications of heptazine-based materials and devices.

Keywords: heptazine, light-emitting, metal ion-containing heptazine, polymeric heptazine, monomeric heptazine

OPEN ACCESS

Edited by:
Haichang Zhang,
Qingdao University of Science and Technology, China

Reviewed by:
Zheng Zhou,
The University of Sydney, Australia
Shengli Zhai,
University of Alberta, Canada

***Correspondence:**
Qiang Guo
qiangguo@cuit.edu.cn

Specialty section:
This article was submitted to Organic Chemistry, a section of the journal Frontiers in Chemistry

Received: *31 May 2021*
Accepted: *10 June 2021*
Published: *18 June 2021*

Citation:
Li J, Tao L, Wang Y, Yao Y and Guo Q (2021) Heptazine-Based π-Conjugated Materials for Light-Emitting. Front. Chem. 9:717569. doi: 10.3389/fchem.2021.717569

INTRODUCTION

Over the last decade, considerable progress in the fields of organic light-emitting diodes (OLEDs) and photocatalysis has triggered intensive effort to develop highly efficient light-emitting materials and photocatalysts (Wu and Ma, 2016; Zhou et al., 2017; Zhou et al., 2019; Yin et al., 2020; Zhou et al., 2020). Among the many kinds of materials investigated, nitrogen-rich heptazine-based materials are highly attractive on account of intriguing photoelectronic and photocatalytic properties (Audebert et al., 2021; Wang et al., 2021). In the 1830s, heptazine-based materials were initially discovered by a Swedish chemist, Jons Jakob Berzelius, after the ignition of mercury thiocyanate, and this work was mentioned and reported by the German chemists, Justus von Liebg and Leopold Gmelin (Liebig, 1834; Gmelin, 1835; Liebig, 1835). Meanwhile, the compound obtained by Berzelius was termed melon by Liebig. However, the study on heptazine derivatives has long been hampered probably by their general insolubility, chemical inertness, and high decomposition temperatures which make their characterization and modification difficult (Kailasam et al., 2013; Sayed et al., 2017). About 100 years later, through the elaborate analysis of a few small crystals by X-ray crystallography, Pauling, and Sturdivant proposed a planar triangular structure as the basic monomer of melon, cyameluric nucleus (C_6N_7), which is the accurate structure of heptazine core (Pauling and Sturdivant, 1937). Much later, the unsubstituted heptazine, 1,3,4,6,7,9,9b-heptaazaphenalene ($C_6N_7H_3$), was firstly synthesized and characterized in the 1980s by the members of Leonard group (Hosmane et al., 1982; Shahbaz et al., 1984). Since 2001, the structure of Berzelius's melon has been systematically

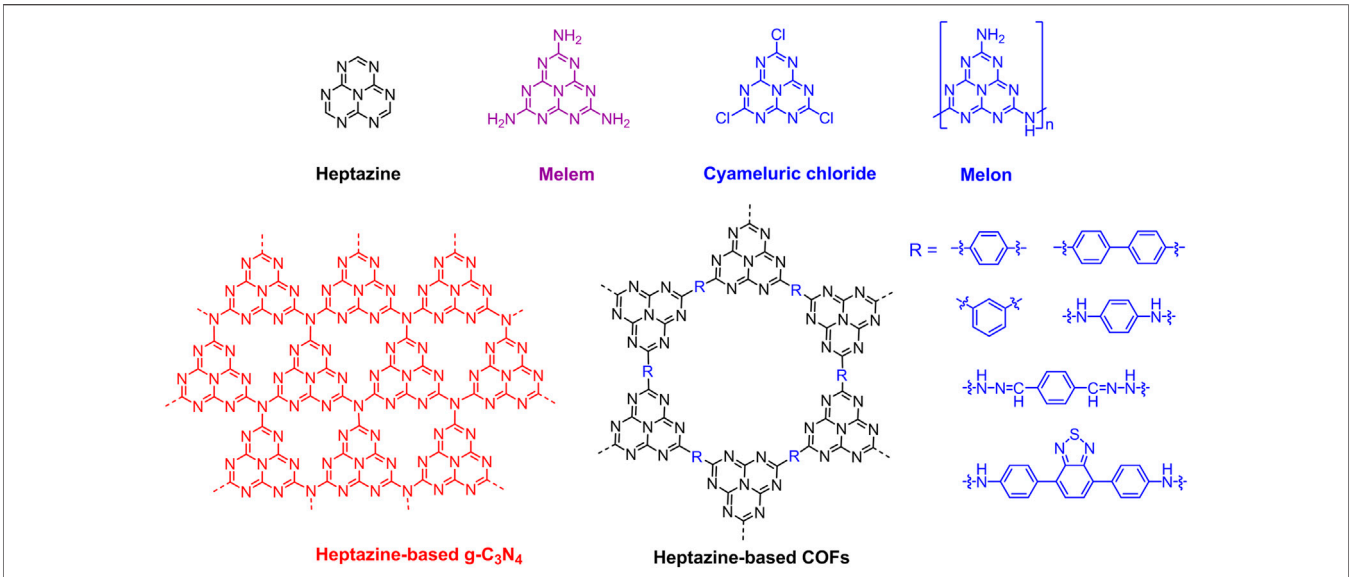

FIGURE 1 | Chemical structures of heptazine, melem, cyameluric chloride, melon, heptazine-based graphitic carbon nitride (g-C_3N_4), and covalent organic frameworks (COFs).

confirmed, which is polymerized with the heptazine units linked through an amine (NH) link (Komatsu, 2001; Lotsch et al., 2007).

The heptazine, also known as tri-*s*-triazine, carbon nitride or C_6N_7, is a type of chemical compound consisting of a triangular structure, or three fused *s*-triazine rings, with three substituents at the corners of the triangle. Namely, the heptazine is a planar and relatively rigid nitrogen-rich heterocyclic system with 6 C=N bonds surrounding an sp^2-hybridized N atom. The heptazine with three amino substituents is called melem (2,5,8-triamino-tri-*s*-triazine), which is an important intermediate during condensation of melamine to graphitic carbon nitride (g-C_3N_4). Jurgens et al. initially ascertained the crystal structure of melem by X-ray powder diffractometry and found that melem molecules are arranged into parallel layers with an interplanar distance of 0.327 nm. Particularly, according to temperature-dependent X-ray powder diffractometry investigations above 560°C, they discovered that the melem would transform into g-C_3N_4 (Jurgens et al., 2003). Similar to cyanuric chloride (trichloro-*s*-triazine, $C_3N_3Cl_3$), cyameluric chloride (trichloro-tri-*s*-triazine, $C_6N_7Cl_3$) is an important starting material for various synthesis of heptazine-based materials, and Kroke et al. comprehensively characterized its crystal structure and photophysical properties (Kroke et al., 2002). As the heptazine-based g-C_3N_4 emerging to be a class of promising metal-free photocatalysts, it received tremendous research interests over the past decade in the fields of hydrogen evolution Wang et al. (2009), Liao et al. (2019), CO_2 reduction Gao et al. (2016), Barrio et al. (2019), photocatalytic degradation of organic pollutants Ong et al. (2016), Zeng Y. et al. (2018), and artificial photosynthesis (Su et al., 2010; Dai et al., 2018). Additionally, heptazine-based covalent organic frameworks (COFs) have also attracted much attention in the past several years due to the photocatalytic performance (Bojdys et al., 2010; Kailasam et al., 2016; Luo et al., 2019; Xing et al., 2020; Zhang et al., 2020). The various applications are significantly associated with the appealing heptazine-based molecular structure in which the sp^2 hybridized carbon and nitrogen induce a delocalized π-conjugated system and consequently result in a moderate band gap of around 2.7 eV, whereby a broad variety of photocatalytic reactions can be carried out (Zhang et al., 2019; Patnaik et al., 2021). The chemical structures of heptazine, melem, cyameluric chloride, melon, heptazine-based g-C_3N_4, and COFs are depicted in **Figure 1**. Considering a number of published review articles with respect to the photocatalysis of g-C_3N_4 and in order to avoid the content overlap, in this article, the heptazine-based materials regarding to light-emitting are mainly reviewed.

METAL ION-CONTAINING HEPTAZINE-BASED LIGHT-EMITTING

In 2012, Makowski et al. synthesized a series of rare-earth melonates $LnC_6N_7(NCN)_3{\bullet}xH_2O$ (Ln = La, Ce, Pr, Nd, Sm, Eu, Tb; x = 8–12) by metathesis reactions in aqueous solution and systematically investigated the photoluminescence (PL) performance of $LnC_6N_7(NCN)_3{\bullet}xH_2O$ (Ln = Eu, Tb; x = 9–12). The terbium melonate showed green emission with an emission peak (λ_{em}) of 545 nm due to the $^5D_4 \rightarrow {}^7F_5$ transition. Meanwhile, they found that the rare-earth melonates exhibited rather low thermal stability probably deriving from the tight binding of crystal water, which resulted in hydrolytic decomposition at elevated temperatures (Makowski et al., 2012). Cheng et al. reported a silver-g-C_3N_4 quantum dots (Ag-g-CNQDs) composite prepared from g-C_3N_4 quantum dots and silver nanoparticles by water phase synthesis (Cheng

et al., 2018). Based on metal-enhanced fluorescence, the Ag-g-CNQDs composite exhibited excitation-dependent red emission with λ_{em} = 600 nm and a PL quantum efficiency (PLQE) of 21%. More importantly, for heparin detection, the emission at 600 nm was enhanced linearly over a concentration range of 0.025–2.5 μM by hydrogen-bonding and electrostatic interaction. This phenomenon has also been successfully applied to determine heparin levels in human serum samples, demonstrating its promising diagnostic applications.

POLYMERIC g-C_3N_4-BASED LIGHT-EMITTING

As an organic semiconducting material, g-C_3N_4 has drawn immense attraction due to its unique optical and electronic properties. In 2008, Iwano et al. studied the possibility for white light emitting devices using carbon nitride thin films prepared by microwave electron cyclotron resonance (ECR)-plasma chemical vapor deposition (CVD). The cathodoluminescence measurement of the film grown by ECR-plasma CVD method showed three peaks of red, green, and blue (Iwano et al., 2008). Barman et al. presented highly blue fluorescent g-C_3N_4 quantum dots (g-CNQDs) with a PLQE of 29% (Barman and Sadhukhan, 2012). Notably, the g-CNQDs can play a dual role for selective and sensitive detection of mercuric ions and iodide ions in aqueous media by "ON-OFF-ON" fluorescence response. Zhou et al. reported a low-temperature solid-phase method to synthesize highly fluorescent g-CNQDs with a PLQE of 42% (Zhou et al., 2013). Interestingly, the emission of g-CNQDs can be tuned from deep blue to green by adjusting the molar ratio of the two reactants, urea and sodium citrate.

Zhang et al. facilely synthesized g-C_3N_4 by the low temperature thermal condensation of melamine between 300–650°C and found that the PL spectra could be continuously tuned from 400 to 510 nm with the control of temperature (Zhang Y. et al., 2013). Chen el al. characterized the fluorescence and electrochemiluminescence (ECL) properties of g-C_3N_4 nanoflake particles (g-C_3N_4 NFPs) and nanoflake films (g-C_3N_4 NFFs). It was found that both g-C_3N_4 NFPs and g-C_3N_4 NFFs showed strong blue emission, and the as-prepared g-C_3N_4 NFFs exhibited strong non-surface state ECL activity in the presence of reductive-oxidative coreactants with λ_{em} = 435 nm (Chen et al., 2013). Two-dimensional nanosheets have attracted tremendous attention because the atomic-thick nanosheets can not only enhance the intrinsic properties of their bulk counterparts but also generate new promising properties. In 2013, Zhang et al. firstly prepared ultrathin g-C_3N_4 nanosheets by a liquid exfoliation route from bulk g-C_3N_4 in water (Zhang X. et al., 2013). In comparison to the bulk g-C_3N_4, the ultrathin blue-emitting g-C_3N_4 nanosheets showed enhanced intrinsic photoabsorption and photoresponse, resulting in an extremely high PLQE of 19.6%, which could be promising candidates for bioimaging application.

To investigate the charge carrier trapping, migration, and transfer of electron-hole pairs, Zhao et al. synthesized a series of g-C_3N_4 under different precursor masses and measured their PL characteristics. All the as-prepared g-C_3N_4 samples showed blue emission with λ_{em} = 440–455 nm. Moreover, CN-2T exhibits the highest PL intensity, which is attributed to the less structural defects (e.g. uncondensed $-NH_2$, $-NH$ groups) in view of more complete condensation of thiourea (Zhao et al., 2015). To better clarify the photocatalytic mechanism of heptazine-based materials, Wen et al. measured the photophysical properties of melamine, melem, and g-C_3N_4. They found that the PL intensities of melem is the highest, g-C_3N_4 second, and melamine the weakest, indicating that the condensation of melamine to melem makes PL stronger, while the condensation of melem to g-C_3N_4 results in weaker PL (Wen et al., 2018). Yang et al. prepared strong blue-emitting porous g-C_3N_4 with λ_{em} = 400 nm and a PLQE of 21% (Yang et al., 2018). Compared with bulk g-C_3N_4 and g-C_3N_4 nanosheets, the porous g-C_3N_4 shows good PLQE, large surface area and great dispersibility, and stability in water. The porous g-C_3N_4 probes showed the remarkable sensitivity and selectivity for uric acid (UA) and were successfully applied to the determination of UA.

Recently, Yadav et al. developed a facile approach to prepare free-standing films comprising of g-C3N4 nanolayers (Yadav et al., 2020). The as-synthesized g-C3N4 film exhibited intense and broad blue emission centered 459 nm. Tang el al. realized the broadband white light luminescence based on electron-deficient porous g-C_3N_4 constructed by supramolecular copolymerization design (Tang et al., 2020). Meanwhile, they successfully narrowed the band gap of g-C3N4 from 2.64 to 1.39 eV. Furthermore, the emission wavelengths of electron-deficient porous g-C3N4 can be tuned from narrow blue to broad-band white range by the addition of 2, 4, 6-triaminopyrimidine (TAP).

MONOMERIC HEPTAZINE-BASED LIGHT-EMITTING

Traditional Fluorescence

Owing to the strong electron-withdrawing ability and three substitution sites at the corners of the triangle of heptazine core, a series of heptazine derivatives have been developed and the PL or electroluminescence (EL) characteristics have been investigated. During the structure determination of cyameluric chloride and melem, their photophysical properties were also measured. Cyameluric chloride showed blue emission with λ_{em} = 466 nm, and melem exhibited ultraviolet emission with λ_{em} = 366 nm and a relatively high PLQE of 40% (Kroke et al., 2002; Jurgens et al., 2003). In 2017, Zheng et al. reported a rod-like structured blue-emitting melem which was synthesized by treating a bulk melem with nitric acid and ethylene glycol (Zheng et al., 2017). Excitingly, the PLQE of the rod-like melem (56.9%) is about 1.6 times higher than that of the ordinary melem (35.2%) and is substantially higher than that of blue-emitting bulk g-C_3N_4 (4.8%). This blue-emitting melem shows great potential for practical applications in many fields.

Bala et al. reported a heptazine-based discotic liquid crystal molecule (Hpz-3C12, **Figure 2**), which presented significant aggregation-induced emission (AIE) behavior as indicated by

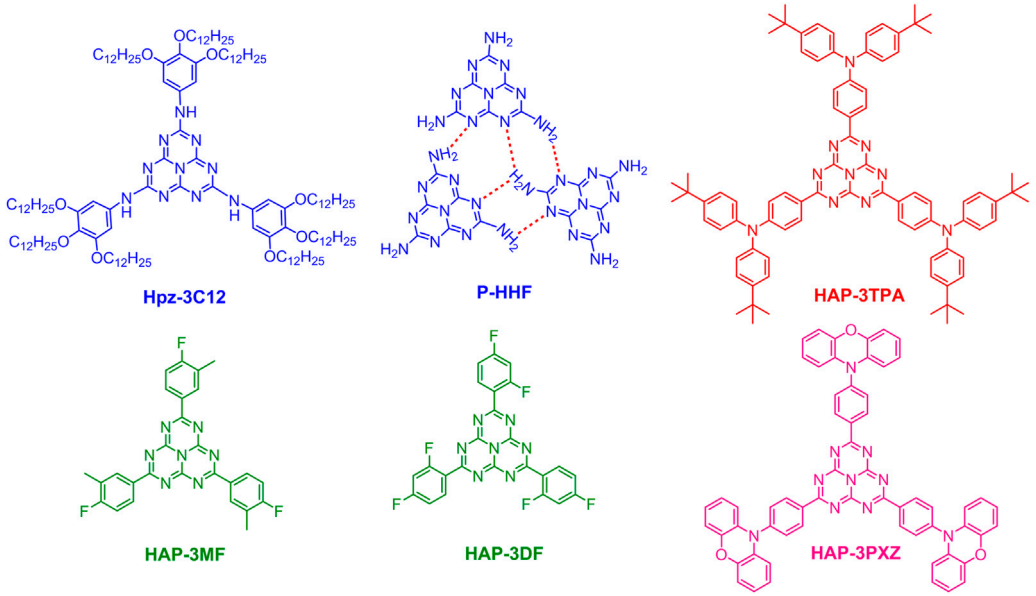

FIGURE 2 | Chemical structures of Hpz-3C12, polymeric hydrogen-bonded heptazine frameworks (P-HHF), HAP-3TPA, HAP-3MF, HAP-3DF, and HAP-3PXZ.

the remarkably increased fluorescence intensity in solid state in comparison to that in solution (Bala et al., 2018). Interestingly, the EL spectra of solution-processed OLEDs containing Hpz-3C12 varied with the host materials. The OLED incorporating 3 wt% Hpz-3C12:CBP exhibited the best performance with a power efficiency of 0.3 lm W^{-1}, a current efficiency of 0.4 cd A^{-1}, an EQE of 1.6% and deep blue emission. Although the EL efficiency is low, it still demonstrates that heptazine-based discotic liquid crystals may contribute to the further development of AIE-based blue emitters. Yang et al. investigated the hydrogen-bonding effect on PLQEs and luminescence stability of polymeric hydrogen-bonded heptazine frameworks (P-HHF, **Figure 2**) and trivalent europium ions incorporated P-HHF (P-HHF-Eu) (Yang et al., 2020). The hydration degrees and the role of hydrogen bonding in the emission properties were analyzed by time-resolved and steady state PL spectroscopies. They found that the bulk P-HHF particles showed blue emission and a moderate PLQE of 35.8%, while enhanced PLQE of 55.9% was obtained when suspending P-HHF into polyvinyl alcohol (PVA) to form hydrogel composites (P-HHF-PVA gel). This work is considerably beneficial to understand the effect of intermolecular hydrogen-bonds on the luminescence characteristics of heptazine-based materials.

Thermally Activated Delayed Fluorescence

Over the past decade, as the third generation organic light-emitting materials with respect to traditional fluorescent and phosphorescent materials, thermally activated delayed fluorescence (TADF) materials exhibit great potential in OLEDs on account of the excellent performance with both high EL efficiency and low cost (Uoyama et al., 2012; Zhang et al., 2014; Sohn et al., 2020). The key design strategy of TADF materials is to realize a small energy gap (ΔE_{ST}) between the lowest excited singlet (S_1) and triplet (T_1) states through an ingenious design to effectively separate the electron densities of the highest occupied molecular orbital (HOMO) and the lowest unoccupied molecular orbital (LUMO) (Endo et al., 2011). One of the most widely used methods in developing highly efficient TADF emitters is to design molecules possessing electron donor-acceptor (DA) structure which is beneficial for the realization of small singlet-triplet splitting during intramolecular charge-transfer (CT) transitions (Zhang et al., 2012; Li et al., 2013; Tanaka et al., 2013; Kawasumi et al., 2015; Chen et al., 2018; Zeng W. X. et al., 2018). Based on the strong electron-withdrawing ability of heptazine core and strong electron-donating feature of triphenylamine, Li et al. designed and synthesized a highly efficient heptazine-based TADF emitter, HAP-3TPA (**Figure 2**), which exhibited a small ΔE_{ST} of 0.27 eV based on density functional theory (DFT) in view of the effective separation of HOMO and LUMO. Meanwhile, HAP-3TPA showed relatively high thermal stability over 500°C and considerably strong absorption centered at 486 nm. Encouragingly, an extremely high PLQE of 91%, red emission with λ_{em} = 610 nm were achieved in a 6 wt% HAP-3TPA:2,6-dicarbazolo-1,5-pyridine (26 mCPy) doped film. More importantly, An OLED incorporating 6 wt% HAP-3TPA: 26 mCPy as an emitting layer exhibited a fairly high external quantum efficiency (EQE) of 17.5 ± 1.3%, up to now, which is still one of the highest EQEs of red TADF emitters (Li et al., 2013). As a result, the realization of highly efficient red emitter makes TADF completely cover the red, green and blue bands, and show promising applications in the fields of lighting and display.

Alternatively, Goushi et al. demonstrated that small ΔE_{ST} can be realized by exciplex formation *via* intermolecular CT between two molecules with electron-donating and electron-accepting

characteristics, respectively (Goushi et al., 2012). Since then, a new class of TADF emitters have been developed (Chapran et al., 2019; Wu et al., 2019; Zhang et al., 2021). In view of the formation mechanism of exciplex, another heptazine derivative (HAP-3MF, **Figure 2**) was designed and synthesized, and an exciplex system was formed by choosing 1,3-di (9*H*-carbazol-9-yl)benzene (mCP) as an electron donor (Li et al., 2014a). Surprisingly, the 8 wt% HAP-3MF:mCP doped film showed efficient exciplex emission with a remarkably high PLQE of 66.1%, a rather small PLQE difference was observed in air and vacuum conditions, indicating the tight molecular packing between HAP-3MF and mCP. Subsequently, the OLED containing 8 wt % HAP-3MF:mCP showed a pretty high EQE of 11.3% with a low roll-off, demonstrating the efficient harvest of triple exciplex excitons through reverse intersystem crossing (RISC) from T_1 to S_1 under electrical excitation. By changing the three substituents of heptazine core from 2-fluorotoluene to 1,3-difluorobenzene, 2,5,8-tris(2,4-difluorophenyl)-1,3,4,6,7,9,9b-heptaazaphenalene (HAP-3DF, **Figure 2**) was obtained (Li et al., 2021). The OLED incorporating 8 wt% HAP-3DF:mCP as an emitting layer exhibited a reasonably high EQE of 10.8%.

Additionally, TADF can be also realized by more localized n→π^* transitions involving the nonbonding lone-pair electrons of heteroatoms and π antibonding molecular orbitals (Turro et al., 2010). Excitingly, through elaborate theoretical analysis and experimental verification, a hidden, efficient TADF pathway was found in HAP-3MF on account of n→π^* transitions (Li et al., 2014b). To verify the contribution of n→π^* transitions and prevent exciplex formation, electron-deficient bis[2-(diphenylphosphino)phenyl] ether oxide (DPEPO) was chosen as the host material. An OLED incorporating 6 wt% HAP-3MF: DPEPO showed a high EQE of 6.0% regarding to the low PLQE of 26%, confirming the hidden n→π^* based TADF pathway. This work demonstrated that the n→π^* emitter is a new TADF material and can be applied to OLED applications. Interestingly, the n→π^* based HAP-3DF exhibited a lower PLQE of 0.16 and an EQE of 3.0%, illustrating that the subtle structural change has a great influence on luminescence properties (Li et al., 2021). According to the energy gap law, the design of efficient red-emitting materials is rather difficult. In 2018, Kang, et al. proposed an efficient heptazine-based red TADF molecule, HAP-3PXZ (**Figure 2**), based on the optimal Hartree-Fock percentage calculation method through enlarging the delocalization of HOMO and LUMO (Kang et al., 2018). Excitingly, HAP-PXZ exhibited deep red emission with λ_{em} = 714 nm and a small ΔE_{ST} of 0.172 eV based on calculation, implying the importance of further experimental research on heptazine derivatives.

CONCLUSION AND OUTLOOK

In summary, we have provided an overview of monomeric and polymeric heptazine-based π-conjugated materials for light-emitting. The historical introduction of heptazine was meticulously described. Benefiting from the intriguing electronic, optical, thermal, and mechanical properties, heptazine-based materials have roused tremendous research interest in the field of light-emitting. The metal ion-containing, polymeric g-C_3N_4-based, monomeric heptazine-based light-emitting materials, and devices are systematically summarized, which is conductive to stimulate numerous efforts in the development of heptazine-based functional materials. By comparison, the number of heptazine-based light-emitting materials is much less than that of heptazine-based photocatalytic ones, although some heptazine derivatives have exhibited great potential in practical applications. Therefore, it could be anticipated that more high performance heptazine-based light-emitting materials and devices will be realized through elaborate molecular design in the near future.

AUTHOR CONTRIBUTIONS

JL and QG conceived the idea and supervised the whole work. LT, YW, and YY collected the articles and revised the manuscript. All authors contributed to the manuscript revision and approved the submitted version.

FUNDING

This work was financially supported by the National Natural Science Foundation of China (61505015, 21801028, 11704050), Department of Science and Technology of Sichuan Province (2019YJ0358, 2017FZ0085, 2020YFG0038, 2020YFH0104), Fundamental Research Funds for the Central Universities (YJ201952) and Department of Human Resources and Social Security of Sichuan Province (2019Z226).

REFERENCES

Audebert, P., Kroke, E., Posern, C., and Lee, S.-H. (2021). State of the Art in the Preparation and Properties of Molecular Monomeric S-Heptazines: Syntheses, Characteristics, and Functional Applications. *Chem. Rev.* 121, 2515–2544. doi:10.1021/acs.chemrev.0c00955

Bala, I., Ming, L., Yadav, R. A. K., De, J., Dubey, D. K., Kumar, S., et al. (2018). Deep-Blue OLED Fabrication from Heptazine Columnar Liquid Crystal Based AIE-Active Sky-Blue Emitter. *Chemistryselect* 3, 7771–7777. doi:10.1002/slct.201801715

Barman, S., and Sadhukhan, M. (2012). Facile Bulk Production of Highly Blue Fluorescent Graphitic Carbon Nitride Quantum Dots and Their Application as Highly Selective and Sensitive Sensors for the Detection of Mercuric and Iodide Ions in Aqueous media. *J. Mater. Chem.* 22, 21832–21837. doi:10.1039/c2jm35501a

Barrio, J., Mateo, D., Albero, J., García, H., and Shalom, M. (2019). A Heterogeneous Carbon Nitride-Nickel Photocatalyst for Efficient Low-Temperature CO2 Methanation. *Adv. Energ. Mater.* 9, 1902738. doi:10.1002/Aenm.201902738

Bojdys, M. J., Wohlgemuth, S. A., Thomas, A., and Antonietti, M. (2010). Ionothermal Route to Layered Two-Dimensional Polymer-Frameworks

Based on Heptazine Linkers. *Macromolecules* 43, 6639–6645. doi:10.1021/ma101008c

Chapran, M., Pander, P., Vasylieva, M., Wiosna-Salyga, G., Ulanski, J., Dias, F. B., et al. (2019). Realizing 20% External Quantum Efficiency in Electroluminescence with Efficient Thermally Activated Delayed Fluorescence from an Exciplex. *ACS Appl. Mater. Inter.* 11, 13460–13471. doi:10.1021/acsami.8b18284

Chen, J. X., Wang, K., Zheng, C. J., Zhang, M., Shi, Y. Z., Tao, S. L., et al. (2018). Red Organic Light-Emitting Diode with External Quantum Efficiency beyond 20% Based on a Novel Thermally Activated Delayed Fluorescence Emitter. *Adv. Sci. (Weinh)* 5, 1800436. doi:10.1002/advs.201800436

Chen, L., Huang, D., Ren, S., Dong, T., Chi, Y., and Chen, G. (2013). Preparation of Graphite-like Carbon Nitride Nanoflake Film with strong Fluorescent and Electrochemiluminescent Activity. *Nanoscale* 5, 225–230. doi:10.1039/C2NR32248J

Cheng, Q., He, Y., Ge, Y., Zhou, J., and Song, G. (2018). Ultrasensitive Detection of Heparin by Exploiting the Silver Nanoparticle-Enhanced Fluorescence of Graphitic Carbon Nitride (G-C3n4) Quantum Dots. *Microchim. Acta* 185, 332. doi:10.1007/s00604-018-2864-9

Dai, Y., Li, C., Shen, Y., Lim, T., Xu, J., Li, Y., et al. (2018). Light-tuned Selective Photosynthesis of Azo- and Azoxy-Aromatics Using Graphitic C3N4. *Nat. Commun.* 9, 60. doi:10.1038/S41467-017-02527-8

Endo, A., Sato, K., Yoshimura, K., Kai, T., Kawada, A., Miyazaki, H., et al. (2011). Efficient Up-Conversion of Triplet Excitons into a Singlet State and its Application for Organic Light Emitting Diodes. *Appl. Phys. Lett.* 98, 083302. doi:10.1063/1.3558906

Gao, G., Jiao, Y., Waclawik, E. R., and Du, A. (2016). Single Atom (Pd/pt) Supported on Graphitic Carbon Nitride as an Efficient Photocatalyst for Visible-Light Reduction of Carbon Dioxide. *J. Am. Chem. Soc.* 138, 6292–6297. doi:10.1021/jacs.6b02692

Gmelin, L. (1835). Ueber einige verbindungen des melon's. *Ann. Pharm.* 15, 252–258. doi:10.1002/jlac.18350150306

Goushi, K., Yoshida, K., Sato, K., and Adachi, C. (2012). Organic Light-Emitting Diodes Employing Efficient Reverse Intersystem Crossing for Triplet-To-Singlet State Conversion. *Nat. Photon* 6, 253–258. doi:10.1038/nphoton.2012.31

Hosmane, R. S., Rossman, M. A., and Leonard, N. J. (1982). Synthesis and Structure of Tri-*s*-triazine. *J. Am. Chem. Soc.* 104, 5497–5499. doi:10.1021/ja00384a046

Iwano, Y., Kittaka, T., Tabuchi, H., Soukawa, M., Kunitsugu, S., Takarabe, K., et al. (2008). Study of Amorphous Carbon Nitride Films Aiming at white Light Emitting Devices. *Jpn. J. Appl. Phys.* 47, 7842–7844. doi:10.1143/jjap.47.7842

Jürgens, B., Irran, E., Senker, J., Kroll, P., Müller, H., and Schnick, W. (2003). Melem (2,5,8-Triamino-Tri-S-Triazine), an Important Intermediate during Condensation of Melamine Rings to Graphitic Carbon Nitride: Synthesis, Structure Determination by X-ray Powder Diffractometry, Solid-State Nmr, and Theoretical Studies. *J. Am. Chem. Soc.* 125, 10288–10300. doi:10.1021/ja0357689

Kailasam, K., Mesch, M. B., Möhlmann, L., Baar, M., Blechert, S., Schwarze, M., et al. (2016). Donor-acceptor-type Heptazine-Based Polymer Networks for Photocatalytic Hydrogen Evolution. *Energy Technol.* 4, 744–750. doi:10.1002/ente.201500478

Kailasam, K., Schmidt, J., Bildirir, H., Zhang, G., Blechert, S., Wang, X., et al. (2013). Room Temperature Synthesis of Heptazine-Based Microporous Polymer Networks as Photocatalysts for Hydrogen Evolution. *Macromol. Rapid Commun.* 34, 1008–1013. doi:10.1002/marc.201300227

Kang, Y., Zhao, L., and Leng, J. (2018). Delocalization of Frontier Orbitals Induced Red Emission for Heptazine Based Thermally Activated Delayed Fluorescence Molecule: First-Principles Study. *Chem. Phys. Lett.* 698, 187–194. doi:10.1016/j.cplett.2018.03.017

Kawasumi, K., Wu, T., Zhu, T., Chae, H. S., Van Voorhis, T., Baldo, M. A., et al. (2015). Thermally Activated Delayed Fluorescence Materials Based on Homoconjugation Effect of Donor-Acceptor Triptycenes. *J. Am. Chem. Soc.* 137, 11908–11911. doi:10.1021/jacs.5b07932

Komatsu, T. (2001). The First Synthesis and Characterization of Cyameluric High Polymers. *Macromol. Chem. Phys.* 202, 19–25. doi:10.1002/1521-3935(20010101)202:1<19::AID-MACP19>3.0.CO;2-G

Kroke, E., Schwarz, M., Horath-Bordon, E., Kroll, P., Noll, B., and Norman, A. D. (2002). Tri-s-triazine Derivatives. Part I. From Trichloro-Tri-S-Triazine to Graphitic C3N4 structuresPart II: Alkalicyamelurates M3[C6N7O3], M = Li, Na, K, Rb, Cs, Manuscript in Preparation. *New J. Chem.* 26, 508–512. doi:10.1039/b111062b

Li, J., Gong, H., Zhang, J., Zhou, S., Tao, L., Jiang, L., et al. (2021). Enhanced Electroluminescence Based on a π-Conjugated Heptazine Derivative by Exploiting Thermally Activated Delayed Fluorescence. *Front. Chem.* 9, 693813. doi:10.3389/fchem.2021.693813

Li, J., Nakagawa, T., MacDonald, J., Zhang, Q., Nomura, H., Miyazaki, H., et al. (2013). Highly Efficient Organic Light-Emitting Diode Based on a Hidden Thermally Activated Delayed Fluorescence Channel in a Heptazine Derivative. *Adv. Mater.* 25, 3319–3323. doi:10.1002/adma.201300575

Li, J., Nomura, H., Miyazaki, H., and Adachi, C. (2014a). Highly Efficient Exciplex Organic Light-Emitting Diodes Incorporating a Heptazine Derivative as an Electron Acceptor. *Chem. Commun.* 50, 6174–6176. doi:10.1039/c4cc01590h

Li, J., Zhang, Q., Nomura, H., Miyazaki, H., and Adachi, C. (2014b). Thermally Activated Delayed Fluorescence from $3n\pi^*$ to $1n\pi^*$ Up-Conversion and its Application to Organic Light-Emitting Diodes. *Appl. Phys. Lett.* 105, 013301. doi:10.1063/1.4887346

Liao, G., Gong, Y., Zhang, L., Gao, H., Yang, G.-J., and Fang, B. (2019). Semiconductor Polymeric Graphitic Carbon Nitride Photocatalysts: The "holy Grail" for the Photocatalytic Hydrogen Evolution Reaction under Visible Light. *Energy Environ. Sci.* 12, 2080–2147. doi:10.1039/c9ee00717b

Liebig, J. (1834). Uber Einige Stickstoff - Verbindungen. *Ann. Pharm.* 10, 1–47. doi:10.1002/jlac.18340100102

Liebig, J. (1835). Ueber Einige Stickstoffverbindungen. *Ann. Phys. Chem.* 110, 570–613. doi:10.1002/andp.18351100403

Lotsch, B. V., Döblinger, M., Sehnert, J., Seyfarth, L., Senker, J., Oeckler, O., et al. (2007). Unmasking Melon by a Complementary Approach Employing Electron Diffraction, Solid-State Nmr Spectroscopy, and Theoretical Calculations-Structural Characterization of a Carbon Nitride Polymer. *Chem. Eur. J.* 13, 4969–4980. doi:10.1002/chem.200601759

Luo, M., Yang, Q., Liu, K., Cao, H., and Yan, H. (2019). Boosting Photocatalytic H2 Evolution on G-C3n4 by Modifying Covalent Organic Frameworks (COFs). *Chem. Commun.* 55, 5829–5832. doi:10.1039/c9cc02144b

Makowski, S. J., Schwarze, A., Schmidt, P. J., and Schnick, W. (2012). Rare-Earth Melonates LnC6N7(NCN)3·xH2O (Ln = La, Ce, Pr, Nd, Sm, Eu, Tb; X = 8-12): Synthesis, Crystal Structures, Thermal Behavior, and Photoluminescence Properties of Heptazine Salts with Trivalent Cations. *Eur. J. Inorg. Chem.* 2012, 1832–1839. doi:10.1002/ejic.201101251

Ong, W.-J., Tan, L.-L., Ng, Y. H., Yong, S.-T., and Chai, S.-P. (2016). Graphitic Carbon Nitride (G-C3n4)-Based Photocatalysts for Artificial Photosynthesis and Environmental Remediation: Are We a Step Closer to Achieving Sustainability?. *Chem. Rev.* 116, 7159–7329. doi:10.1021/acs.chemrev.6b00075

Patnaik, S., Sahoo, D. P., and Parida, K. (2021). Recent Advances in Anion Doped G-C3n4 Photocatalysts: A Review. *Carbon* 172, 682–711. doi:10.1016/j.carbon.2020.10.073

Pauling, L., and Sturdivant, J. H. (1937). The Structure of Cyameluric Acid, Hydromelonic Acid and Related Substances. *Proc. Natl. Acad. Sci.* 23, 615–620. doi:10.1073/pnas.23.12.615

Sayed, S. M., Deng, L. L., Lin, B. P., and Yang, H. (2017). A Room-Temperature Heptazine Core Discotic Liquid crystal. *Liq. Cryst.* 44, 2175–2183. doi:10.1080/02678292.2017.1371343

Shahbaz, M., Urano, S., LeBreton, P. R., Rossman, M. A., Hosmane, R. S., and Leonard, N. J. (1984). Tri-*s*-triazine: Synthesis, Chemical Behavior, and Spectroscopic and Theoretical Probes of Valence Orbital Structure. *J. Am. Chem. Soc.* 106, 2805–2811. doi:10.1021/ja00322a014

Sohn, S., Ha, M. W., Park, J., Kim, Y.-H., Ahn, H., Jung, S., et al. (2020). High-efficiency Diphenylpyrimidine Derivatives Blue Thermally Activated Delayed Fluorescence Organic Light-Emitting Diodes. *Front. Chem.* 8, 356. doi:10.3389/fchem.2020.00356

Su, F., Mathew, S. C., Lipner, G., Fu, X., Antonietti, M., Blechert, S., et al. (2010). mpg-C3N4-Catalyzed Selective Oxidation of Alcohols Using O2and Visible Light. *J. Am. Chem. Soc.* 132, 16299–16301. doi:10.1021/ja102866p

Tanaka, H., Shizu, K., Nakanotani, H., and Adachi, C. (2013). Twisted Intramolecular Charge Transfer State for Long-Wavelength Thermally Activated Delayed Fluorescence. *Chem. Mater.* 25, 3766–3771. doi:10.1021/cm402428a

Tang, W., Tian, Y., Chen, B., Xu, Y., Li, B., Jing, X., et al. (2020). Supramolecular Copolymerization Strategy for Realizing the Broadband White Light

Luminescence Based on N-Deficient Porous Graphitic Carbon Nitride (G-C3n4). *ACS Appl. Mater. Inter.* 12, 6396–6406. doi:10.1021/acsami.9b19338

Turro, N. J., Ramamurthy, V., and Scaiano, J. C. (2010). *Modern Molecular Photochemistry of Organic Molecules*. Melville, NY, USA: University Science Books.

Uoyama, H., Goushi, K., Shizu, K., Nomura, H., and Adachi, C. (2012). Highly Efficient Organic Light-Emitting Diodes from Delayed Fluorescence. *Nature* 492, 234–238. doi:10.1038/nature11687

Wang, S., Zhang, J., Li, B., Sun, H., and Wang, S. (2021). Engineered Graphitic Carbon Nitride-Based Photocatalysts for Visible-Light-Driven Water Splitting: A Review. *Energy Fuels* 35, 6504–6526. doi:10.1021/acs.energyfuels.1c00503

Wang, X., Maeda, K., Thomas, A., Takanabe, K., Xin, G., Carlsson, J. M., et al. (2009). A Metal-free Polymeric Photocatalyst for Hydrogen Production from Water under Visible Light. *Nat. Mater* 8, 76–80. doi:10.1038/NMAT2317

Wen, J., Li, R., Lu, R., and Yu, A. (2018). Photophysics and Photocatalysis of Melem: A Spectroscopic Reinvestigation. *Chem. Asian J.* 13, 1060–1066. doi:10.1002/asia.201800186

Wu, T. L., Liao, S. Y., Huang, P. Y., Hong, Z. S., Huang, M. P., Lin, C. C., et al. (2019). Exciplex Organic Light-Emitting Diodes with Nearly 20% External Quantum Efficiency: Effect of Intermolecular Steric Hindrance between the Donor and Acceptor Pair. *ACS Appl. Mater. Inter.* 11, 19294–19300. doi:10.1021/acsami.9b04365

Wu, Z., and Ma, D. (2016). Recent Advances in white Organic Light-Emitting Diodes. *Mater. Sci. Eng. R: Rep.* 107, 1–42. doi:10.1016/j.mser.2016.06.001

Xing, Y., Yin, L., Zhao, Y., Du, Z., Tan, H.-Q., Qin, X., et al. (2020). Construction of the 1D Covalent Organic Framework/2D G-C3n4 Heterojunction with High Apparent Quantum Efficiency at 500 Nm. *ACS Appl. Mater. Inter.* 12, 51555–51562. doi:10.1021/acsami.0c15780

Yadav, R. M., Kumar, R., Aliyan, A., Dobal, P. S., Biradar, S., Vajtai, R., et al. (2020). Facile Synthesis of Highly Fluorescent Free-Standing Films Comprising Graphitic Carbon Nitride (G-C3n4) Nanolayers. *New J. Chem.* 44, 2644–2651. doi:10.1039/c9nj05108b

Yang, C., Folens, K., Du Laing, G., Artizzu, F., and Van Deun, R. (2020). Improved Quantum Yield and Excellent Luminescence Stability of Europium-Incorporated Polymeric Hydrogen-Bonded Heptazine Frameworks Due to an Efficient Hydrogen-Bonding Effect. *Adv. Funct. Mater.* 30, 2003656. doi:10.1002/adfm.202003656

Yin, X., He, Y., Wang, X., Wu, Z., Pang, E., Xu, J., et al. (2020). Recent Advances in Thermally Activated Delayed Fluorescent Polymer-Molecular Designing Strategies. *Front. Chem.* 8, 725. doi:10.3389/fchem.2020.00725

YunYang, Y., Lei, W., Xu, Y., Zhou, T., Xia, M., and Hao, Q. (2018). Determination of Trace Uric Acid in Serum Using Porous Graphitic Carbon Nitride (G-C3n4) as a Fluorescent Probe. *Mikrochim Acta* 185, 39. doi:10.1007/s00604-017-2533-4

Zeng, W. X., Lai, H. Y., Lee, W. K., Jiao, M., Shiu, Y. J., Zhong, C., et al. (2018a). Achieving Nearly 30% External Quantum Efficiency for orange-red Organic Light Emitting Diodes by Employing Thermally Activated Delayed Fluorescence Emitters Composed of 1,8-Naphthalimide-Acridine Hybrids. *Adv. Mater.* 30, 1704961. doi:10.1002/adma.201704961

Zeng, Y., Liu, X., Liu, C., Wang, L., Xia, Y., Zhang, S., et al. (2018b). Scalable One-step Production of Porous Oxygen-Doped G-C3n4 Nanorods with Effective Electron Separation for Excellent Visible-Light Photocatalytic Activity. *Appl. Catal. B: Environ.* 224, 1–9. doi:10.1016/j.apcatb.2017.10.042

Zhang, M., Zheng, C.-J., Lin, H., and Tao, S.-L. (2021). Thermally Activated Delayed Fluorescence Exciplex Emitters for High-Performance Organic Light-Emitting Diodes. *Mater. Horiz.* 8, 401–425. doi:10.1039/d0mh01245a

Zhang, Q., Li, B., Huang, S., Nomura, H., Tanaka, H., and Adachi, C. (2014). Efficient Blue Organic Light-Emitting Diodes Employing Thermally Activated Delayed Fluorescence. *Nat. Photon* 8, 326–332. doi:10.1038/Nphoton.2014.12

Zhang, Q., Li, J., Shizu, K., Huang, S., Hirata, S., Miyazaki, H., et al. (2012). Design of Efficient Thermally Activated Delayed Fluorescence Materials for Pure Blue Organic Light Emitting Diodes. *J. Am. Chem. Soc.* 134, 14706–14709. doi:10.1021/ja306538w

Zhang, S., Gu, P., Ma, R., Luo, C., Wen, T., Zhao, G., et al. (2019). Recent Developments in Fabrication and Structure Regulation of Visible-Light-Driven G-C3n4-Based Photocatalysts towards Water Purification: A Critical Review. *Catal. Today* 335, 65–77. doi:10.1016/j.cattod.2018.09.013

Zhang, W., Xu, C., Kobayashi, T., Zhong, Y., Guo, Z., Zhan, H., et al. (2020). Hydrazone-Linked Heptazine Polymeric Carbon Nitrides for Synergistic Visible-Light-Driven Catalysis. *Chem. Eur. J.* 26, 7358–7364. doi:10.1002/chem.202000934

Zhang, X., Xie, X., Wang, H., Zhang, J., Pan, B., and Xie, Y. (2013a). Enhanced Photoresponsive Ultrathin Graphitic-phase C3N4 Nanosheets for Bioimaging. *J. Am. Chem. Soc.* 135, 18–21. doi:10.1021/ja308249k

Zhang, Y., Pan, Q., Chai, G., Liang, M., Dong, G., Zhang, Q., et al. (2013b). Synthesis and Luminescence Mechanism of Multicolor-Emitting G-C3n4 Nanopowders by Low Temperature thermal Condensation of Melamine. *Sci. Rep.* 3, 1943. doi:10.1038/srep01943

Zhao, Z., Sun, Y., Luo, Q., Dong, F., Li, H., and Ho, W.-K. (2015). Mass-Controlled Direct Synthesis of Graphene-like Carbon Nitride Nanosheets with Exceptional High Visible Light Activity. Less Is Better. *Sci. Rep.* 5, 14643. doi:10.1038/srep14643

Zheng, H. B., Chen, W., Gao, H., Wang, Y. Y., Guo, H. Y., Guo, S. Q., et al. (2017). Melem: An Efficient Metal-free Luminescent Material. *J. Mater. Chem. C* 5, 10746–10753. doi:10.1039/c7tc02966g

Zhou, J., Yang, Y., and Zhang, C.-y. (2013). A Low-Temperature Solid-phase Method to Synthesize Highly Fluorescent Carbon Nitride Dots with Tunable Emission. *Chem. Commun.* 49, 8605–8607. doi:10.1039/c3cc42266f

Zhou, Z., Pei, Z., Wei, L., Zhao, S., Jian, X., and Chen, Y. (2020). Electrocatalytic Hydrogen Evolution under Neutral pH Conditions: Current Understandings, Recent Advances, and Future Prospects. *Energ. Environ. Sci.* 13, 3185–3206. doi:10.1039/d0ee01856b

Zhou, Z., Wei, L., Wang, Y., Karahan, H. E., Chen, Z., Lei, Y., et al. (2017). Hydrogen Evolution Reaction Activity of Nickel Phosphide Is Highly Sensitive to Electrolyte pH. *J. Mater. Chem. A.* 5, 20390–20397. doi:10.1039/c7ta06000a

Zhou, Z., Yuan, Z., Li, S., Li, H., Chen, J., Wang, Y., et al. (2019). Big to Small: Ultrafine Mo 2 C Particles Derived from Giant Polyoxomolybdate Clusters for Hydrogen Evolution Reaction. *Small* 15, 1900358. doi:10.1002/Smll.201900358

Conflict of Interest: The authors declare that the research was conducted in the absence of any commercial or financial relationships that could be construed as a potential conflict of interest.

frontiers in Chemistry

ORIGINAL RESEARCH
published: 06 August 2021
doi: 10.3389/fchem.2021.727631

Design and Synthesis of AIE-Based Small-Molecule and Nanofibrous Film for Fluorescent Sensing Application

Chunping Ma[1,2], Zhiyi Li[1], Chenglin Zhang[3], Gaoyi Xie[3], Yancheng Wu[1], Yangfan Zhang[1], Jinpeng Mo[1], Xi Liu[1]*, Ke Wang[4], Dong Xie[4] and Yang Li[2]**

[1]Guangdong-Hong Kong Joint Laboratory for New Textile Materials, School of Textile Materials and Engineering, Wuyi University, Jiangmen, China, [2]School of Materials and Energy Engineering, Guizhou Institute of Technology, Guiyang, China, [3]School of Biotechnology and Health Sciences, Wuyi University, Jiangmen, China, [4]Institute of Bioengineering, Guangdong Academy of Sciences, Guangzhou, China

Fluorescent sensors that respond to environmental conditions (temperature, pressure, and pH) have attracted widespread attention in recent years. Generally, traditional solid-state fluorescent materials tend to suffer from aggregation-induced quenching (ACQ) and difficulty of film forming, limiting their extensive applications. Therefore, researchers are focusing more and more attention on fluorescent sensors with aggregation-induced emission (AIE) effects. Herein, the article reports an AIE molecule (TPEBZMZ) containing tetraphenylethylene (TPE) and benzimidazole fragments. The fluorescence properties of TPEBZMZ in solution and aggregation states have been investigated, and the luminescence performance and aggregation structures of solid-state TPEBZMZ after force and acid treatments have been explored. The results show obvious AIE and fluorescent sensing properties of TPEBZMZ, presenting force- and acid-induced discolorations. Moreover, the TPEBZMZ-based fluorescent nanofibrous film is fabricated by electrospinning the solution of TPEBZMZ blended with polylactic acid (PLA), which shows a good nanofiber film structure and exhibits reversible acid-induced discoloration property, even with only 0.5 wt% TPEBZMZ. This work provides a simple strategy to achieve stimulus-responsive fluorescent film.

Keywords: fluorescent sensing, AIE, nanofibrous film, acid-induced discoloration, luminescence performance

OPEN ACCESS

Edited by:
Haichang Zhang,
Qingdao University of Science and Technology, China

Reviewed by:
Cheng Zhou,
National University of Singapore, Singapore
Zhu Mao,
Shenzhen Institutes of Advanced Technology (CAS), China

****Correspondence:***
Gaoyi Xie
xiegaoyi@126.com
Xi Liu
liuxi_wyu@163.com
Yang Li
20130214@git.edu.cn

Specialty section:
This article was submitted to Organic Chemistry, a section of the journal Frontiers in Chemistry

Received: *19 June 2021*
Accepted: *06 July 2021*
Published: *06 August 2021*

Citation:
Ma C, Li Z, Zhang C, Xie G, Wu Y, Zhang Y, Mo J, Liu X, Wang K, Xie D and Li Y (2021) Design and Synthesis of AIE-Based Small-Molecule and Nanofibrous Film for Fluorescent Sensing Application. Front. Chem. 9:727631. doi: 10.3389/fchem.2021.727631

INTRODUCTION

Fluorescent films composed of π-conjugated materials-based fluorescent sensors and membranous materials are promising sensor technology due to their real-time detection, easy fabrication, non-invasiveness detection, and mechanical stability and flexibility (Guan et al., 2015; Miao et al., 2016). In recent years, they have been widely used in detecting residual pesticides (Peng et al., 2021), enzymes (Zhao et al., 2017a; Zhao et al., 2017b), pollutants (Lee et al., 2019; Zhao et al., 2020b; Sun et al., 2021), explosives (Zhou et al., 2014; Sun et al., 2015; Li et al., 2018; Hao et al., 2021), metal ions (Chen et al., 2020), gases (Moscoso et al., 2020), and temperature and humidity (Jiang et al., 2020; Li et al., 2020), which greatly expanded the applications of fluorescence sensors. Generally, high selectivity and sensitivity are the key characteristics of a successful membranous fluorescent sensor (Sun et al., 2015). Selectivity is mainly related to the specific interaction between fluorescent probe and environmental stimulus or detection objects (Zhou et al., 2017), showing differentiated luminescence characteristics, while sensitivity is primarily determined by fluorescence intensity

(Song et al., 2015). Traditional fluorescent materials usually present weak fluorescence in the solid state but high fluorescence in solution due to the widely known aggregation-caused quenching (ACQ) effect. ACQ greatly limits the application of traditional fluorescence materials (Hong et al., 2011). Aggregation-induced emission (AIE), proposed by Tang's research team in 2001, can be used as a perfect solution to the ACQ issue (Luo et al., 2001). AIE behavior is just the opposite of the ACQ fluorescence behavior of traditional fluorescent compounds: AIE luminogen (AIEgen) emits weak fluorescence in solution, whereas it emits strong fluorescence when aggregated or in a solid state (Luo et al., 2001). The AIE phenomenon is related to intermolecular rotation, restricting these rotations in solid state, inducing the fluorescent emission of the corresponding compound (Qin et al., 2012; Liu et al., 2019; Zhao et al., 2020a). Therefore, AIEgen-based films will show specifically emissive characteristics. Thus, AIEgen-based fluorescent films will provide an effective strategy for the development of fluorescent film sensors.

Electrospinning is an effective method to obtain polymer-based nanofibrous films, compared with casting films, showing a larger specific surface area and higher porosity (Xue et al., 2019). Thus, fluorescent films fabricated by electrospinning can improve the sensitivity and response rate (Zhao et al., 2017b). Therefore, much attention has been devoted to nanofibrous fluorescent films to explore their specific sensing properties. For example, Li et al. (2019) have developed an epoxy resin system functionalized with the typical AIE tetraphenylethylene (TPE) groups, forming nanofibrous films by electrospinning, and finally obtained temperature-sensitive fluorescent films probes. Yang et al. (Yang et al., 2018) have reported specific composite nanofibrous films by electrospinning of AIE small molecules (oME-TPA) and polyvinyl alcohol (PVA) and further studied its piezochromic properties related to sensitivities. Zhao et al. (2017a) have grafted TPE derivatives and phloxine B onto electrospun nanofiber film, inducing the static quenching of phloxine B through protamine adsorption and combining them with the aggregation of TPE-based groups, promoting fluorescence emission of nanofiber, which realized effective monitoring of different concentrations of heparin. Therefore, the design and development of novel AIE molecules containing nanofiber fluorescent films will benefit the realization of efficient fluorescent sensing applications.

Herein, we report a novel compound (TPEBZMZ) containing the classic AIE group tetraphenylethylene (TPE) and benzimidazole unit. The TPE group renders the TPEBZMZ molecule AIE property, and the structure of the benzimidazole unit will offer the potential of acid-induced discoloration. The relationship between the structure, aggregate, and luminescence properties of TPEBZMZ in different states and force and acid treatments has been systematically studied. Specifically, TPEBZMZ shows an obvious AIE phenomenon and fluorescent sensing properties of force- and acid-induced discolorations. More importantly, we prepared TPEBZMZ-based fluorescent nanofibrous film by electrospinning the solution of TPEBZMZ blended with polylactic acid (PLA), and the nanofibrous film displays a good reversible acid-induced discoloration property. Significantly, this work provides a simple strategy to prepare fluorescent sensing film.

MATERIALS AND METHODS

Materials

1-Bromo-1,2,2-triphenylethene (P_3Br) was purchased from Macklin Biochemical Co., Ltd. (Shanghai, China). 4-Formylphenylboronic acid, tetrabutylammonium bromide (TBAB), tetrakis(triphenylphosphine) palladium [$Pd(PPh_3)_4$], 2-(cyanomethyl) benzimidazole, and tetrabutylammonium hydroxide (TBAH) were purchased from Energy Chemical. Polylactic acid (PLA, 4032D) was purchased from NarureWorks (America). All of the above reagents were used as received. Potassium carbonate (K_2CO_3), potassium hydroxide (KOH), tetrahydrofuran (THF), ethanol, and dichloromethane (DCM) were purchased the analytical grade from Guangzhou Chemical Reagent Factory (Guangzhou, China) and used without further purification.

Synthesis of P_4A and (E)-2-(1H-Benzo[d] imidazol-2-yl)-3-(4-(1,2,2-triphenylvinyl) phenyl) Acrylonitrile (TPEBZMZ)

The intermediate of P_4A was synthesized according to a previous literature method (Xu et al., 2013).

P_4A (1.080 g, 3 mmol), 2-(cyanomethyl) benzimidazole (0.471 g, 3 mmol), and ethanol (20 ml) were mixed and stirred in a 50 ml two-necked round-bottomed flask at room temperature. After adding tetrabutylammonium hydroxide (TBAH, 0.8 M, 10 drops) dropwise, the mixture was stirred continually at room temperature for 4 h. The precipitate was filtrated and washed three times using ethanol, resulting in a yellow powder (1.087 g, yield 72.6%). ^{1}H NMR (500 MHz, $CDCl_3$) δ (ppm): 9.58 (s, 1 H), 8.41 (s, 1 H), 7.77 (d, 2 H, J = 8.32 Hz), 7.34 (dd, 2 H, J = 3.12, 6.09 Hz), 6.01–7.23 (m, 19 H). ^{13}C NMR (125 MHz, $CDCl_3$) δ (ppm): 148.35, 146.46, 146.34, 143.19, 143.09, 143.01, 139.81, 132.19, 131.37, 131.33, 131.29, 130.55, 129.61, 127.99, 127.95, 127.71, 127.12, 126.86, 117.01, 98.63. FT-IR (KBr): 2924, 2854, 1593, 1491, 1443, 747, 700, 616. ESI-MS, m/z: 500.21 ([M + H+], calcd for C36H26N3, 500.20).

Characterization

^{1}H NMR and ^{13}C NMR spectra were recorded on a Bruker AVANCE NEO 500 spectrometer. Mass spectra were measured on an LTQ Orbitrap LCMS spectrometer. FT-IR spectra were recorded using Nicolet iS5 spectrometer (KBr pellet). UV–visible absorption spectra (UV–vis) were obtained via a SHIMADZU UV-2700 spectrophotometer. Fluorescence spectra (PL) were determined by a Shimadzu RF-6000 spectrometer with a slit width of 3 nm for excitation and 5 nm for emission. Thermal behaviors were studied using differential scanning calorimetry (DSC) on a NETZSCH thermal analyzer (DSC214Polyma) with both heating and cooling rates of 20°C/min under a N_2 atmosphere. Powder X-ray diffraction (PXRD) measurements were carried out at 298 K on a Rigaku X-ray

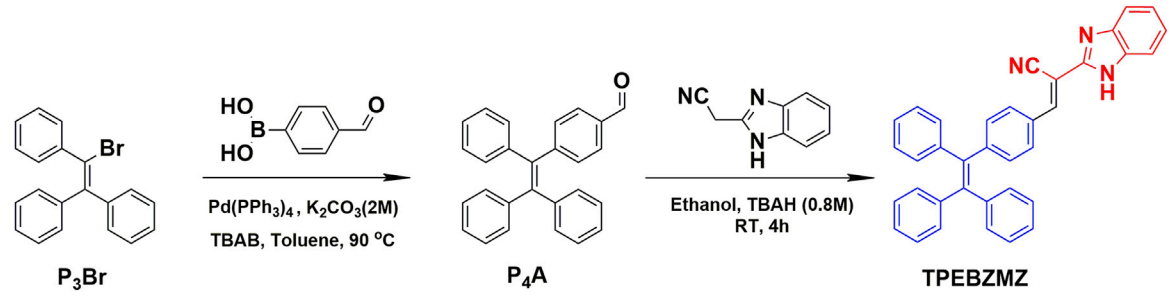

SCHEME 1 | Synthetic route and chemical structure of TPEBZMZ.

diffractometer (Ultima IV, Japan) with an X-ray source of Cu Kα (λ = 0.1541 nm) at 40 kV and 40 mA, at a scan rate of 5°(2θ)/min from 5° to 60°. The frontier molecular orbital distributions of TPEBZMZ and acid fumed TPEBZMZ (TPEBZMZ-HCl) were determined using density functional theory (DFT) using Gaussian 09 at the B3LYP/6-311G(d,p) level. After 1 min of gold coating, the surface morphologies of nanofibers were observed by a scanning electron microscope (Sigma 500, Zeiss, German) equipped with an in-lens detector at 15 kV. Fluorescent microscopic images were recorded on a laser confocal microscope (Leica DMI8, Germen) in an XY scan mode, using an argon ion laser source with a wavelength of 488 nm.

Electrospinning Process of PLA-TPEBZMZ and PLA Nanofibrous Films

The electrospinning process was performed on an E05 electrospinning apparatus (supplied by Lepton Technology Co., Ltd., Foshan, China), using a 10 wt% PLA/(DMF:DCM = 1:2) solution with or without 0.05 wt% TPEBZMZ as a spinning solution. The nanofibers were collected by a rotating metal cylinder (100 r/min) covered with release paper, with an immobile distance of 20 cm away from the needle tip of the spinneret (0.7 mm inner diameter). The spinning voltage and fluid flow rate were set to 12 kV and 2 ml/h, respectively. The obtained nanofibrous films were dried in a vacuum oven at 70°C for another 12 h to remove the residual solvent completely.

RESULT AND DISCUSSION

Synthesis and Characterization

The synthetic route of TPEBZMZ is shown in **Scheme 1**. The intermediate molecule P_4A was acquired *via* Suzuki coupling from P_3Br and 4-formylphenylboronic acid. The final product TPEBZMZ was obtained by Knoevenagel reaction with P_4A and 2-(cyanomethyl) benzimidazole. As shown in **Supplementary Figures 1–4**, TPEBZMZ was characterized using ^{1}H NMR and ^{13}C NMR spectroscopies, mass spectrometry, and Fourier transform infrared spectroscopy, confirming that the target compound TPEBZMZ has been successfully synthesized. The thermal stability of TPEBZMZ was investigated by thermal gravity analysis (TGA) under a nitrogen atmosphere, and the result is presented in **Supplementary Figure 5**. TPEBZMZ showed good thermal stability with 5% weight loss at a temperature (T_d) of 366°C.

AIE Property of TPEBZMZ

Due to the state-of-the-art AIE functional unit, TPE, we proposed that the TPEBZMZ molecule can exhibit the AIE effect, which was firstly examined by the photoluminescence (PL) fluorescence emission spectra of TPEBZMZ/THF/H_2O solutions with different water content. The resulting spectra, the plot of PL intensity vs. water fraction, and the fluorescence photo images of specific water fraction are shown in **Figure 1A**. The fluorescence emission of the TPEBZMZ/THF solution in the presence of only the good solvent THF is very weak, and the fluorescence of the solution is almost invisible to the naked eye. When the water content is lower than 70%, the fluorescence spectra show few changes. In contrast, the fluorescence intensity increases sharply, when the water content reaches 80%, and the fluorescence intensity is about 36 times compared to 0% water content. The fluorescence intensity begins to decrease after the water content is further increased to 90%, within a sharp drop of fluorescence intensity at 98% of water content. We speculate that the reason for the change in fluorescence intensity is because TPEBZMZ aggregation started with 80% of water content, and the size of aggregates increased gradually when the water fraction increased to 98%, leading to a remarkable light scattering phenomenon (Thomas et al., 2007). Thus, the PL fluorescence experiment preliminarily confirmed the AIE property of TPEBZMZ.

Optical absorption properties of TPEBZMZ/THF/H_2O solutions with different water content were investigated using UV–vis absorption spectroscopy. As shown in **Figure 1B**, the solution absorption spectra exhibit similar characteristics under 0–70% water content, while the obvious decreases of absorption intensities were demonstrated in >80% water content solutions. Moreover, the spectra of >80% water content show the obvious tailing phenomenon in absorption curves, especially presented in the 98% water content solution, which can be attributed to the Mie scattering effect of nano aggregates (Zhang et al., 2015). The tendency of absorption spectra is consistent with the results of fluorescence emission spectra of TPEBZMZ/THF/H_2O mixture solution with different water content. These results further

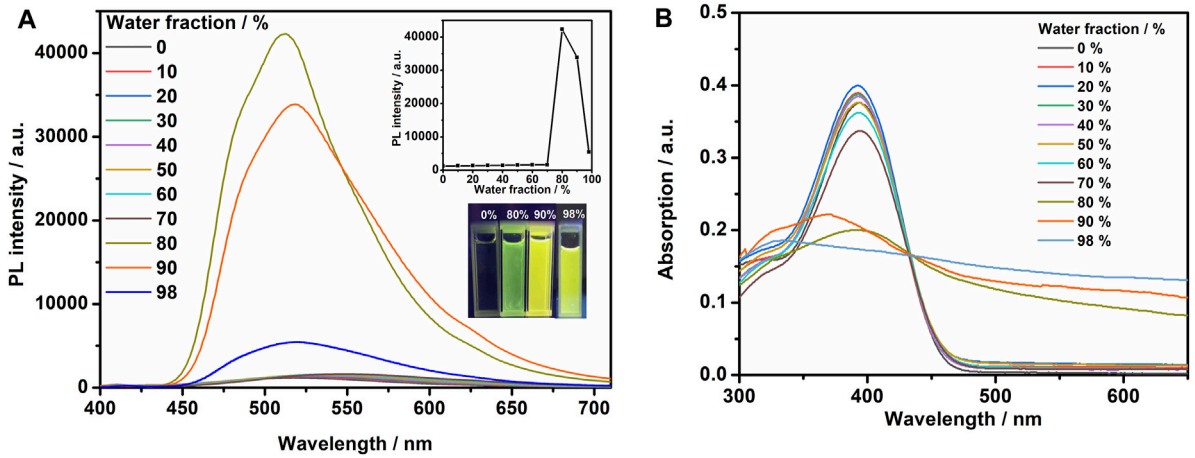

FIGURE 1 | (A) Fluorescence spectra of TPEBZMZ in THF/water mixed solvents (10 mM) with different water fractions. The insets show changes in peak intensity of the fluorescence spectra and emission images of the compounds in different water fraction mixtures under 365 nm UV illumination. **(B)** UV–vis absorption spectra of TPEBZMZ in THF/water mixed solvents (10 mM) with different water fractions.

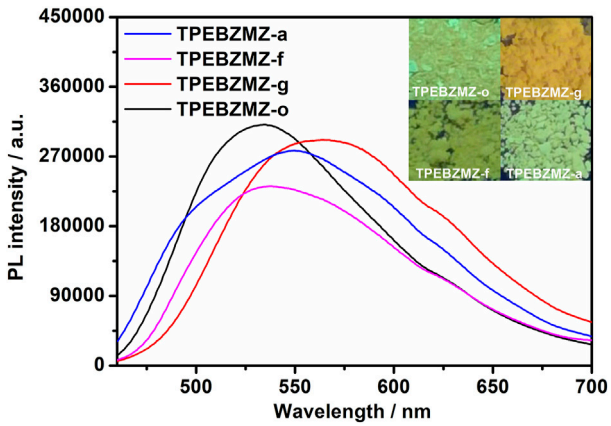

FIGURE 2 | Fluorescence spectra and images of TPEBZMZ: TPEBZMZ-o, the original powder; TPEBZMZ-g, ground powder from TPEBZMZ-o; TPEBZMZ-f, CH_2Cl_2-fumed (2 h) powder from TPEBZMZ-g; TPEBZMZ-a, annealed (240°C, 1 h) powder from TPEBZMZ-g.

confirmed that TPEBZMZ shows the AIE effect, which will benefit its further fluorescent sensor application.

Mechanochromism Property of TPEBZMZ

To evaluate the stimulus-response characteristic of TPEBZMZ, we first tested the fluorescence performance of the original TPEBZMZ (TPEBZMZ-o) powder. As shown in **Figure 2**, TPEBZMZ-o shows a strong yellow-green fluorescence emission with a PL peak at 534 nm. The ground powder (TPEBZMZ-g) was obtained by grinding TPEBZMZ-o, which releases an orange-yellow fluorescence emission with a PL peak of 565 nm. The 31 nm red shift of fluorescence peaks of TPEBZMZ-o and TPEBZMZ-g demonstrated that the preliminary mechanochromism property of TPEBZMZ. The fluorescence color returned to yellow-green when the TPEBZMZ-g sample was treated with dichloromethane (DCM) fumigation (TPEBZMZ-f), and TPEBZMZ-f shows a blue-shift fluorescence spectrum, showing a similar wavelength range of TPEBZMZ-o. The annealed sample (TPEBZMZ-a) of TPEBZMZ-g also exhibits a similar effect with a blue-shift of fluorescence spectrum. Moreover, the results of the cycling measurement (**Supplementary Figure 6**) indicate that TPEBZMZ displays good reversible mechanochromism properties.

Solid-state TPEBZMZ changes from yellow-green to orange-yellow after being mechanically stimulated. We speculate that the reason is the change in the aggregation state of the TPEBZMZ molecules due to the action of external mechanical forces (Ma et al., 2016; Ma et al., 2017). Accordingly, the aggregate structures of the TPEBZMZ powder with different treatments were investigated by powder X-ray diffraction (PXRD) measurements. As shown in **Figure 3A**, a large number of sharp diffraction peaks appeared in the PXRD curve of TPEBZMZ-o, suggesting a relatively regular molecular arrangement and good crystallinity presented in the initial state of TPEBZMZ. While the ground sample TPEBZMZ-g shows weak and even disappeared diffraction peaks, it indicates a relatively disordered and amorphous state exhibited in the TPEBZMZ-g sample. Moreover, the diffraction peaks are partially restored while TPEBZMZ-g is annealed, and the major peaks of the fumed TPEBZMZ-f are also restored and similar to those of TPEBZMZ-o. These results demonstrated the varied aggregated structures of TPEBZMZ with different treatments, which is consistent with its mechanochromism property.

Aggregate structures of TPEBZMZ with different treatments were further characterized by differential scanning calorimetry (DSC) measurements. As shown in **Figure 3B**, in the first heating curves, TPEBZMZ-o shows an obvious melting peak at 298°C (enthalpy of 25.80 J/g), while TPEBZMZ-g displays a weak melting peak at 290°C with an enthalpy of 4.63 J/g, suggesting

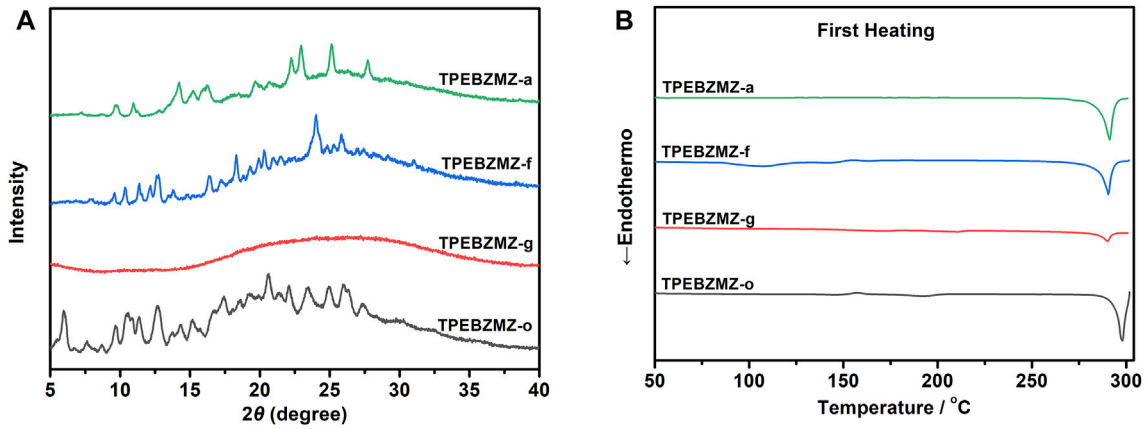

FIGURE 3 | (A) The PXRD patterns of TPEBZMZ; **(B)** DSC curves of TPEBZMZ.

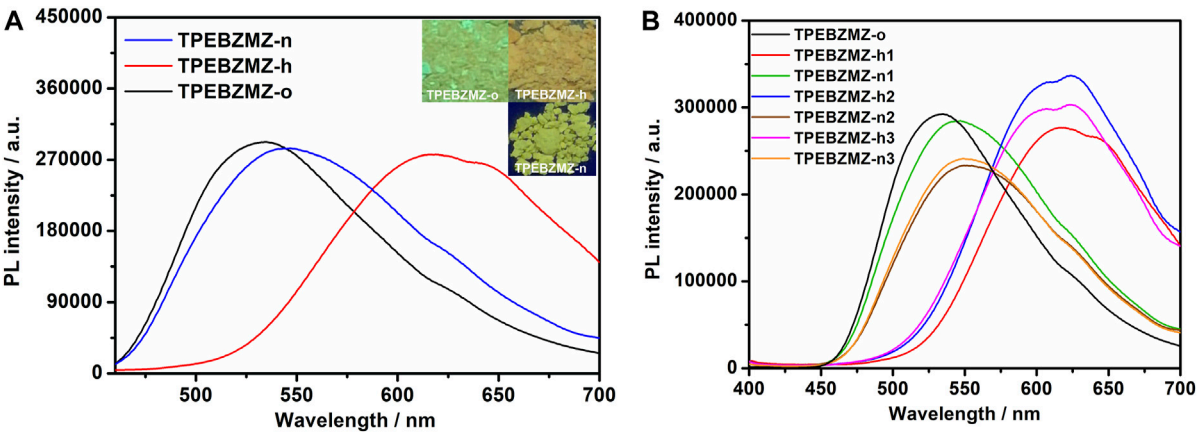

FIGURE 4 | (A) Fluorescence spectra and images of TPEBZMZ: TPEBZMZ-o, the original powder; TPEBZMZ-h, HCl-fumed (10 min) powder from TPEBZMZ-o (HCl gas was released from a 37% concentrated HCl aqueous solution); TPEBZMZ-n, NH_3-fumed (15 min) powder from TPEBZMZ-o (NH_3 gas was released from a 25% concentrated NH_3 aqueous solution). **(B)** Repeated fluorescence switch of TPEBZMZ by HCl fuming and NH_3 fuming cycles.

that the mainly amorphous state is presented in the TPEBZMZ-g sample. TPEBZMZ-f and TPEBZMZ-a also have obvious crystal melting peaks near 290°C, but the melting enthalpies (23.77 J/g and 25.90 J/g, respectively) are slightly lower than or almost the same as TPEBZMZ-o, indicating that a certain rearrangement of amorphous structure of the TPEBZMZ sample appeared under annealing or DCM fumigation treatments.

Acid-Base Discoloration Property of TPEBZMZ

The protonateable benzimidazole unit presented in the TPEBZMZ molecule renders the variable electron cloud density of TPEBZMZ after being protonated, further, in turn, affecting its fluorescence performance. Thus, TPEBZMZ-o was fumigated by hydrogen chloride gas to obtain the protonated acid-fumigated TPEBZMZ powder (TPEBZMZ-h). As shown in **Figure 4A**, the TPEBZMZ-h sample displays orange fluorescence with an emission peak at 589 nm, which shows an obvious red shift of 55 nm compared to the TPEBZMZ-o solid. Furthermore, the TPEBZMZ-h solid fumigated NH_3 vapor (TPEBZMZ-n) shows a fluorescence color turning back to yellow-green, and its fluorescence spectrum is almost restored to that of TPEBZMZ-o. **Figure 4B** shows the repeated fluorescence spectra of TPEBZMZ by HCl fuming and NH_3 fuming cycles, displaying modest repeatability of acid-base discoloration under three cycles. These results prove that the TPEBZMZ powder exhibits good reversible acid-base discoloration performance.

The proposed reaction mechanism about TPEBZMZ treated with HCl and NH_3 is shown in **Figure 5**, and the frontier molecular orbital distributions of TPEBZMZ and HCl-protonated TPEBZMZ (TPEBZMZ-HCl) were further determined using DFT by Gaussian 09 at the B3LYP/6-311G(d,p) level. The electron density distribution of the lowest unoccupied molecular orbital (LUMO) of TPEBZMZ is localized in the central molecule and tends to be fastened to the cyano unit.

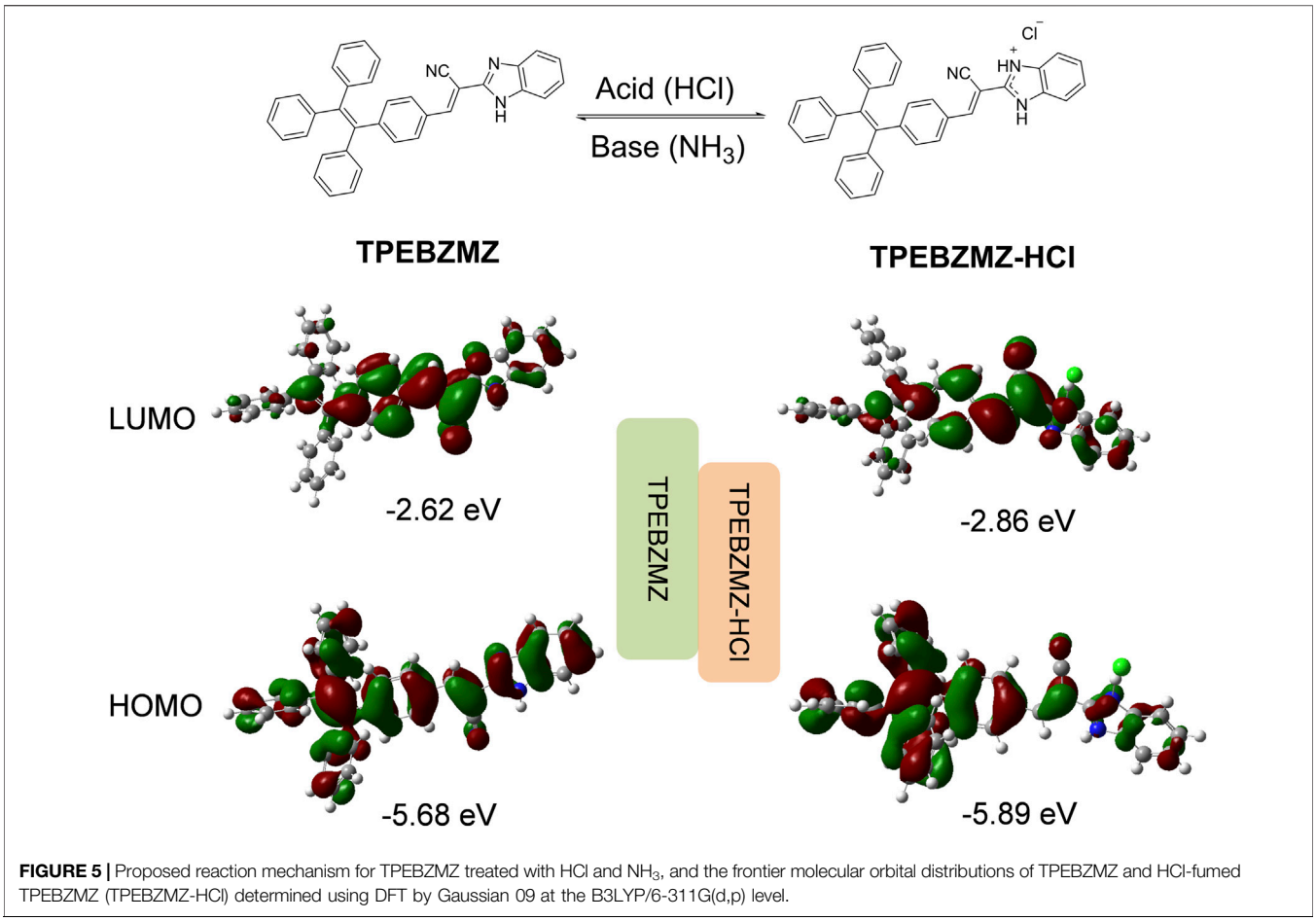

FIGURE 5 | Proposed reaction mechanism for TPEBZMZ treated with HCl and NH_3, and the frontier molecular orbital distributions of TPEBZMZ and HCl-fumed TPEBZMZ (TPEBZMZ-HCl) determined using DFT by Gaussian 09 at the B3LYP/6-311G(d,p) level.

The highest occupied molecular orbital (HOMO) of TPEBZMZ shows a well-proportioned electron density distribution. Moreover, the electron density distributions of the LUMO and HOMO of TPEBZMZ-HCl exhibit a delocalization effect, which tends to localize in the benzimidazole hydrochloride unit and TPE unit, respectively. Correspondingly, TPEBZMZ and TPEBZMZ-HCl exhibit LUMO/HOMO levels of −2.62/−5.68 and −2.86/−5.89 eV, respectively, presenting the bandgaps of 3.06 and 3.03 eV. The red-shift fluorescence spectra of HCl-protonated TPEBZMZ could be attributed to the delocalization effect of its electron density distributions, which may explain the acid-base discoloration property of TPEBZMZ.

Fluorescent Sensing Property of TPEBZMZ-Based Nanofibrous Film

Generally, small-molecule fluorescent powders exhibit poor film-forming properties requiring expensive film-forming equipment (e.g., vacuum evaporator), which will limit their practical application (Hong et al., 2011). To overcome this drawback, TPEBZMZ was blended with a PLA dimethylformamide (DMF)/DCM mix solution by electrospinning to obtain the TPEBZMZ-based nanofibrous film (TPEBZMZ-m). The morphology of TPEBZMZ-m and a pure PLA nanofibrous film was tested using scanning electron microscopy (SEM). The corresponding SEM images are shown in **Figures 6A–D**. TPEBZMZ-m shows an almost similar microstructure compared to that of the pure PLA nanofibrous film, both of which possess filaments with diameters of 500–800 nm.

To evaluate the fluorescent sensing property of TPEBZMZ-m, the acid-induced discoloration experiment was performed. The results of the acid-induced discoloration experiment are shown in **Figure 7A**. Unlike the pure PLA nanofibrous film (**Supplementary Figure 7B**), the nascent TPEBZMZ-m film emits significant green fluorescence under ultraviolet light (confirmed by laser confocal microscope, **Supplementary Figures 7C–E**), even with only 0.5 wt% TPEBZMZ. After fuming by HCl vapor, the resulting film (TPEBZMZ-m-h) exhibits an obvious yellow fluorescence color. Moreover, when the TPEBZMZ-m-h sample was fumed with a NH_3 vapor (TPEBZMZ-m-n), the fluorescence of the sample became green again. To quantitatively characterize the fluorescence emission wavelength of TPEBZMZ-m after different treatments, we used fluorescence spectroscopy to test the electrospinning nanofibrous film samples after different treatments. As shown in **Figure 7A**, the TPEBZMZ-m sample shows a fluorescence emission peak of 496 nm, while the TPEBZMZ-m-h sample exhibits a fluorescence emission peak

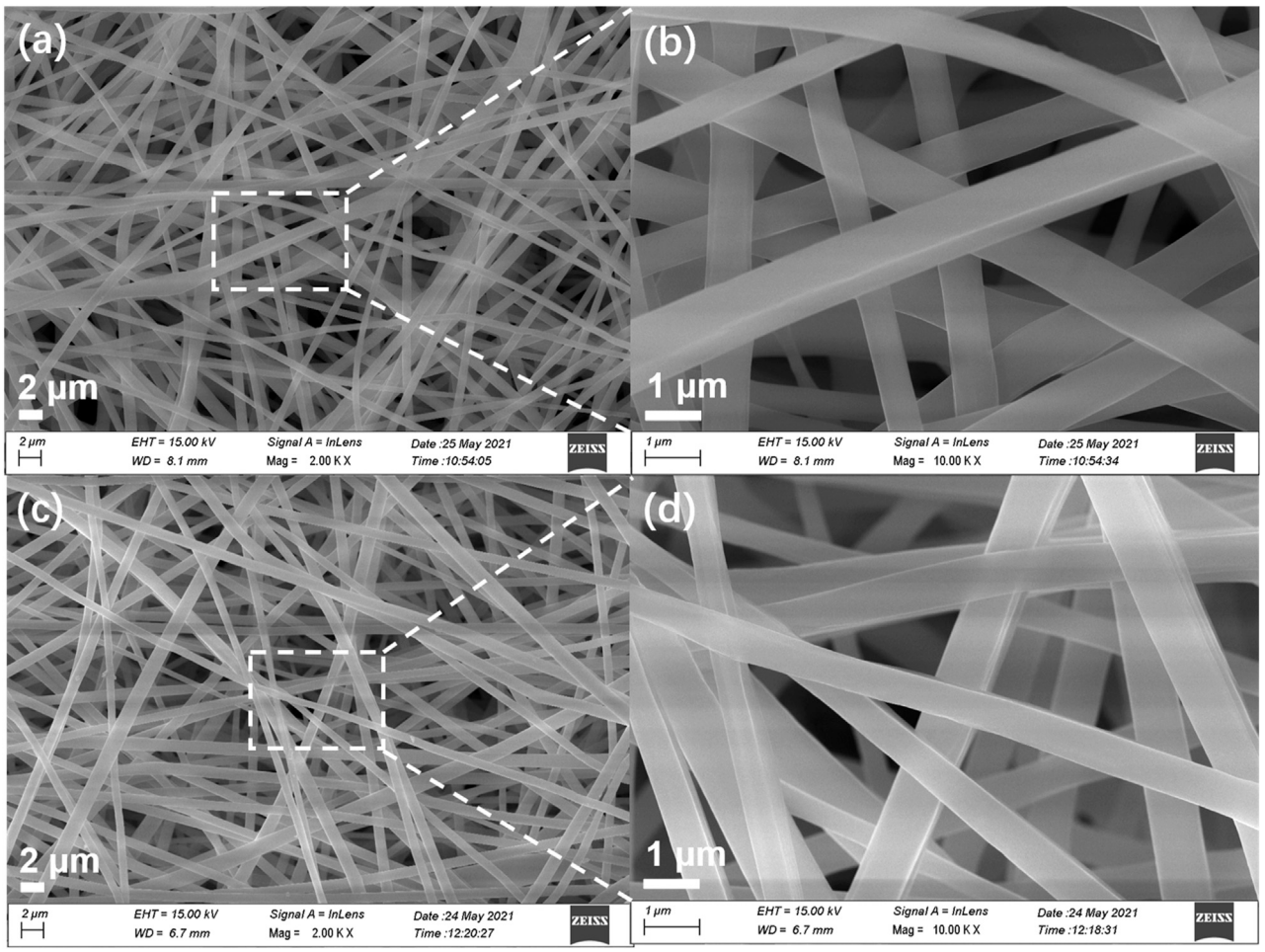

FIGURE 6 | SEM images of **(A,B)** PLA nanofibrous film and **(C,D)** TPEBZMZ-m. **(A,C)** Large scale; **(B,D)** high resolution.

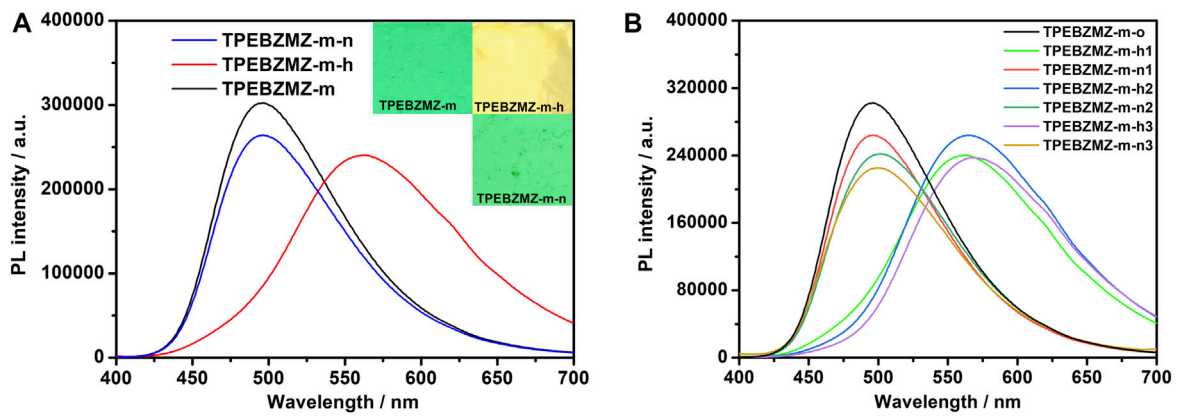

FIGURE 7 | (A) Fluorescence spectra and images of TPEBZMZ-m: TPEBZMZ-m, the original TPEBZMZ-based nanofibrous film; TPEBZMZ-m-h, HCl-fumed (24 h) film from TPEBZMZ-m (HCl gas was released from a 37% concentrated HCl aqueous solution); TPEBZMZ-m-n, NH_3-fumed (15 min) film from TPEBZMZ-m-h (NH_3 gas was released from a 25% concentrated NH_3 aqueous solution). **(B)** Repeated fluorescence switch of TPEBZMZ-m by HCl fuming and NH_3 fuming cycles.

of 563 nm, with a red shift of 67 nm compared to TPEBZMZ-m. Meanwhile, the TPEBZMZ-m-n sample shows an obvious blue-shift fluorescence emission compared to the TPEBZMZ-m-h sample and presenting a fluorescence emission peak at 496 nm, coinciding with the spectroscopy of TPEBZMZ-m. **Figure 7B** shows the repeated fluorescence spectra of TPEBZMZ-m by HCl fuming and NH_3 fuming cycles, displaying good repeatability of acid-base discoloration under three cycles. The well acid-base discoloration repeatability of TPEBZMZ-based nanofibrous film suggests its good potential on fluorescent film sensors application. These results demonstrated that electrospinning acts as a simple and efficient method to prepare TPEBZMZ-based nanofibrous fluorescent film with good reversible acid-induced discoloration property, which provides an effective strategy for developing fluorescent film sensors.

CONCLUSION

In conclusion, we have developed an AIE molecule (TPEBZMZ) containing tetraphenylethylene (TPE) and benzimidazole fragments, which is synthesized from 2-cyanomethylbenzimidazole and 4-(1,2,2-tristyryl) benzaldehyde. TPEBZMZ powder shows obvious AIE and fluorescent sensing properties and exhibits force- and acid-induced discoloration phenomena. More importantly, the TPEBZMZ-based fluorescent nanofibrous film is fabricated by electrospinning the solution of TPEBZMZ blended with polylactic acid (PLA), exhibiting a good nanofiber film structure and well reversible acid-induced discoloration properties. This work demonstrates a simple strategy to achieve stimulus-responsive fluorescent film, which will benefit the development of fluorescent film sensors.

DATA AVAILABILITY STATEMENT

The original contributions presented in the study are included in the article/**Supplementary Material**; further inquiries can be directed to the corresponding author/s.

AUTHOR CONTRIBUTIONS

All authors listed have made a substantial, direct, and intellectual contribution to the work and approved it for publication.

FUNDING

This work was supported by the Guizhou Province Science and Technology Planning Project ((2019)1419, (2019)2845), the Education Department of Guizhou Province (KY(2018)059), the National Natural Science Foundation of China (51803039, 22005224), the Jiangmen City Basic and Theoretical Scientific Research Science and Technology Planning Project (2020JC01019), the Guangdong Basic and Applied Basic Research Funds (2019A1515110944), the Guangdong Science and Technology Major Special Fund (No. 2019-252), the Youth Innovation Talent Project for the Universities of Guangdong Province (2019KQNCX161), and the Wuyi University–Hong Kong/Macau Joint Research Funds (2019WGALH02).

SUPPLEMENTARY MATERIAL

The Supplementary Material for this article can be found online at: https://www.frontiersin.org/articles/10.3389/fchem.2021.727631/full#supplementary-material

REFERENCES

Chen, M., An, J., Hu, Y., Chen, R., Lyu, Y., Hu, N., et al. (2020). Swelling-shrinking Modified Hyperstatic Hydrophilic Perovskite Polymer Fluorescent Beads for Fe(III) Detection. *Sensors Actuators B: Chem.* 325, 128809. doi:10.1016/j.snb.2020.128809

Guan, W., Zhou, W., Lu, J., and Lu, C. (2015). Luminescent Films for Chemo- and Biosensing. *Chem. Soc. Rev.* 44, 6981–7009. doi:10.1039/c5cs00246j

Hao, H., Xu, C., Luo, H., Yang, J., Liu, C., Xu, B., et al. (2021). An AIE Luminogen-Based Electropolymerized Film: an Ultrasensitive Fluorescent Probe for TNP and Fe3+ in Water. *Mater. Chem. Front.* 5, 492–499. doi:10.1039/d0qm00543f

Hong, Y., Lam, J. W. Y., and Tang, B. Z. (2011). Aggregation-induced Emission. *Chem. Soc. Rev.* 40, 5361. doi:10.1039/C1CS15113D

Jiang, Y., Zhang, X., Xiao, L., Yan, R., Xin, J., Yin, C., et al. (2020). Preparation of Dual-Emission Polyurethane/carbon Dots Thermoresponsive Composite Films for Colorimetric Temperature Sensing. *Carbon* 163, 26–33. doi:10.1016/j.carbon.2020.03.013

Lee, S., Kim, K. Y., Lim, N. Y., Jung, J. H., Lee, J. H., Choi, M. Y., et al. (2019). Terpyridine-based Complex Nanofibers with Eu3+ as a Highly Selective Chemical Probes for UO22+. *J. Hazard. Mater.* 378, 120713. doi:10.1016/j.jhazmat.2019.05.106

Li, K., Yu, R.-H., Shi, C.-M., Tao, F.-R., Li, T.-D., and Cui, Y.-Z. (2018). Electrospun Nanofibrous Membrane Based on AIE-Active Compound for Detecting Picric Acid in Aqueous Solution. *Sensors Actuators B: Chem.* 262, 637–645. doi:10.1016/j.snb.2018.02.032

Li, M., Lyu, Q., Sun, L., Peng, B., Zhang, L., and Zhu, J. (2020). Fluorescent Metallosupramolecular Elastomers for Fast and Ultrasensitive Humidity Sensing. *ACS Appl. Mater. Inter.* 12, 39665–39673. doi:10.1021/acsami.0c11278

Li, W., Ding, Y., Tebyetekerwa, M., Xie, Y., Wang, L., Li, H., et al. (2019). Fluorescent Aggregation-Induced Emission (AIE)-based Thermosetting Electrospun Nanofibers: Fabrication, Properties and Applications. *Mater. Chem. Front.* 3, 2491–2498. doi:10.1039/c9qm00342h

Liu, Z., Jiang, Z., Yan, M., and Wang, X. (2019). Recent Progress of BODIPY Dyes with Aggregation-Induced Emission. *Front. Chem.* 7, 712. doi:10.3389/fchem.2019.00712

Luo, J., Xie, Z., Lam, J. W. Y., Cheng, L., Tang, B. Z., Chen, H., et al. (2001). Aggregation-induced Emission of 1-Methyl-1,2,3,4,5-Pentaphenylsilole. *Chem. Commun.* 18, 1740–1741. doi:10.1039/B105159H

Ma, C., Zhang, X., Yang, L., Li, Y., Liu, H., Yang, Y., et al. (2017). Alkyl Length Dependent Mechanofluorochromism of AIE-Based Phenothiazinyl Fluorophenyl Acrylonitrile Derivatives. *Dyes Pigm.* 136, 85–91. doi:10.1016/j.dyepig.2016.08.031

Ma, C., Zhang, X., Yang, Y., Ma, Z., Yang, L., Wu, Y., et al. (2016). Effect of Alkyl Length Dependent Crystallinity for the Mechanofluorochromic Feature of Alkyl Phenothiazinyl Tetraphenylethenyl Acrylonitrile Derivatives. *J. Mater. Chem. C* 4, 4786–4791. doi:10.1039/c6tc00939e

Miao, R., Peng, J., and Fang, Y. (2016). Recent Advances in Fluorescent Film Sensing from the Perspective of Both Molecular Design and Film Engineering. *Mol. Syst. Des. Eng.* 1, 242–257. doi:10.1039/c6me00039h

Moscoso, F. G., Almeida, J., Sousaraei, A., Lopes-Costa, T., Silva, A. M. G., Cabanillas-Gonzalez, J., et al. (2020). Luminescent MOF Crystals Embedded in PMMA/PDMS Transparent Films as Effective NO(2)gas Sensors. *Mol. Syst. Des. Eng.* 5, 1048. doi:10.1039/c9me00164f

Peng, X.-X., Bao, G.-M., Zhong, Y.-F., Zhang, L., Zeng, K.-B., He, J.-X., et al. (2021). Highly Sensitive and Rapid Detection of Thiabendazole Residues in Oranges Based on a Luminescent Tb3+-Functionalized MOF. *Food Chem.* 343, 128504. doi:10.1016/j.foodchem.2020.128504

Qin, A., Lam, J. W. Y., and Tang, B. Z. (2012). Luminogenic Polymers with Aggregation-Induced Emission Characteristics. *Prog. Polym. Sci.* 37, 182–209. doi:10.1016/j.progpolymsci.2011.08.002

Song, N., Chen, D.-X., Xia, M.-C., Qiu, X.-L., Ma, K., Xu, B., et al. (2015). Supramolecular Assembly-Induced Yellow Emission of 9,10-distyrylanthracene Bridged Bis(pillar[5] arene)s. *Chem. Commun.* 51, 5526–5529. doi:10.1039/C4CC08205B

Sun, X., Wang, Y., and Lei, Y. (2015). Fluorescence Based Explosive Detection: from Mechanisms to Sensory Materials. *Chem. Soc. Rev.* 44, 8019–8061. doi:10.1039/c5cs00496a

Sun, Z., Yan, F., Xu, J., Zhang, H., and Chen, L. (2021). Solvent-controlled Synthesis Strategy of Multicolor Emission Carbon Dots and its Applications in Sensing and Light-Emitting Devices. *Nano Res.* [Epub ahead of print] doi:10.1007/s12274-021-3495-8

Thomas, S. W., Joly, G. D., and Swager, T. M. (2007). Chemical Sensors Based on Amplifying Fluorescent Conjugated Polymers. *Chem. Rev.* 107, 1339–1386. doi:10.1021/cr0501339

Xu, B., Xie, M., He, J., Xu, B., Chi, Z., Tian, W., et al. (2013). An Aggregation-Induced Emission Luminophore with Multi-Stimuli Single- and Two-Photon Fluorescence Switching and Large Two-Photon Absorption Cross Section. *Chem. Commun.* 49, 273–275. doi:10.1039/c2cc36806d

Xue, J., Wu, T., Dai, Y., and Xia, Y. (2019). Electrospinning and Electrospun Nanofibers: Methods, Materials, and Applications. *Chem. Rev.* 119, 5298–5415. doi:10.1021/acs.chemrev.8b00593

Yang, H., Sun, Z., Lv, C., Qile, M., Wang, K., Gao, H., et al. (2018). Ratiometric Piezochromism of Electrospun Polymer Films: Intermolecular Interactions for Enhanced Sensitivity and Color Difference. *Chempluschem* 83, 132–139. doi:10.1002/cplu.201800080

Zhang, X., Zhang, X., Wang, K., Liu, H., Gu, Z., Yang, Y., et al. (2015). A Novel Fluorescent Amphiphilic Glycopolymer Based on a Facile Combination of Isocyanate and Glucosamine. *J. Mater. Chem. C* 3, 1738–1744. doi:10.1039/C4TC02556C

Zhao, E., Lai, P., Xu, Y., Zhang, G., and Chen, S. (2020a). Fluorescent Materials with Aggregation-Induced Emission Characteristics for Array-Based Sensing Assay. *Front. Chem.* 8, 288. doi:10.3389/fchem.2020.00288

Zhao, L., Wang, T., Wu, Q., Liu, Y., Chen, Z., and Li, X. (2017a). Fluorescent Strips of Electrospun Fibers for Ratiometric Sensing of Serum Heparin and Urine Trypsin. *ACS Appl. Mater. Inter.* 9, 3400–3410. doi:10.1021/acsami.6b14118

Zhao, L., Xie, S., Song, X., Wei, J., Zhang, Z., and Li, X. (2017b). Ratiometric Fluorescent Response of Electrospun Fibrous Strips for Real-Time Sensing of Alkaline Phosphatase in Serum. *Biosens. Bioelectron.* 91, 217–224. doi:10.1016/j.bios.2016.12.025

Zhao, L., Zhang, Z., Liu, Y., Wei, J., Liu, Q., Ran, P., et al. (2020b). Fibrous Strips Decorated with Cleavable Aggregation-Induced Emission Probes for Visual Detection of Hg2+. *J. Hazard. Mater.* 385, 121556. doi:10.1016/j.jhazmat.2019.121556

Zhou, H., Ye, Q., Neo, W. T., Song, J., Yan, H., Zong, Y., et al. (2014). Electrospun Aggregation-Induced Emission Active POSS-Based Porous Copolymer Films for Detection of Explosives. *Chem. Commun.* 50, 13785–13788. doi:10.1039/c4cc06559j

Zhou, J., Yu, G., and Huang, F. (2017). Supramolecular Chemotherapy Based on Host-Guest Molecular Recognition: a Novel Strategy in the Battle against Cancer with a Bright Future. *Chem. Soc. Rev.* 46, 7021–7053. doi:10.1039/C6CS00898D

Conflict of Interest: The authors declare that the research was conducted in the absence of any commercial or financial relationships that could be construed as a potential conflict of interest.

Publisher's Note: All claims expressed in this article are solely those of the authors and do not necessarily represent those of their affiliated organizations, or those of the publisher, the editors and the reviewers. Any product that may be evaluated in this article, or claim that may be made by its manufacturer, is not guaranteed or endorsed by the publisher.

frontiers in Chemistry

MINI REVIEW
published: 24 August 2021
doi: 10.3389/fchem.2021.723718

Hydrogen-Bonded Conjugated Materials and Their Application in Organic Field-Effect Transistors

*Xin Shi and Weiwei Bao**

National and Local Joint Engineering Laboratory for Slag Comprehensive Utilization and Environmental Technology, School of Materials Science and Engineering, Shaanxi University of Technology (SNUT), Hanzhong, China

Recent research on organic semiconductors has revealed that the composition of the constituent organic material, as well as the subtle changes in its structure (the stacking order of molecules), can noticeably affect its bulk properties. One of the reasons for this is that the charge transport in conjugated materials is strongly affected by their structure. Further, the charge mobility increases significantly when the conjugated materials exhibit self-assembly, resulting in the formation of ordered structures. However, well-organized nanostructures are difficult to obtain using classical solution processing methods, owing to their disordered state. A simple strategy for obtaining well-ordered material films involves synthesizing new conjugated materials that can self-organize. Introducing hydrogen bonding in the materials to yield hydrogen-bonded material superstructures can be a suitable method to fulfill these critical requirements. The formed hydrogen bonds will facilitate the assembly of the molecules into a highly ordered structure and bridge the distance between the adjacent molecules, thus enhancing the intermolecular charge transfer. In this minireview, hydrogen-bonded small molecules and polymers as well as the relationship between their chemical structures and performances in organic field-effect transistors are discussed.

Keywords: hydrogen bonding, conjugated materials, small molecules, polymers, organic field-effect transistors

OPEN ACCESS

Edited by:
Haichang Zhang,
Qingdao University of Science and Technology, China

Reviewed by:
Yiqun Wang,
Chengdu University of Technology, China
Zhao Li,
Xi'an Shiyou University, China
Haiyan Yan,
Xi'an Technological University, China

****Correspondence:***
Weiwei Bao
baowei1834@163.com

Specialty section:
This article was submitted to Organic Chemistry, a section of the journal Frontiers in Chemistry

Received: *11 June 2021*
Accepted: *29 July 2021*
Published: *24 August 2021*

Citation:
Shi X and Bao W (2021) Hydrogen-Bonded Conjugated Materials and Their Application in Organic Field-Effect Transistors. Front. Chem. 9:723718. doi: 10.3389/fchem.2021.723718

INTRODUCTION

Hydrogen bonds have been receiving increasing attention by scientists since 1989 when Peter Atkins stated that "hydrogen bonding, a noncovalent interaction in structural organic chemistry, is a link formed by a hydrogen atom lying between two strongly electronegative atoms" (Atkins, 1989). A hydrogen atom can be shared between a hydrogen-bond donor and a hydrogen-bond acceptor, i.e., a molecular with electron lone pairs. Thus, hydrogen bonds exist ubiquitously, including in biological systems, dyes and pigments, ionic conductors, and organic semiconductors (Cooksey, 2001; Meot-Ner, 2005; Glowacki et al., 2013). Furthermore, hydrogen bond, as a kind of directional intermolecular interaction, can affect the configuration and optical physical properties of the molecules forming hydrogen bond. It has been found in studies that hydrogen bond can effectively modulate the electron transfer process between molecules. It can facilitate the self-assembly of molecules, endowing the material with a more ordered or crystalline structure in the solid state. This is beneficial for the charge transport across neighboring molecules in the semiconductor layers of organic field-effect transistors (OFETs) (Zhang et al., 2018a; Deng et al., 2018; Zhang et al., 2020). The charge-transfer mobility of OFETs plays a key role in ensuring their high performance; notably, however, the charge-transport mobility of the current OFETs is

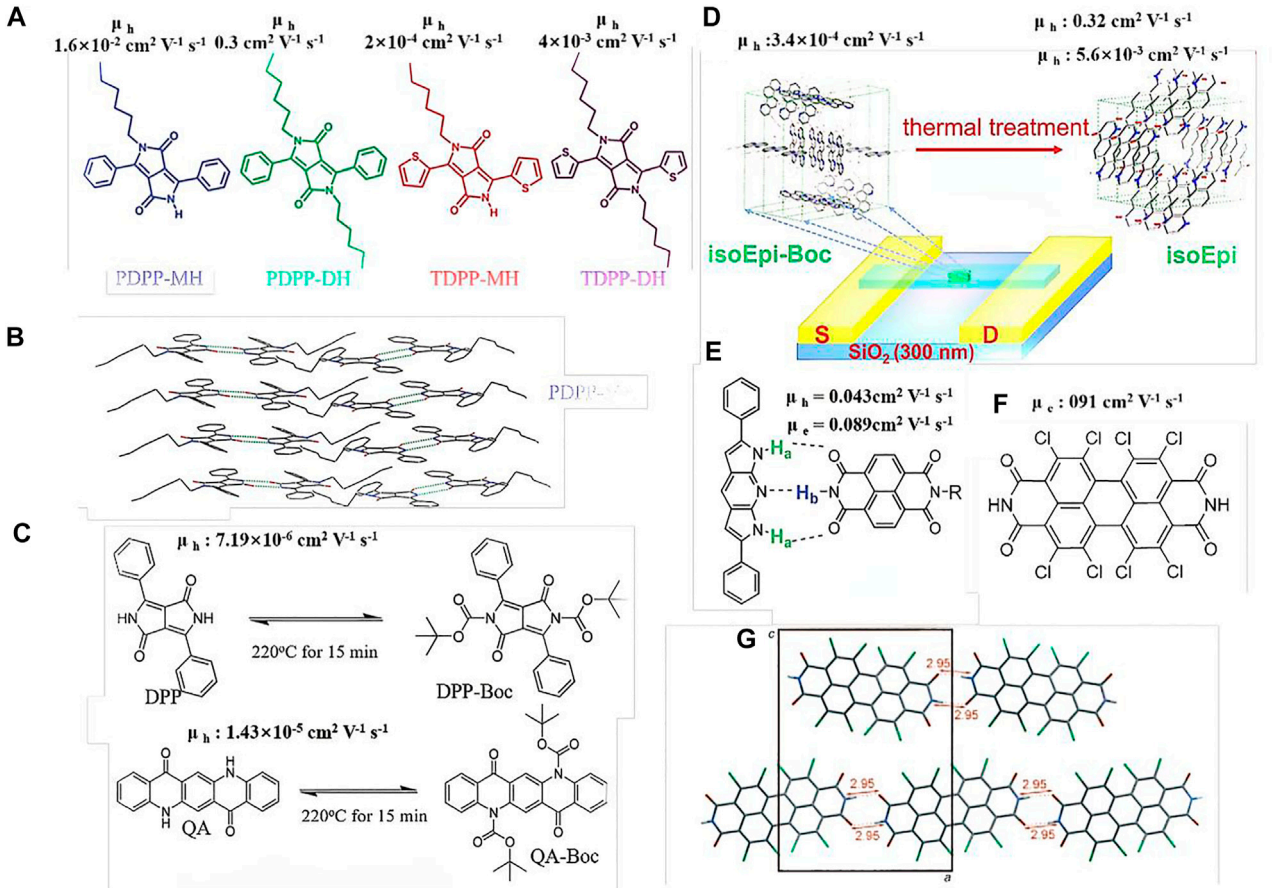

FIGURE 1 | (A,C,E,F) Chemical structures of the small molecules; **(B,G)** crystal structures of PDPP-MH and Cl8PTCDI; **(D)** diagram of the isoEpi-Boc crystal OFET transition to hydrogen-bonded isoEpi crystal OFET.

considerably lower than those of silicon-based field-effect transistors (Zhang et al., 2018b; Bao et al., 2020; Zou et al., 2021). Thus, the development of high-performance OFETs through structural modification to obtain hydrogen-bonded semiconductor materials with high charge-transport mobilities within individual molecules or between adjacent molecules is imperative.

Although hydrogen-bonded self-assembling materials can significantly enhance the performance of OFETs, their application has not been extensively investigated. In this minireview, small molecules and polymers of hydrogen-bonded π-conjugated materials, as well as the relationship between their chemical structures and performances in OFETs, are reviewed. In addition, this minireview provides development prospects of ideal hydrogen-bonded π-conjugated semiconductor materials with high performance.

HYDROGEN-BONDED SMALL MOLECULES

In small-molecule organic semiconductors, charge carriers need to be frequently transferred among individual molecules; therefore, the molecular crystal size and packing are crucial for efficient charge transport (Zhang et al., 2017a). Hydrogen bonding can facilitate the reorganization of the molecular packing *via* self-assembly. The charge transfer among hydrogen-bonded small molecules often results in their poor solubility in most organic solvents, owing to their strong hydrogen bonding association, which results in the formation of crosslinked netlike materials in the solid state. These materials are often difficult to utilize in the direct fabrication of OFETs *via* solution processing.

In 2014, Patil et al. introduced an alkyl chain into the substituted single N position of diketopyrrolopyrrole (DPP) to obtain mono-alkylated PDPP-MH and TDPP-MH (**Figure 1A**) (Dhar et al., 2015). The alkyl chain not only facilitated hydrogen bonding formation, but also enhanced the material solubility. Conversely, the other NH units formed hydrogen bonds with the O = C units of neighboring molecules, resulting in dimer-like molecules (**Figure 1B**). PDPP-DH and TDPP-DH, which have similar chemical structures with dialkyl substituents and no hydrogen bonding, showed a hole-transfer mobility of almost two orders of magnitude higher than those of the other molecules above. Crystal analysis revealed that the mono-alkylated DPP exhibited cofacial layered structures, attributed to the

intermolecular hydrogen bonding through the free amide group in the DPP core, while the dihexyl DPP-based molecules showed herring bone-packing arrangements. The present study revealed that hydrogen bonding not only affects the molecular packing, but also improves the charge-transport speed.

In addition to mono-alkylation, tert-butoxycarbonyl (t-Boc), which can be decomposed by thermal annealing or ultraviolet (UV) light exposure, has also been incorporated into small molecules *via* latent hydrogen bonding. Yanagisawa et al. incorporated t-Boc units into DPP and quinacridone (QA) to obtain t-Boc DPP and t-Boc QA, respectively (Hiroyuki et al., 2008). These two molecules exhibited good solubility in most organic solvents, permitting the fabrication of OFETs by the spin-coating technique and offering a low-cost fabrication process, rather than the expensive vacuum technology. During the thermal-annealing process at 220°C for 15 min, the t-Boc DPP and t-Boc QA molecules were converted into DPP and QA, respectively (**Figure 1C**). Studies on OFET devices have shown that the hole-transfer mobilities of the DPP or QA materials formed *via* t-Boc annealing are similar to those of the related DPP or QA materials formed *via* the vacuum-deposition technique. The present study demonstrated a simple and useful method to fabricate hydrogen-bonded OFETs through solution processing, which involves the introduction of a functional group that can be easily decomposed by thermal annealing, such as t-Boc, to replace the pigments with latent hydrogen bonds.

Recently, Zhang et al. reported several t-Boc-substituted conjugated pigment molecules with fused hydrogen bonds (Zhang et al., 2017b; Zhang et al., 2018a). In the present study, the authors observed that a solid-state t-Boc substituted conjugated pigment crystal could transition to a hydrogen-bonded pigment crystal *via* annealing, and the molecular packing was changed significantly. This occurred because the t-Boc units were decomposed during the thermal annealing process, while the NH units emerged (**Figure 1D**). Before the donor units (NH) coordinated with the acceptor units (C=O) to form hydrogen bonds, the molecules remained mobile, owing to the elevated temperature and relatively weak intermolecular interactions. Therefore, the molecules may have undergone crystallization to form hydrogen-bonded crystals. With the emergence of hydrogen bonds, the molecules were arranged to form a brick-in-wall structure with π-stacking along the crystal growth axis, leading to a significant enhancement in the charge mobility along the crystal growth direction (the hole mobility increased from 3.4×10^{-4} to 0.32 $cm^2 V^{-1} s^{-1}$, and the electron mobility increased from non-detectable to 5.6×10^{-3} $cm^2 V^{-1} s^{-1}$). The significantly improved charge-transfer mobility could be ascribed to the hydrogen bonding that not only reorganized the molecular packing, but also afforded high-density materials. It is also proved that strong hydrogen bonding between the regulatory units can induce the formation of enhanced π-π interaction (close, coplanar accumulation) and highly ordered supramolecular assembly between the conjugated units, which can better improve the migration properties of the materials. This study provides a useful strategy for preparing crystalline hydrogen-bonded small-molecule OFETs *via* solution processing.

In addition to pure conjugated materials, hydrogen bonds can be formed between two or more composite materials. In 2014, Perepichka introduced dipyrrolopyridine (DP) as a donor semiconductor capable of undergoing complementary hydrogen bonding with naphthalenediimide (NDI) acceptors (**Figure 1E)** (Black and Perepichka, 2014). In this system, the hydrogen bonds formed between the NH groups of the DP and the C = O or NH units of NDI were confirmed by nuclear magnetic resonance (NMR) spectroscopy and crystal analysis. Due to the hydrogen bonding, the two white or yellow materials changed into a dark–green material. The cocrystal mixture with a ratio of 1:1 (DP:NDI) exhibited relatively balanced ambipolar transport with hole and electron mobilities of 0.043 and 0.089 $cm^2 V^{-1} s^{-1}$, respectively, which were among the highest reported values for cocrystals at the time. This study provides a foundation for the advanced solid-state engineering of organic electronics, capitalizing on the complementary hydrogen bonding.

Most hydrogen-bonded small molecules often exhibit poor solubility in most common organic solvents, such as DPP, indigo, and octachloroperylene, due to their strong intermolecular interactions. Therefore, the OFETs based on these hydrogen-bonded molecules are often processed by the thermal vapor deposition technique. Bao et al. synthesized 1,2,5,6,7,8,11,12-tetrachloro-substituted perylene 3,4:9,10-tetracarboxylic diimides (Cl8PTCDI) and investigated their packing properties by X-ray diffraction (XRD) analysis (**Figure 1F**) (Li et al., 2010). The results showed that a strong hydrogen bond was formed between the two adjacent molecules with a distance of 2.95 Å, and a brick stone crystal packing arrangement was observed (**Figure 1G**). The crystalline Cl8PTCDI OFET showed an electron mobility as high as 0.91 $cm^2 V^{-1} s^{-1}$ with an air-stable operation. This high electron mobility could be due to the brick stone packing arrangement, which provides two-dimensional percolation paths for the charge-carrier transport in organic semiconductors. Recently, Geng and his team found that the addition of furan rings at 3,6-positions of DPP unit remarkably improved the solubility of the polymers (Wang et al., 2021).

3 HYDROGEN-BONDED POLYMERS

Compared to that in π-conjugated small molecules, the charge transport in polymers is considerably more complicated. This is because polymers are usually semicrystalline; thus, the charge carriers need to travel across both amorphous and crystalline regions (Zhang et al., 2017a). Therefore, the charge mobility of polymers is governed not only by the crystallinity of the polymer film but also by the connections between the crystalline aggregates. Polymer is essentially between traditional semiconductor and molecular intermediates, can form a variety of nanostructures with complex energy band structures and optical properties. The hydrogen bonds with self-assembly recognition have obvious chiral inductive characteristics on the planar II conjugated molecular skeleton. While the melting hydrogen bonds are essential for molecular rearrangement to form new solid crystals. That is to say, hydrogen bonding could

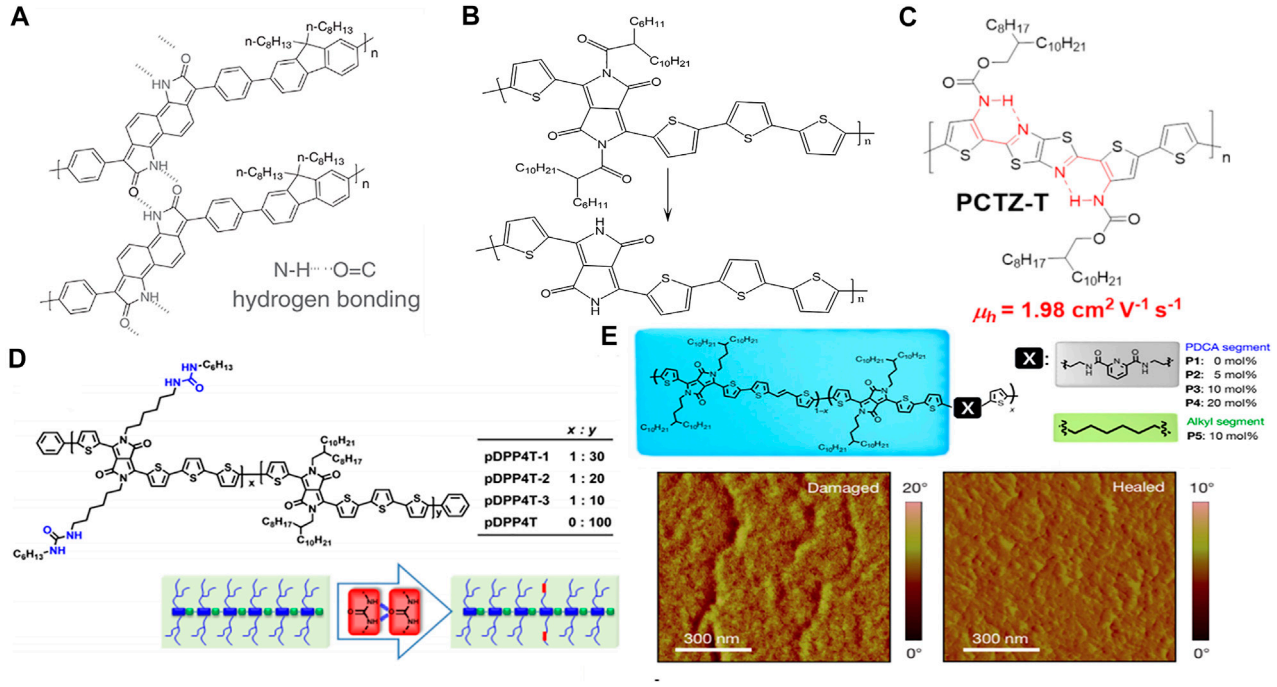

FIGURE 2 | (A) Hydrogen-bonded cross-linked netlike NDP-based polymer; **(B)** the 2-octyldodecanoyl-substituted DPP-based polymer transition to a hydrogen-bonded DPP-based polymer; **(C)** chemical structure of polymer PCTZ-T; **(D)** chemical structures of the polymers and illustrations of the design rationale for incorporating urea groups into the side chains of conjugated polymers; **(E)** chemical structure of the DPP-based polymers, as well as the atomic force microscopy (AFM) phase image of the damaged and healed films.

facilitate the self-assembly of the molecules, affording more crystalline regions in the polymers and consequently improving the charge-carrier transfer speed.

Hydrogen bonds can be formed directly on the polymer backbone with conjugated units. In 2017, Zhang et al. reported two soluble π-conjugated polymers containing t-Boc-substituted benzodipyrrolidone (BDP) or naphthodipyrrolidone (NDP) units with latent hydrogen bonds on the main chain (Zhang et al., 2017b). Upon thermal annealing, the t-Boc units decomposed, forming hydrogen-bonded crosslinked netlike polymers (**Figure 2A**). The hydrogen-bonded polymers exhibited not only a bathochromic shift in the optical absorption and a small bandgap, but also better coplanarity and a stronger π–π interaction, compared to that of the pristine polymer. OFET studies have shown that the hydrogen-bonded polymer based on NDP affords an air-stable n-type semiconductor with an electron mobility 40 times that of its precursor polymer *via* latent hydrogen bonding. This is due to the strong aggregation and the planar polymer backbone, as confirmed by Cao et al. (Liu et al., 2015). To be solution-processable, polymer semiconductors require the incorporation of a large portion of solubilizing side chains to oppose the strong aggregation tendency of the polymer backbones in solution. To modify the t-Boc units, 2-octyldodecanoyl groups with long alkyl chains were designed and introduced into the DPP-based polymers by Li's group (Sun et al., 2012). Similar to the t-Boc units, 2-octyldodecanoyl undergoes decomposition *via* thermal annealing while NH units emerge to form hydrogen bonds (**Figure 2B**). High performance organic semiconductor polymers were realized by using intramolecular resonance-assisted hydrogen bonding (RAHB). Based on this, Gao Xike's group Liu et al. (2021) synthesized polymer PCTZ-T and PCTZ-B with Rahb interaction in the study of OFET devices, and PCTZ-T achieved an average carrier mobility of 1.98 $cm^2V^{-1}s^{-1}$ (**Figure 2C**). This is the highest mobility of thiazole-containing or dythiazole-containing polymer materials in P-type OFET devices.

Apart from the polymer backbone, hydrogen bonding can also be formed with the side chain. Yao et al. introduced urea-containing alkyl chains *vs*. branching alkyl chains into DPP-based polymers to investigate the effect of hydrogen bonding on the OFET performance (**Figure 2D**) (Yao et al., 2016). The authors discovered that the hydrogen bonding-induced assembly significantly improved the polymer packing, typically the alky chain packing, which resulted in a thin film with thick nanofibers after thermal annealing. By increasing the ratio of hydrogen bonding from 10 to 30%, the hole-transfer mobility increased from 5.5 to 13.1 $cm^2 V^{-1} s^{-1}$. This study demonstrates not only the application of a urea moiety as a new functional group to design hydrogen-bonded materials, but also the incorporation of other functional moieties with hydrogen bonding into the alkyl side chains of conjugated polymers to tune the interchain interactions/packing, thereby improving the semiconductor performance.

Hydrogen bonding dissociation and association could afford a thin film semiconductor with self-healing abilities. In Oh et al. (2016) introduced non-conjugated, alkylated 2,6-pyridine dicarboxamide units into a DPP-based polymer backbone. Hydrogen bonding could be formed between the NH units and the C = O units of the neighboring molecules (**Figure 2E**). The linear polymer formed crosslinked polymers, owing to the hydrogen bonding, affording polymer films with hole mobilities ranging from 1.32 to 0.11 $cm^2 V^{-1} s^{-1}$, along the direction of the applied strain. Subsequently, the mobility recovered to $1.00\,cm^2 V^{-1} s^{-1}$ upon releasing the applied strain. However, the polymers with similar chemical structures and without hydrogen bonding were unable to recover upon stress release. The damaged hydrogen-bonded film could be healed by thermal annealing or solvent-vapor processing (**Figure 2E**). This study shows that combining hydrogen bonds into the polymer not only makes the material stretch-resistant, but also achieves efficient charge transfer.

CONCLUSION AND OUTLOOK

The formation of hydrogen bonding, a strong noncovalent interaction, between neighboring molecules in the solid state results not only in molecular reassembly with more ordered and crystalline structures, but also in strong aggregations and improved π–π stacking. In addition, the hydrogen bonding could afford conjugated materials with a planar backbone. This is beneficial for the charge transfer within individual molecules and across adjacent molecules. Thus, it is possible to fabricate a good organic hydrogen-bonded conjugated semiconductor with excellent charge-transport performance. Hydrogen bonding can be formed between conjugated units, such as molecular backbones, and non-conjugated units, such as alky chains, as well as the unconjugated part of the molecular backbone. Hydrogen bonding could result in the formation of cross-linked netlike materials with poor solubility in most organic solvents; these materials cannot be utilized to build devices through solution processing. To solve this issue, t-Boc units or other functional groups can be introduced into the material structure to break the hydrogen bonding, affording soluble materials with latent hydrogen bonding. Hydrogen-bonded conjugated materials are one of the most promising semiconductor materials employed in OFETs. Thus, a series of different types of functional units with latent potential strong hydrogen bonding could be explored in the near future.

AUTHOR CONTRIBUTIONS

XS collected materials and prepared the manuscript. WB revised the manuscript and supervised the whole work.

FUNDING

This study was financially supported by the National and Local Joint Engineering Laboratory for Slag Comprehensive Utilization and Environmental Technology Open Fund (SLGPT2019KF01-03).

REFERENCES

Atkins, P. (1989). *General Chemistry*. New York: Scientic American Books.

Bao, W. W., Li, R., Dai, Z. C., Tang, J., Shi, X., Geng, J. T., et al. (2020). Diketopyrrolopyrrole (DPP)-Based Materials and its Applications: A Review. *Front. Chem.* 8, 679. doi:10.3389/fchem.2020.00679

Black, H. T., and Perepichka, D. F. (2014). Crystal Engineering of Dual Channel P/n Organic Semiconductors by Complementary Hydrogen Bonding. *Angew. Chem. Int. Ed.* 53, 2138–2142. doi:10.1002/anie.201310902

Cooksey, C. (2001). Tyrian Purple: 6,6'-Dibromoindigo and Related Compounds. *Molecules* 6, 736–769. doi:10.3390/60900736

Deng, Z., Yang, K., Li, L., Bao, W., Hao, X., Ai, T., et al. (2018). Solution Processed Air-Stable P-Channel Organic crystal Field-Effect Transistors of Aminobenzodifuranone. *Dyes Pigm.* 151, 173–178. doi:10.1016/j.dyepig.2017.12.052

Dhar, J., Karothu, D. P., and Patil, S. (2015). Herringbone to Cofacial Solid State Packing via H-Bonding in Diketopyrrolopyrrole (DPP) Based Molecular Crystals: Influence on Charge Transport. *Chem. Commun.* 51, 97–100. doi:10.1039/C4CC06063F

Głowacki, E. D., Irimia-Vladu, M., Bauer, S., and Sariciftci, N. S. (2013). Hydrogen-bonds in Molecular Solids - from Biological Systems to Organic Electronics. *J. Mater. Chem. B.* 1, 3742–3753. doi:10.1039/c3tb20193g

Hiroyuki, Y., Jin, M., Aramaki, S., and Sakai, Y. (2008). Organic Field-Effffect Transistor Devices Based on Latent Pigments of Unsubstituted Diketopyrrolopyrrole or Quinacridone. *Jpn. J. Appl. Phys.* 47 (6R), 4728–4731. doi:10.1143/JJAP.47.4728

Li, Y.-S., Liang, F.-Y., Bux, H., Feldhoff, A., Yang, W.-S., and Caro, J. (2010). Inside Cover: Molecular Sieve Membrane: Supported Metal-Organic Framework with High Hydrogen Selectivity (Angew. Chem. Int. Ed. 3/2010). *Angew. Chem. Int. Edition* 49, 464. doi:10.1002/anie.200906852

Liu, B., Li, J., Zeng, W., Yang, W., Yan, H., Li, D.-c., et al. (2021). High-Performance Organic Semiconducting Polymers by a Resonance-Assisted Hydrogen Bonding Approach. *Chem. Mater.* 33 (2), 580–588. doi:10.1021/acs.chemmater.0c03720

Liu, C., Dong, S., Cai, P., Liu, P., Liu, S., Chen, J., et al. (2015). Donor-Acceptor Copolymers Based on Thermally Cleavable Indigo, Isoindigo, and DPP Units: Synthesis, Field Effect Transistors, and Polymer Solar Cells. *ACS Appl. Mater. Inter.* 7, 9038–9051. doi:10.1021/am5089956

Meot-Ner, M. (2005). The Ionic Hydrogen Bond. *Chem. Rev.* 105 (1), 213–284. doi:10.1021/cr9411785

`Oh, J. Y., Rondeau-Gagné, S., Chiu, Y.-C., Chortos, A., Lissel, F., Wang, G.-J. N., et al. (2016). Intrinsically Stretchable and Healable Semiconducting Polymer for Organic Transistors. *NATURE* 539, 411–415. doi:10.1038/nature20102

Sun, B., Hong, W., Aziz, H., and Li, Y. (2012). Diketopyrrolopyrrole-based Semiconducting Polymer Bearing Thermocleavable Side Chains. *J. Mater. Chem.* 22, 18950–18955. doi:10.1039/c2jm33818a

Wang, Z., Shi, Y., Deng, Y., Han, Y., and Geng, Y. (2021). Toward High Mobility Green Solvent-Processable Conjugated Polymers: A Systematic Study on Chalcogen Effect in Poly(Diketopyrrolopyrrole- Alt -Terchalcogenophene)s. *Adv. Funct. Mater.* 2104881, 2104881. doi:10.1002/adfm.202104881

Yao, J., Yu, C., Liu, Z., Luo, H., Yang, Y., Zhang, G., et al. (2016). Significant Improvement of Semiconducting Performance of the Diketopyrrolopyrrole-Quaterthiophene Conjugated Polymer through Side-Chain Engineering via

Hydrogen-Bonding. *J. Am. Chem. Soc.* 138, 173–185. doi:10.1021/jacs.5b09737

Zhang, H., Deng, R., Wang, J., Li, X., Chen, Y.-M., Liu, K., et al. (2017a). Crystalline Organic Pigment-Based Field-Effect Transistors. *ACS Appl. Mater. Inter.* 9 (26), 21891–21899. doi:10.1021/acsami.7b03170

Zhang, H., Li, R., Deng, Z., Cui, S., Wang, Y., Zheng, M., et al. (2020). π-Conjugated Oligomers Based on Aminobenzodifuranone and Diketopyrrolopyrrole. *Dyes Pigm.* 181, 108552. doi:10.1016/j.dyepig.2020.108552

Zhang, H., Liu, K., Wu, K.-Y., Chen, Y.-M., Deng, R., Li, X., et al. (2018a). Hydrogen-Bonding-Mediated Solid-State Self-Assembled Isoepindolidiones (isoEpi) Crystal for Organic Field-Effect Transistor. *J. Phys. Chem. C* 122 (11), 5888–5895. doi:10.1021/acs.jpcc.7b11992

Zhang, H., Yang, K., Chen, Y. M., Bhatta, R., Tsige, M., Cheng, S. Z. D., et al. (2017b). Polymers Based on Benzodipyrrolidone and Naphthodipyrrolidone with Latent Hydrogen-Bonding on the Main Chain. *Macromol. Chem. Phys.* 218, 1600617. doi:10.1002/macp.20160061713

Zhang, H., Yang, K., Zhang, K., Zhang, Z., Sun, Q., and Yang, W. (2018b). Thionating Iso-Diketopyrrolopyrrole-Based Polymers: from P-type to Ambipolar Field Effect Transistors with Enhanced Charge Mobility. *Polym. Chem.* 9, 1807–1814. doi:10.1039/c8py00292d

Zou, X., Cui, S., Li, J., Wei, X., and Zheng, M. (2021). Diketopyrrolopyrrole Based Organic Semiconductor Materials for Field-Effect Transistors. *Front. Chem.* 9, 671294. doi:10.3389/fchem.2021.671294

Conflict of Interest: The authors declare that the research was conducted in the absence of any commercial or financial relationships that could be construed as a potential conflict of interest.

Publisher's Note: All claims expressed in this article are solely those of the authors and do not necessarily represent those of their affiliated organizations, or those of the publisher, the editors and the reviewers. Any product that may be evaluated in this article, or claim that may be made by its manufacturer, is not guaranteed or endorsed by the publisher.

frontiers in Chemistry

PERSPECTIVE
published: 25 August 2021
doi: 10.3389/fchem.2021.732935

Efficient Colorimetric Fluoride Anion Sensor Based on π-Conjugated Carbazole Small Molecule

Zhifeng Deng[1†], *Cheng Wang*[2†], *Junqiang Li*[3] *and Meng Zheng*[2,3*]

[1]National and Local Joint Engineering Laboratory for Slag Comprehensive Utilization and Environmental Technology, School of Materials Science and Engineering, Shaanxi University of Technology (SNUT), Hanzhong, China, [2]Key Laboratory of Rubber–Plastic of Ministry of Education (QUST), School of Polymer Science and Engineering, Qingdao University of Science and Technology, Qingdao, China, [3]Qingdao Haiwan Science and Technology Industry Research Institute Co. Ltd., Qingdao, China

The ability to detect fluoride anions with high selectivity and sensitivity by using the naked eye is crucial yet challenging. In this study, a novel, simple conjugated organic dye, *N-tert*-butyldimethylsilyl-3,6-diiodocarbazole (CA-TBMDS) was developed and used for the first time as a colorimetric sensor for fluoride. CA-TBMDS was found to be a highly sensitive fluoride chemosensor, with a detection limit as low as 3×10^{-5} M. The reaction of CA-TBMDS with fluoride anions in a tetrahydrofuran solution resulted in a color change from colorless to yellow under ambient light, which can be discriminated by the naked eye. The sensor operated via intermolecular proton transfer between the amide units and the fluoride anion, as confirmed by proton nuclear magnetic resonance titration. CA-TBMDS is not only highly sensitive to fluoride anions, but also exhibits high sensitivity in the presence of various ions. This work demonstrates that *N*-butyldimethylchlorosilane-based organic dyes have prospective utility as a type of fluoride anion chemosensor.

Keywords: fluoride anion sensors, naked eye detection, carbazole, intermolecular proton transfer, color change

OPEN ACCESS

Edited by:
Qixin Zhou,
University of Akron, United States

Reviewed by:
Yalong Wang,
Hainan University, China
Xiaohuan Sun,
Yangzhou University, China

****Correspondence:***
Meng Zheng
zhengmeng.555@hotmail.com

†These authors have contributed equally to this work

Specialty section:
This article was submitted to Organic Chemistry, a section of the journal Frontiers in Chemistry

Received: *29 June 2021*
Accepted: *11 August 2021*
Published: *25 August 2021*

Citation:
Deng Z, Wang C, Li J and Zheng M (2021) Efficient Colorimetric Fluoride Anion Sensor Based on π-Conjugated Carbazole Small Molecule. Front. Chem. 9:732935. doi: 10.3389/fchem.2021.732935

INTRODUCTION

Fluoride is among the most electronegative ions and is the smallest anion, with a high charge density. Fluoride plays a key role in human health and chemical engineering because: (i) the fluoride anion is easily absorbed by the animal or human body, but it is excreted slowly. As a result, people or animals develop bone and thyroid activity disorders if they are overexposed to fluoride (Wade et al., 2010). (ii) Fluoride anions play a crucial role in organic synthesis, the chemical industry, biological and medical processes, and the military fields (Kleerekoper, 1998; Cametti and Rissanen, 2009; Wade et al., 2010; Xuan et al., 2013; Zhou et al., 2014; Li et al., 2018). An appropriate amount of fluoride anions in the environment is healthy for humans. However, a large amount of fluoride in the environment is hazardous and even toxic (Kaur and Choi, 2015). With the rapid development of the chemical industry, fluoride anions are present not only in aqueous environments, but also in organic media, such as waste organic liquor (Clark, 1980). The development of highly sensitive and selective fluoride anion sensors capable of qualitative and quantitative detection is crucial and could provide a diversity of optical chemosensors for fluoride anions in organic solutions.

In the past few years, many scientific studies have focused on the development of novel fluoride anion sensors with high sensitivity and selectivity (Yang et al., 2013; Feng et al., 2018; Wang et al., 2018; Antonio et al., 2020). Very recently, aminobenzodifuranone dyes for F^- chemosensors were developed by our group, which could not only detect F^-, but could also distinguish it from F^- containing solvents (Deng et al., 2020). Yuan et al. developed a new (3Z, 3′Z)-3,3'-(4,4,9,9-tetrakis

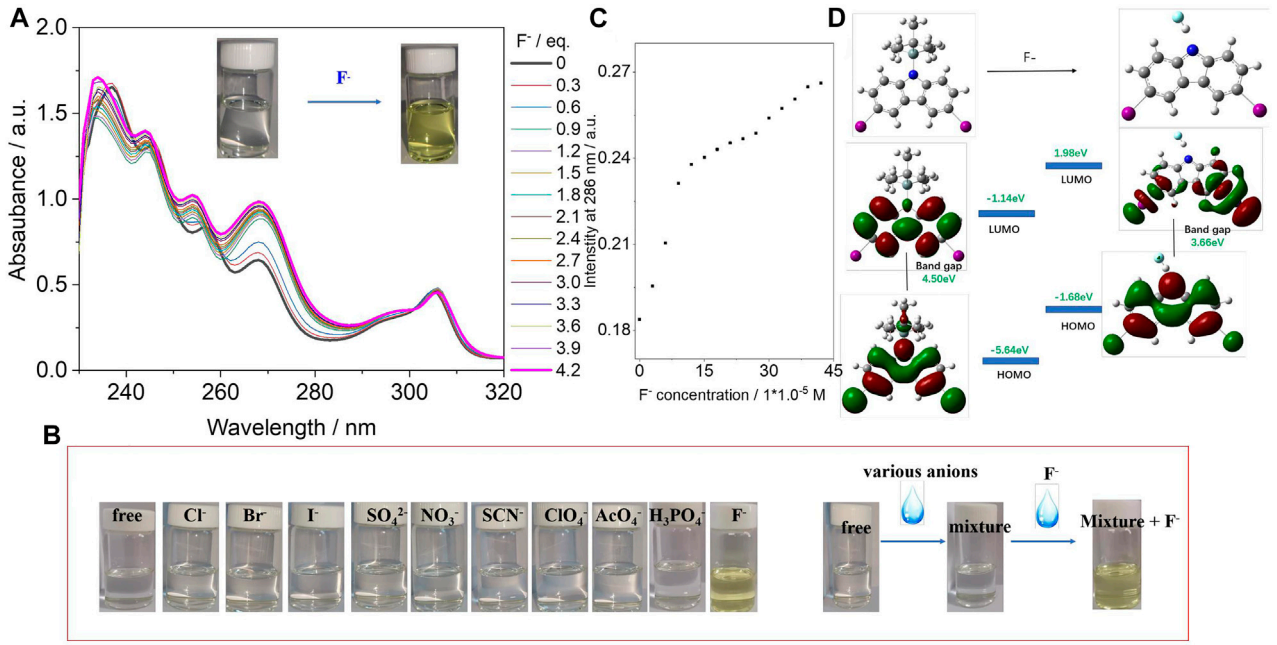

FIGURE 1 | (A) UV/vis absorption spectra of CA-TBMDS (1.0×10^{-4} M) in the presence of F^- (0–4.2 eq.) in THF. Inset shows photograph of CA-TBMDS solution with or without adding different amounts of fluoride anion under ambient light. **(B)** Photographs of CA-TBMDS (5×10^{-5} M) in THF before and after adding different anions, as well the addition of other anions together with and without F^-. **(C)** Optical absorption intensity at 286 nm against the concentration of fluoride anion. **(D)** Molecular orbital surfaces of the HOMO and LUMO energy levels of CA-TBMDS at the B3LYP/6–31G (d, p) level, before and after adding fluoride anion.

(4-hexylphenyl)-4,9-dihydro-s-indaceno [1,2-b:5,6-b']dithiophene)-2,7-diylbis (methan-1-yl-1-ylidene))bis (6-bromo-indolin-2-one) (IDTI) dye with a detection limitation as low as 1×10^{-7} M for the fluoride anion (Yuan et al., 2020). Additionally, Zhang and co-workers developed a DPP-based polymer from *t*-butoxy carbonyl (*t*-Boc) units that detect fluoride anions, and also extract fluoride anions from organic solutions (Zhang et al., 2018).

The reported fluoride anion sensors generally react with fluoride anions, resulting in changes in the UV-vis absorption and/or fluorescence emission spectra of the sensors. Among these, the sensors that allow for the detection of color with the naked eye are more interesting and promising because fluoride anions can be detected easily and simply without the need for auxiliary equipment. Herein, a new organic conjugated carbazole small molecule, which can allow for fluoride detection with the naked eye, was developed for use as a fluoride anion chemosensor.

MATERIALS AND METHODS

N-Tert-Butyldimethylsilyl-3,6-Diiodocarbazole (CA-TBMDS)

In a dry flask under nitrogen protection, 3,6-diiodocarbazole (2.00 g, 4.77 mmol) was dissolved in anhydrous tetrahydrofuran (THF; 30 ml) at room temperature. Sodium hydride (172 mg, 7.2 mmol) was added to the stirred solution, which was further stirred at room temperature for another 30 min *tert*-Butyldimethylsilyl chloride (0.79 g, 5.3 mmol) was then added and the reaction was stirred at room temperature for a further 17 h. The reaction mixture was then poured into ice water (50 ml) and extracted three times with dichloromethane. The combined organic layers were dried over $MgSO_4$ before the solvent was removed *in vacuo*, which afforded an off-white solid. The crude product was purified through a plug of silica in a fitted funnel with hexane/dichloromethane (9:1) as the eluent. After removing the solvent *in vacuo*, the product was obtained (2.06 g, yield: 81%). ^{1}H NMR (500 MHz, d_6-DMSO) δ ppm: 8.61 (s, 2H), 7.65–7.67 (d, J = 10 Hz, 2H), 7.51–7.53 (d, J = 10 Hz, 2H), 0.96 (s, 9H), 0.75(s, 3H).

RESULTS AND DISCUSSION

The synthesis of CA-TBMDS is described in the *Materials and Methods* section. CA-TBMDS showed good solubility in most common organic solvents. The interaction between the CA-TBMDS chromophore and fluoride anions was first investigated by using the naked eye to determine the color change. As shown in the inset of **Figure 1A**, the pure CA-TBMDS solution was colorless. Once the fluoride anion was introduced, the color of the solution immediately changed to yellow. This indicated that in the presence of CA-TBMDS, fluoride anions could be detected by the naked eye without additional equipment. Additionally, CA-TBMDS presented blue emission, which is sensitive to the naked eyes. A spectrophotometric titration was used to investigate the interaction between the CA-TBMDS chromophore and

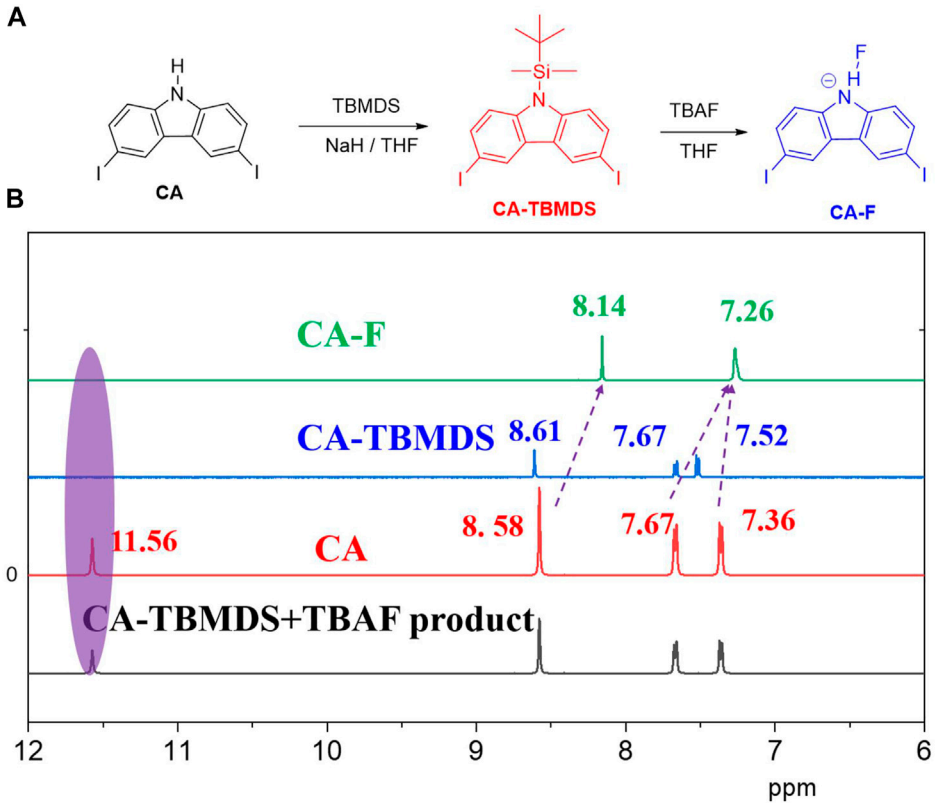

FIGURE 2 | (A) Synthesis of CA-TBMDS, and reaction between CA-TBMDS and fluoride anion. **(B)** Partial ^{1}H NMR titration spectra of CA and CA-TBMDS before and after adding fluoride anion (4 eq.) in DMSO-d_6.

fluoride anion in THF solution. A standard solution of tetrabutylammonium fluoride (TBAF, 1.0×10^{-2} M) was gradually added to a 1.0×10^{-4} M solution of CA-TBMDS in THF. As shown in **Figure 1A**, with the progressive addition of fluoride anions, the absorption intensity at 306 nm showed almost no change, but other absorption peaks were slightly blue-shifted, which enhanced the absorption intensity. For example: (i) the absorption peak at 268 nm with an intensity of 0.61 shifted to 267 nm with an intensity of 0.99; (ii) the absorption peak at 256 nm with an intensity of 0.80 shifted to 254 nm with an intensity of 1.01; (iii) the absorption peak at 245 nm with an intensity of 1.27 shifted to 244 nm with an intensity of 1.38; (iv) the absorption peak at 236 nm with an intensity of 1.31 shifted to 234 nm with an intensity of 1.70. In addition, the optical absorption intensity of the spectra vs the concentration of fluoride anion was calculated which was described in **Figure 1C**. **Figure 1C** showed that the detection limit of CA-TBMDS for the fluoride anions was at least 3×10^{-5} M. As shown in **Figure 1B**, apart from F^- (as tetrabutylammonium salts), anions (4 equivalents) such as Cl^-, Br^-, I^-, SO_4^{2-}, NO_3^-, SCN^-, ClO_4^-, AcO_4^-, and $H_2PO_4^-$ caused almost no change in the color of the CA-TBMDS solution. Interestingly, there was no noticeable color change upon the addition of other anions together with F^-, although F^- by itself led to an immediate change from colorless to yellow (**Figure 2B**). This observation indicates that fluoride anions can be detected without interference from other anions. Thus, CA-TBMDS seems to be a highly sensitive and selective sensor for fluoride anions.

The changes in the color and optical absorption spectrum are plausibly associated with the decomposition of *t*-butyldimethylchlorosilane (TBMDS) from CA-TBMDS. Once CA-TBMDS interacted with the fluoride anion, the CA-TBMDS molecules were transformed to CA, which generated N-H units. This was confirmed by the NMR test. The CA-TBMDS solution was added by TABF solution, subsequently the mixture was stirred for 15 min under room temperature. The mixture was purified by the saturated NH_4Cl (aq) and extracted with toluene. The combined organic layers were washed with deionized water then dried by $MgSO_4$ before the solvent was removed in vacuo to afford the white product. The NMR of the product was measured, which showed the same peaks compared to the CA. Compare to the CA-TBMDS, the peaks of the product were shifted into slightly lower ppm, for instance the proton of the carbazone core of 8.61 ppm shifted into 8.58 ppm, while 7.72 ppm was moved to 7.36 ppm. The lactam NH moiety from the CA core was able to interact with the fluoride anions, which easily deprotonated the -NH protons (inter-molecular proton transfer, IPT, **Figure 2A** (Zhang et al., 2018)).^{1}H NMR experiments were carried out in DMSO-d_6 to confirm our assumption and further understand the interaction between

the fluoride anion and the CA-TBMDS acceptor. As shown in **Figure 2B**, except for the signal of the amino proton at 11.56 ppm, the specific signals from the carbazole core of CA and CA-TBMDS were similar. Once the fluoride anions were added, the proton signal of carbazole at 8.58 ppm shifted to 8.14 ppm, while the respective proton signals at 7.67 and 7.36 ppm shifted to 7.26 ppm. This may be due to the IPT process, which severed the TBMDS units from the CA core, and resulted in hydrogen bonding between the fluoride anion and the proton on the amino N-H. In addition, the signals of the amino protons at 11.56 ppm for CA did not appear, which further confirmed this assumption.

To further understand the electron distributions before and after fluoride anion binding, the Frontier molecular orbital (FMO) energy was calculated at the B3LYP/6–31 (d, p) level using CA-TBMDS. As shown in **Figure 1D**, the distribution of the highest occupied molecular orbital (HOMO) and lowest unoccupied molecular orbital (LUMO) orbitals of CA-TBMDS was similar because these orbitals were mainly localized on the core of CA. After binding with the fluoride anions, the HOMO orbital distributions showed almost no change, but the electron distribution of the LUMO, which was associated with the binding of CA to the fluoride anions, was mainly located at both ends of the CA core. This indicates that when the CA became excited, electron transfer from the core of CA to both ends took place at the fluoride-bonded CA. In addition, after binding with the fluoride anions, the bandgap of the molecules decreased.

CONCLUSION

A novel colorimetric chemosensor for detecting fluoride anions was designed and studied. This novel sensor, CA-TBMDS, based on carbazole, exhibits high sensitivity and selectivity for fluoride. CA-TBMDS reacts with fluoride anions in organic solvents, resulting in a visible color change from colorless to yellow, which can be detected with the naked eye. The color change is associated with severance of the TBMDS units from CA-TBMDS by the fluoride anion and simultaneous formation of NH units, leading to intermolecular proton transfer between CA-TBMDS and the fluoride anions. Spectroscopic studies show that for CA-TBMDS, the detection limit for the fluoride anion was as low as 3×10^{-5} M. This work demonstrates that CA-TBMDS, with its high sensitivity and selectivity, is a promising dye for fluoride chemosensors, enabling naked eye detection of target analytes. In addition, N-TBMDS units containing organic dyes can be used to produce fluoride anion sensors.

DATA AVAILABILITY STATEMENT

The original contributions presented in the study are included in the article/**Supplementary Material**, further inquiries can be directed to the corresponding author.

AUTHOR CONTRIBUTIONS

ZD and CW carried out in experiment and prepared the article. MZ and JL supervised the whole work. All authors discussed and commented on the paper.

FUNDING

This study was financially supported by the National & Local Joint Engineering Laboratory for Slag Comprehensive Utilization and Environmental Technology Open Fund (SLGPT2019KF01-01), Research Projects of Shaanxi University of Technology (SLG 1901) and Qingdao Postdoctoral Applied Research Project of Shandong Province (No. QDBSHYYYJXM202001-28).

SUPPLEMENTARY MATERIAL

The Supplementary Material for this article can be found online at: https://www.frontiersin.org/articles/10.3389/fchem.2021.732935/full#supplementary-material

REFERENCES

Cametti, M., and Rissanen, K. (2009). Recognition and Sensing of Fluoride Anion. *Chem. Commun.* 28, 2809–2829. doi:10.1039/b902069a

Clark, J. H. (1981). ChemInform Abstract: FLUORIDE ION AS A BASE IN ORGANIC SYNTHESIS. *Chemischer Informationsdienst.* 12, 80429–80452. doi:10.1002/chin.198121368

Deng, Z. F., Li, R., Geng, J. T., Zheng, M., Li, L. Q., Shi, X., et al. (2020). Efficient Colorimetric Fluoride Anion Chemosensors with Varied Colors Based on Simple Aminobenzodifuranone Organic Π-Conjugated Dyes. *Front. Chem.* 8, 231. doi:10.3389/fchem.2020.00231

Feng, Y., Li, X., Ma, H., Zhang, Z., Zhang, M., and Hao, S. (2018). A Simple Fluorescent Film Probe for the Detection of Fluoride Anion in Organic Solution. *Dyes Pigm.* 153, 200–205. doi:10.1016/j.dyepig.2018.02.004

Kaur, M., and Choi, D. H. (2015). Diketopyrrolopyrrole: Brilliant Red Pigment Dye-Based Fluorescent Probes and Their Applications. *Chem. Soc. Rev.* 44, 58–77. doi:10.1039/c4cs00248b

Kleerekoper, M. (1998). The Role of Fluoride in the Prevention of Osteoporosis. *Endocrinol. Metab. Clin. North America.* 27, 441–452. doi:10.1016/S0889-8529(05)70015-3

Li, M., Liu, Z., Wang, H.-C., Sedgwick, A. C., Gardiner, J. E., Bull, S. D., et al. (2018). Dual-function Cellulose Composites for Fluorescence Detection and Removal of Fluoride. *Dyes Pigm.* 149, 669–675. doi:10.1016/j.dyepig.2017.11.033

Sánchez-Ruiz, A., González-Alfaro, S., García-Martínez, J. C., and Rodríguez-López, J. (2020). A Study of Silylated Tris(styryl)benzenes as Potential Fluorescent Sensors for Aqueous Fluoride. *Dyes Pigm.* 182, 108610. doi:10.1016/j.dyepig.2020.108610

Wade, C. R., Broomsgrove, A. E. J., Aldridge, S., and Gabbaï, F. P. (2010). Fluoride Ion Complexation and Sensing Using Organoboron Compounds. *Chem. Rev.* 110, 3958–3984. doi:10.1002/chin.20104125010.1021/cr900401a

Wang, R., Li, J., Li, G., Hao, C., Zhang, Y., Wang, S., et al. (2018). Synthesis of 1-Amino-12-Hydroxyl-Perylene Tetra-(alkoxycarbonyl) for Selective Sensing of Fluoride. *Dyes Pigm.* 156, 225–232. doi:10.1016/j.dyepig.2018.04.012

Xuan, W., Cao, Y., Zhou, J., and Wang, W. (2013). A FRET-Based Ratiometric Fluorescent and Colorimetric Probe for the Facile Detection of Organophosphonate Nerve Agent Mimic DCP. *Chem. Commun.* 49, 10474–10476. doi:10.1039/c3cc46095a

Yang, C., Zheng, M., Li, Y., Zhang, B., Li, J., Bu, L., et al. (2013). N-monoalkylated 1,4-Diketo-3,6-Diphenylpyrrolo[3,4-C]pyrroles as Effective One- and Two-Photon Fluorescence Chemosensors for Fluoride Anions. *J. Mater. Chem. A.* 1, 5172–5178. doi:10.1039/C3TA00160A

Yuan, X., Shi, X., Wang, C., Du, Y., Jiang, P., Jiang, X., et al. (2020). IDTI Dyes for Fluoride Anion Chemosensors. *Front. Chem.* 8, 591860. doi:10.3389/fchem.2020.591860

Zhang, H., Yang, K., Chen, C., Wang, Y., Zhang, Z., Tang, L., et al. (2018). 1,4-Diketo-pyrrolo[3,4-c]pyrroles (DPPs) Based Insoluble Polymer Films with Lactam Hydrogens as Renewable Fluoride Anion Chemosensor. *Polymer* 149, 266–272. doi:10.1016/j.polymer.2018.07.011

Zhou, Y., Zhang, J. F., and Yoon, J. (2014). Fluorescence and Colorimetric Chemosensors for Fluoride-Ion Detection. *Chem. Rev.* 114, 5511–5571. doi:10.1021/cr400352m

Conflict of Interest: MZ and JL belong to the commercial affiliation of Qingdao Haiwan Science and Technology Industry Research Institute Co., Ltd. declare that the research was conducted in the absence of any commercial or financial relationships that could be construed as a potential conflict of interest.

frontiers in Chemistry

MINI REVIEW
published: 06 September 2021
doi: 10.3389/fchem.2021.732132

Conjugated Conductive Polymer Materials and its Applications: A Mini-Review

Huizhi Lu[1], *Xunlai Li*[1]* *and Qingquan Lei*[2]*

[1]College of Economics and Management, Qingdao University of Science and Technology, Qingdao, China, [2]Institute of Advanced Electrical Materials, Qingdao University of Science and Technology, Qingdao, China

Since their discovery 50 years ago, conjugated conducting polymers have received increasing attention owing to their unique conductive properties and potential applications in energy storage, sensors, coatings, and electronic devices such as organic field-effect transistors, photovoltaic cells, and light-emitting devices. Recently, these materials have played a key role in providing a more comfortable environment for humans. Consequently, the development of novel, high-performance conjugated conductive materials is crucial. In this mini-review, the progress of conjugated conductive materials in various applications and the relationship between the chemical structures and their performances is reviewed. This can aid in the molecular design and development of novel high-performance conjugated polymer materials.

Keywords: conjugated polymers, organic field-effect transistors, sensors, organic solar cells, coating

OPEN ACCESS

Edited by:
Qixin Zhou,
University of Akron, United States

Reviewed by:
Maning Liu,
Tampere University, Finland
Shian Ying,
Shandong University of Science and Technology, China

***Correspondence:**
Xunlai Li
lixunlai@163.com
Qingquan Lei
lei_qingquan@sins.com

Specialty section:
This article was submitted to Organic Chemistry, a section of the journal Frontiers in Chemistry

Received: *28 June 2021*
Accepted: *24 August 2021*
Published: *06 September 2021*

Citation:
Lu H, Li X and Lei Q (2021) Conjugated Conductive Polymer Materials and its Applications: A Mini-Review. Front. Chem. 9:732132. doi: 10.3389/fchem.2021.732132

INTRODUCTION

Conjugated conducting polymers can be divided into the following three categories according to their structural characteristics and conducting mechanism: electron conducting polymers, ionic conducting polymer, and redox polymer. Among these, the carriers of electron conducting polymers are free electrons and their common characteristic is a long π-conjugated system in the molecular skeleton, which results in delocalised electrons. Thus, these molecules are called conjugated conducting polymers. To efficiently increase the movement of electrons in the π-system, the energy level difference caused by energy band splitting should be reduced to easily overcome the energy difference between the full and empty bands. The 'doping' method can be used to change the distribution state of electrons in the energy band because conjugated polymers are easily oxidised or reduced. Therefore, almost 50 years ago, scientists found that the conductivity of polyacetylene can be improved by more than 10 orders *via* chemical doping, which was the first report on conjugated conducting polymers with conductive properties (Shirakawa et al., 1977). Recently, with the gradual development and understanding of the conjugated conductive polymer mechanism, conjugated conducting polymers have become a popular topic. They are widely used in organic solar cells (OSCs), organic field effect transistors (OFETs), sensors, and colour-changing coatings, due to advantages including light weight, low cost, good stability, and excellent optical and electrical properties (Zhang et al., 2019a; Bao et al., 2020; Deng et al., 2020; Zhang et al., 2020; Dai et al., 2021). Recently, conjugated conductive polymers have played a key role in improving our standard of living. The development of novel, high-performance conjugated conductive materials as well as their applications is crucial. Despite the rapid development of conjugated conducting polymers, their application has rarely been reviewed (Guo et al., 2014; Yi et al., 2015; Deng et al., 2019). In this mini-review, the research progress of conjugated conducting polymers in OSCs, OFETs, sensors, coatings,

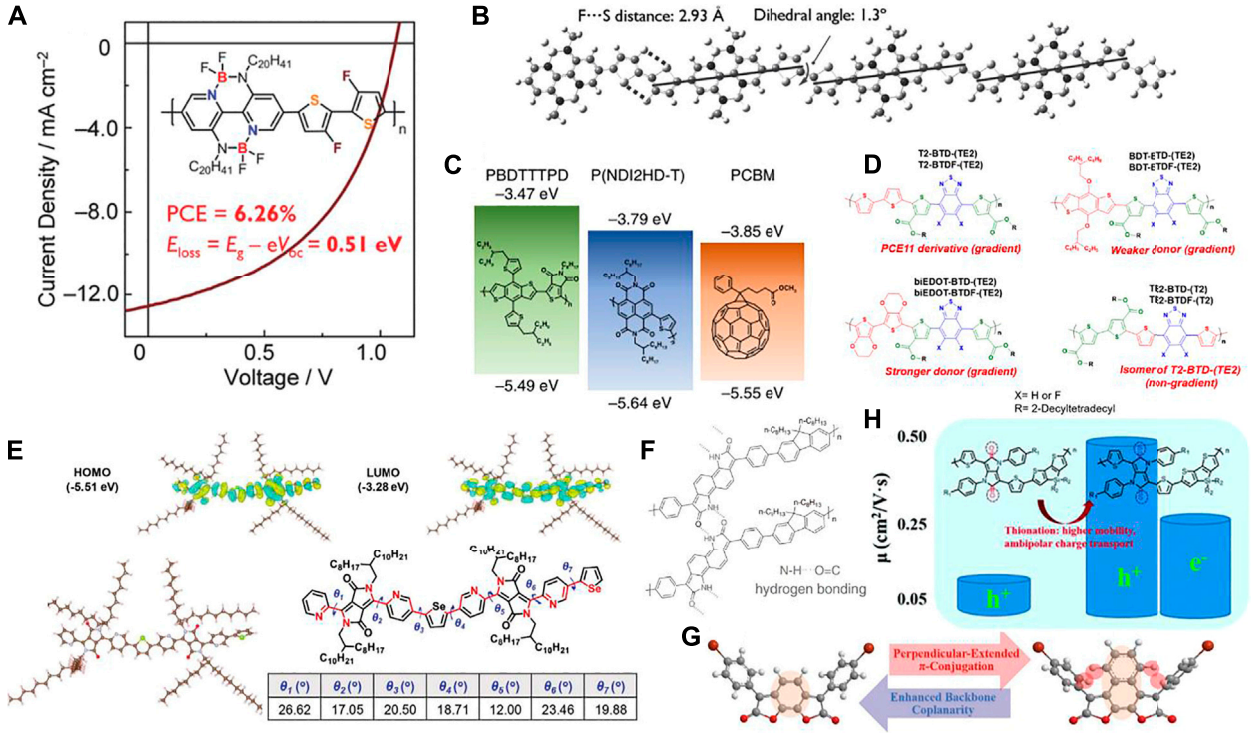

FIGURE 1 | (A) Chemical structure of the polymer as well as the J–V curves of OSC device **(B)** Optimised configuration of the model compound of P-BNBP-fBT, **(C)** Chemical structures and energy levels of PBDTTTPD, PCBM, and P(NDI2HD-T), **(D)** Chemical structures of the eight polymers, **(E)** DFT calculations for polymer dimer with full side chains, **(F)** Hydrogen-bonded naphthodipyrrolidione-based polymer, **(G)** Chemical structures of 1,8-benzodifuranone and 1,10-naphthodifuranone, **(H)** Chemical structures of the two polymers as well as their charge transfer mobility.

and other applications, as well as the relationship between the chemical structures and their performances, is reviewed. Furthermore, this review provides not only a reference and prospect for future applications, but also the development prospects of ideal conjugated conductive materials.

ORGANIC SOLAR CELL

The core of organic solar cells is the use of photosensitive organic materials as semiconductor materials which can generate voltage and current to achieve solar power generation *via* the photovoltaic effect. Recently, organic solar cell-based organic conjugated polymers, which are the leading third-generation low-cost photovoltaic technology, have attracted increasing attention due to their easy processing and low cost (Chen et al., 2016; Liu et al., 2017; Li et al., 2020). Till now, the organic solar cells exhibited efficiency over 17% has reported, which is compete-able with the commercial silicon based solar cells (Zhan et al., 2020).

For the conjugated polymer in OSC applications, the materials should not only have broad optical absorption matching well with the solar energy spectrum, but also have suitable energy levels as well as good charge transfer mobility. Thus, the molecular design is crucial. In 2016, Long et al. reported a polymer, P-BNBP-fBT, based on alternating copolymerisation with double B←N bridged bipyridine (BNBP) and 3, 3′-difluoro-2, 2′-bithiophene (fBT) by the Schiff-base formation reaction, which exhibited a power conversion efficiency (PCE) of up to 6.26% at a photon energy loss (E_{loss}) of only 0.51 eV (**Figure 1A**) (Long et al., 2016). The high PCE could be attributed to: 1) the polymer has a good planar structure because its planar conformation can be 'locked' by the F. . .S interaction, which has been confirmed by the B3LYP/6–31G* level of theory (**Figure 1B**); 2) a large number of F atoms in the easily modified main chain of the polymer helps to deepen the LUMO energy level and N atoms are conducive to the formation of intermolecular hydrogen bonds to improve the stability of the molecule. The polymer backbone configuration and the 'locked' coplanar conformation of the fBT unit endow P-BNBP-fBT with good crystallinity and high electron mobility as an excellent donor in OSCs. This work demonstrates the potential of conjugated conducting polymers in OSCs, such that advances in all-polymer solar cell (all-PSC) device performance can be achieved.

The development of solar cells should include improved efficiency, while simultaneously overcoming the difficulties in practical applications that are ubiquitous in daily life. Theoretical performance and practical application should be considered. Kim et al. developed highly efficient and mechanically robust all-PSCs using poly[4, 8-bis(5-(2-ethylhexyl) thiophen-2-yl)benzo[1, 2-b: 4, 5-b']dithiophene-alt-1, 3-bis(thiophen-2-yl)-5-(2-hexyldecyl)-4H-thieno[3,4-c]pyrrole-4, 6 (5H)-dione] (PBDTTTPD) as the

electron donor and poly[[N,N′-bis(2-hexyldecyl)-naphthalene-1, 4, 5, 8-bis(dicarboximide)-2, 6-diyl]-alt-5, 5′-thiophene] (P(NDI2HD-T)) as the electron acceptor, which achieved a high PCE of 6.64%, higher than that of control fullerene PSCs (PCE = 6.12%) (**Figure 1C**) (Kim et al., 2016). The enhanced performance of all-PSCs is mainly attributed to the high V_{OC} (1.06 V) due to the better alignment of highest occupied molecular orbital (HOMO) and lowest unoccupied molecular orbital (LUMO) energy levels. In addition, many S atoms on PBDTTTPD enhance the electron-donating ability of the molecule, and the large conjugated structure and good molecular planarity provide conditions for high carrier mobility and PCE. This work not only shows the high performance of conjugated conductive polymers in OSCs, but also provides strong operability for extensive use in daily life.

Recently, research has focused on non-fullerene acceptors (NFAs) in OSCs because of their advantages, including greater optical, electrochemical, and structural flexibility compared to their fullerene counterparts (Lin et al., 2015; Nielsen et al., 2015; Hou et al., 2018; Zhang et al., 2018a). In 2019, Reynolds's et al. reported a series of polymers by minimal structure modification with varying electron donors (**Figure 1D**) (Jones et al., 2019). These polymers are consisted of a fluorinated/non-fluorinated benzothiadiazole strong acceptor moiety, a thiophene ester weak acceptor, and various donor units composed of bithiophene, biEDOT, and benzodithiophene to form six acceptor gradient and two non-gradient polymers. The results showed that optimised NFA solar cells based on ITIC-4F paired with each of the top-performing polymers produced an average PCE of up to 7.3% for TE2-BTDF-(T2) (non-gradient) and 3.6% for T2-BTDF-(TE2) (gradient). The differences might be due to the formation of an intramolecular charge transfer that occurred for the acceptor gradient. This work stresses the importance of acquiring accurate ionisation energies and electron affinities when characterising solar cell energetics, since differences as small as 0.1 eV in the offsets can make a significant impact on overall charge collection.

ORGANIC FIELD EFFECT TRANSISTOR

Organic field-effect transistors (FETs) are indispensable electronic devices based on organic materials, which use electric fields to control the conductivity of materials. Research on conjugated conductive polymers has become an important aspect in OFETs owing to advantages including flexibility, easy processing, rich variety, and low cost. Further breakthroughs in the business and industry of OFETs is expected (Zou et al., 2021). However, the low carrier mobility of these conjugated polymers compared to the silicon-based field-effect transistors is a major disadvantage which needs to be addressed.

There are three factors that affect the high-performance OFET: charge transfer mobility, threshold voltage, and current on/off ratio. Among these, the charge carrier mobility is one of the most important and challenging, typically for high electron transfer mobility. The polymer molecular structure and device fabrication techniques are essential to obtain high-performance OFETs. In 2020, Liu et al. developed a new method to improve carrier mobility in OFETs using the synergistic effect of pyridine and selenophene in the backbone of a DPP-based copolymer (**Figure 1E**) (Liu et al., 2020). The study found that the pyridine DPP- and selenophene-based copolymer (PDPPy-Se) exhibited low LUMO and HOMO energy levels due to molecular packing and ordering, which increased the hole transfer barrier and decreased the electron transfer barrier. In addition, the study concluded that the annealing process increases the formation of microcrystals and improves π-stacking and lamellar stacking, which is beneficial to carrier migration. This work demonstrated that the synergistic use of pyridine and selenophene in the backbone of a diketopyrrolopyrrole-based copolymer is a favourable energy level, typically to reduce the LUMO energy level, for electron injection and relatively ordered molecular packing, which is a feasible method to improve carrier mobility and plays a key role in the development of n-type bipolar organic transistors. It also highlights the promising future of conjugated conductive polymers in OFETs.

In 2018, Zhang et al. (2017) reported that introducing hydrogen bonding between the amide and carbonyl into the polymer not only result in polymer self-assembly, but also increases the electron mobility by a factor of 40 compared to its precursor polymer (**Figure 1F**). Recently, Deng et al. (2018) introduced S and F atoms to adjust the polymer backbone and obtained a polymer with hole mobility up to 0.65 $cm^2 V^{-1} s^{-1}$. Zhang et al. then reported that the main chain coplanarity of polymer semiconductors is more essential than the sole extension of π-conjugation (especially perpendicularly to polymer main chains) after investigating two benzo/naphtodifuranone-based polymers (**Figure 1G**) (Li et al., 2021). The same group also found that substituting the oxygen atoms for sulfur atoms in the diketopyrrolopyrrole core could not only improve the charge transfer mobility, but also convert p-type materials into ambipolar type semiconductors (**Figure 1H**) (Zhang et al., 2018c; Zhang et al., 2019a).

SENSORS

A sensor is a type of detection device that can respond to external conditions and transform the stimulation into electrical signals or other required output information to meet the requirements of information transmission, storage, control, monitor, display, as well as recording (Charoenthai et al., 2011; Pattanatornchai et al., 2013; Xu et al., 2013; Lu et al., 2014).

Sensors are one of the key applications of conjugated conductive polymers. In most cases, sensors provide a signal as a response to the stimulation of environmental conditions such as light, gas, anions, and solvents. In 2020, Stewart et al. developed a volatile organic compound (VOC) gas sensor with highly sensitive and selective characteristics using p-conjugated polymer (P3HT)/solid-state ionic liquid (SSIL) blends. They determined that the strong chemical interaction between π-CP and SSIL adjusts the conductivity by applying an electric field (Stewart et al., 2020). The sensor will exhibit different conductivity and transmit signals to distinguish different

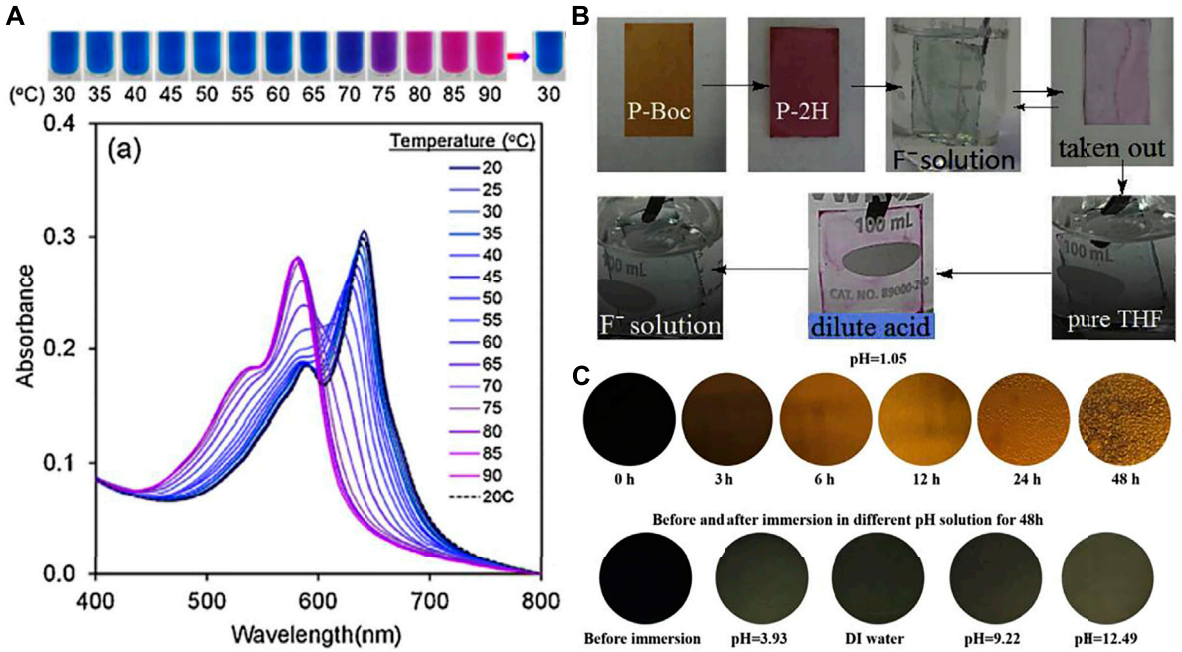

FIGURE 2 | (A) Absorption spectra of PDA(8, 9)/PVP10 nanocomposites measured upon increasing temperature. Dashed lines represent spectra measured upon the consecutive cooling (photographs of the colour transition are illustrated above the spectra), **(B)** Photos of dried P-2H film in THF solution of fluoride anion or HCl with solute concentration of 10^{-5} M **(C)** Colour change in the 1,4-BDF-based epoxy coating samples after immersion in different pH solutions and digital images of the coating samples after immersion in the other pH solutions (from pH = 3.93 to pH = 12.49).

substances under exposure with VOCs of different polarity. The results show that the sensor has better accuracy and stability. This work proved that conjugated conductive polymers have potential applications in the creation of more accurate, cheaper, and easier-to-fabricate sensing arrays.

In addition to gas, the conjugated polymers change colour under different temperatures which can be used for temperature monitoring, biosensors, building materials, and intelligent screens. Kamphan et al. introduced different lengths of side chains into a polydiacetylene (PDA) system, resulting in a series of PDA-based polymers. These polymers exhibited λ_{max} at approximately 640 nm, where λ_{max} shifted to approximately 585 nm when the temperature increased to 75°C, that is, a colour change from blue to purple was noticed (**Figure 2A**) (Kamphan et al., 2016). The colour change might be because the extended π-conjugation system results in an absorption peak at 640 nm, appearing blue, while the twisting of the polymer backbone as well as the changes in the degree of conjugation in the system result in a red colour. Recently, a series of PDA-based polymers with reversible colour change responses to temperature have been reported; these could be potentially used in various applications, including biomedicine, optical storage, sensing, building materials, and anti-counterfeiting.

Various anions exist in the environment. Although anions are generally beneficial for human health, an excessive amount is disadvantageous for human and animal health. Thus, the development of highly sensitive and selective sensors is important. These materials can also be found in conjugated conductive polymers. Recently, Zhang et al. developed a diketopyrrolo[3,4-c] pyrrole (DPP)-based polymer with NH units on the polymer backbone. The functional group NH reacts with the fluoride anions in the organic solvents, resulting in a colour change from red to blue, which is visible to the naked eye (**Figure 2B**). Moreover, these polymers not only detect the fluoride anion with high sensitivity and selectivity with a detection limit as low as 10–^{8} M, but also work as fluoride anion extractors (Zhang et al., 2018b). Very recently, some novel designed insulated conjugated bimetallopolymer for the sensor application were also developed (Kaneko et al., 2020; Masai et al., 2020).

COATING

Coating is a material that covers the surface of objects *via* different construction processes to form a solid film with firm adhesion, a certain strength, and continuity. This kind of material is widely used in building decoration, functional coating, intelligent control, and other daily-life applications.

Further development of high-performance coatings is necessary (typically functionality coating) as they have significantly improved daily life. Recently, Zhang and Zhou et al. introduced conjugated benzodifuranone dyes into an epoxy-polyamine-composited polymer system (Zeng et al., 2019). This coating exhibited a change from dark blue into yellow in response to a change in temperature, PH values, or after exposure to UV-light (**Figure 2C**). Subsequently, the same

group investigated the mechanism and found that the colour change is ascribed to the dissociation of the hydrogen bonding (Zhang et al., 2019b). These types of coatings are potentially used in temperature or UV-light sensors.

Coating, on the top of the materials, worked as a protective functionality. In 2009, Yan et al. reported a neutral conjugated polymer with the ability to cathodically protect exposed alloy in a defect, which was the first report of cathodic protection of an all-organic coating based on a conjugated conductive polymer. In this experiment, SVET current density maps were generated to illustrate the ability of the reaction with the oxygen of the neutral conjugated polymer (Yan et al., 2009). The results showed that oxidation current centered on the defect and most of the reduction current distributed on the surface of the polymer after 2 h, which determined that the polymer is oxidised on the cathode instead of the metal electrode so as to better protect the cathode. In summary, this type of material can protect the cathode. Applications for conjugated conductive polymer coatings are currently being investigated.

CONCLUSION AND FUTURE PROSPECTS

In summary, a series of conjugated conductive polymers and their applications are reviewed. Regarding OSC-conjugated materials, novel chemical structures with broad optical absorption (typically absorbing light from the visible light to the NIR region), high charge mobility, and low LUMOs as non-fullerene acceptors are popular. Conjugated polymers with multi-fluorides, nitrogen, and sulfur atoms in the backbone are promising. High PCE and device stability are important to modify the OSCs. The chemical structures of conjugated polymers, typically the backbone, play a key role in the performance OFETs. To obtain high charge mobility semiconductors, the materials should be produced taking all factors into account, including a good planar backbone, strong aggregating and π–π stacking, and increased crystallinity. In addition, n-type and ambipolar type semiconductors are essential as the most successful electron mobility of OFETs is much smaller than the hole transfer mobility. Regarding sensors, highly selective and sensitive sensors still require further research and development of conjugated polymers. Different applications of sensors have different molecular design concepts. Traditional coatings act as a protective material, while several of them alter the colour of the surfaces. The development of conjugated polymer coatings with multiple functions is promising, including the coating combined as semiconductors and sensors. In the near futures, applications regarding to conjugated polymers are expected to be developed in the direction of interdisciplinary such as OFETs with sensitive of X-ray or light sensors, bio-sensors with functionality of cure disease and so on. In addition, the conjugated polymers used in the energy storage and light-emitting devices are also should be further developed.

AUTHOR CONTRIBUTIONS

HL collected materials and prepared the manuscript. XL revised the manuscript. QL provided ideas. XL and QL supervised the whole work. All authors discussed and commented on the paper.

FUNDING

This study was financially supported by Shandong Provincial Key Research and Development Program (Soft Science) Project (No. 2019RZB01069).

REFERENCES

Bao, W. W., Li, R., Dai, Z. C., Tang, J., Shi, X., Geng, J. T., et al. (2020). Diketopyrrolopyrrole (DPP)-Based Materials and its Applications: A Review. *Front. Chem.* 8, 679. doi:10.3389/fchem.2020.00679

Charoenthai, N., Pattanatornchai, T., Wacharasindhu, S., Sukwattanasinitt, M., and Traiphol, R. (2011). Roles of head group architecture and side chain length on colorimetric response of polydiacetylene vesicles to temperature, ethanol and pH. *J. Colloid Interf. Sci.* 360 (2), 565–573. doi:10.1016/j.jcis.2011.04.109

Chen, R., Zheng, C., Li, C., Li, H., Wang, Z., Tang, Y., et al. (2016). Efficient synthesis and photovoltaic properties of highly rigid perylene-embedded benzothiazolyls. *Polym. Chem.* 7 (4), 780–784. doi:10.1039/c5py01791b

Dai, Z., Ai, T., Zhou, Q., and Zhang, H. (2021). Editorial: Design, Synthesis, and Application of Novel π-Conjugated Materials. *Front. Chem.* 8, 634698. doi:10.3389/fchem.2020.634698

Deng, Z., Ai, T., Li, R., Yuan, W., Zhang, K., Du, H., et al. (2019). Conjugated Polymers Containing Building Blocks 1,3,4,6-Tetraarylpyrrolo[3,2-b]pyrrole-2,5-dione (isoDPP), Benzodipyrrolidone (BDP) or Naphthodipyrrolidone (NDP): A Review. *Polymers* 11 (10), 1683. doi:10.3390/polym11101683

Deng, Z. F., Li, R., Geng, J. T., Zheng, M., Li, L. Q., Shi, X., et al. (2020). Efficient Colorimetric Fluoride Anion Chemosensors with Varied Colors Based on Simple Aminobenzodifuranone Organic Π-Conjugated Dyes. *Front. Chem.* 8, 231. doi:10.3389/fchem.2020.00231

Deng, Z., Li, L., Ai, T., Hao, X., and Bao, W. (2018). Centrosymmetric Thiophenemethyleneoxindole-Based Donor-Acceptor Copolymers for Organic Field-Effect Transistors. *Macromol. Rapid Commun.* 39 (11), 1800073. doi:10.1002/marc.201800073

Guo, X., Facchetti, A., and Marks, T. J. (2014). Imide- and amide-functionalized polymer semiconductors. *Chem. Rev.* 114 (18), 8943–9021. doi:10.1021/cr500225d

Hou, J., Inganäs, O., Friend, R. H., and Gao, F. (2018). Organic solar cells based on non-fullerene acceptors. *Nat. Mater.* 17 (2), 119–128. doi:10.1038/nmat5063

Jones, A. L., Zheng, Z., Riley, P., Pelse, I., Zhang, J., Abdelsamie, M., et al. (2019). Acceptor Gradient Polymer Donors for Non-fullerene Organic Solar Cells. *Chem. Mater.* 31 (23), 9729–9741. doi:10.1021/acs.chemmater.9b03327

Kamphan, A., Khanantong, C., Traiphol, N., and Traiphol, R. (2017). Structural-thermochromic relationship of polydiacetylene (PDA)/polyvinylpyrrolidone (PVP) nanocomposites: Effects of PDA side chain length and PVP molecular weight. *J. Ind. Eng. Chem.* 46, 130–138. doi:10.1016/j.jiec.2016.10.023

Kaneko, S., Masai, H., Yokoyama, T., Liu, M., Tachibana, Y., Fujihara, T., et al. (2020). Complementary Color Tuning by HCl via Phosphorescence-to-Fluorescence Conversion on Insulated Metallopolymer Film and its Light-Induced Acceleration. *Polymers* 12, 244. doi:10.3390/polym12010244

Kim, T., Kim, J.-H., Kang, T. E., Lee, C., Kang, H., Shin, M., et al. (2015). Flexible, highly efficient all-polymer solar cells. *Nat. Commun.* 6, 8547. doi:10.1038/ncomms9547

Li, R., Dai, Z., Zheng, M., Wang, C., Deng, Z., Zhuang, T., et al. (2021). Benzo/Naphthodifuranone-Based Polymers: Effect of Perpendicular-Extended Main Chain π-Conjugation on Organic Field-Effect Transistor Performances. *Macromol. Rapid Commun.* 42 (7), 2000703. doi:10.1002/marc.202000703

Li, Y., Sun, X., Zhang, X., Zhang, D., Xia, H., Zhou, J., et al. (2020). Built-in voltage enhanced by *In Situ* electrochemical polymerized Undoped conjugated hole-transporting modifiers in organic solar cells. *J. Mater. Chem. C* 8, 2676–2681. doi:10.1039/c9tc06140a

Lin, Y., Wang, J., Zhang, Z.-G., Bai, H., Li, Y., Zhu, D., et al. (2015). An Electron Acceptor Challenging Fullerenes for Efficient Polymer Solar Cells. *Adv. Mater.* 27 (7), 1170–1174. doi:10.1002/adma.201404317

Liu, M., Makuta, S., Tsuda, S., Russo, S., Seki, S., Terao, J., et al. (2017). Fluorene-Thiophene Copolymer Wire on TiO2: Mechanism Achieving Long Charge Separated State Lifetimes. *J. Phys. Chem. C* 121, 25672–25681. doi:10.1021/acs.jpcc.7b07295

Liu, Q., Kumagai, S., Manzhos, S., Chen, Y., Angunawela, I., Nahid, M. M., et al. (2020). Synergistic Use of Pyridine and Selenophene in a Diketopyrrolopyrrole-Based Conjugated Polymer Enhances the Electron Mobility in Organic Transistors. *Adv. Funct. Mater.* 30 (34), 2000489. doi:10.1002/adfm.202000489

Long, X., Ding, Z., Dou, C., Zhang, J., Liu, J., and Wang, L. (2016). Polymer Acceptor Based on Double B←N Bridged Bipyridine (BNBP) Unit for High-Efficiency All-Polymer Solar Cells. *Adv. Mater.* 28 (30), 6504–6508. doi:10.1002/adma.201601205

Lu, S., Jia, C., Duan, X., Zhang, X., Luo, F., Han, Y., et al. (2014). Polydiacetylene vesicles for hydrogen peroxide detection. *Colloids Surf. A: Physicochemical Eng. Aspects* 443, 488–491. doi:10.1016/j.colsurfa.2013.11.029

Masai, H., Yokoyama, T., Miyagishi, H. V., Liu, M., Tachibana, Y., Fujihara, T., et al. (2020). Insulated conjugated bimetallopolymer with sigmoidal response by dual self-controlling system as a biomimetic material. *Nat. Commun.* 11, 408. doi:10.1038/s41467-019-14271-2

Nielsen, C. B., Holliday, S., Chen, H.-Y., Cryer, S. J., and Mcculloch, I. (2015). Non-Fullerene Electron Acceptors for Use in Organic Solar Cells. *Acc. Chem. Res.* 48 (11), 2803–2812. doi:10.1021/acs.accounts.5b00199

Pattanatornchai, T., Charoenthai, N., Wacharasindhu, S., Sukwattanasinitt, M., and Traiphol, R. (2013). Control over the color transition behavior of polydiacetylene vesicles Using different alcohols. *J. Colloid Interf. Sci.* 391 (1), 45–53. doi:10.1016/j.jcis.2012.10.004

Shirakawa, H., Louis, E. J., Macdiarmid, A. G., Chiang, C. K., and Heeger, A. J. (1977). Synthesis of electrically conducting organic polymers: halogen derivatives of polyacetylene, (CH) x. *J. Chem. Soc. Chem. Commun.* 16, 578–580. doi:10.1039/C39770000578

Stewart, K., Limbu, S., Nightingale, J., Pagano, K., Park, B., Hong, S., et al. (2020). Molecular Understanding of a π-conjugated polymer/solid-state ionic liquid complex as a highly sensitive and selective gas sensor. *J. Mater. Chem. C* 8 (43), 15268–15276. doi:10.1039/D0TC03093G

Xu, Y., Li, J., Hu, W., Zou, G., and Zhang, Q. (2013). Thermochromism and supramolecular chirality of the coumarin-substituted polydiacetylene LB films. *J. Colloid Interf. Sci.* 400, 116–122. doi:10.1016/j.jcis.2013.02.049

Yan, M. C., Tallman, D. E., Rasmussen, S. C., and Bierwagen, G. P. (2009). Corrosion Control Coatings for Aluminum Alloys Based on Neutral and n-Doped Conjugated Polymers. *J. Electrochem. Soc.* 156 (10), C360–C366. doi:10.1149/1.3190162

Yi, Z., Wang, S., and Liu, Y. (2015). Design of High-Mobility Diketopyrrolopyrrole-Based π-Conjugated Copolymers for Organic Thin-Film Transistors. *Adv. Mater.* 27 (24), 3589–3606. doi:10.1002/adma.201500401

Zeng, W., Deng, Z., Wang, H., Zhang, H., and Zhou, Q. (2019). Benzodifuranone based color-changing epoxy-polyamine coating. *Dyes Pigm.* 164, 198–205. doi:10.1016/j.dyepig.2019.01.016

Zhan, L., Li, S., Lau, T., Cui, Y., and Lu, X. (2020). Over 17 % efficiency ternary organic solar cells enabled by two non-fullerene acceptors working in an alloy-like mode. *Energ. Environ. Sci.* 13, 635–645. doi:10.1039/C9EE03710A

Zhang, G., Zhao, J., Chow, P. C. Y., Jiang, K., Zhang, J., Zhu, Z., et al. (2018a). Nonfullerene Acceptor Molecules for Bulk Heterojunction Organic Solar Cells. *Chem. Rev.* 118 (7), 3447–3507. doi:10.1021/acs.chemrev.7b00535

Zhang, H., Li, R., Deng, Z., Cui, S., Wang, Y., Zheng, M., et al. (2020). π-Conjugated oligomers based on aminobenzodifuranone and diketopyrrolopyrrole. *Dyes Pigm.* 181, 108552. doi:10.1016/j.dyepig.2020.108552

Zhang, H., Liu, M., Yang, W., Judin, L., Hukka, T. I., Priimagi, A., et al. (2019a). Thionation Enhances the Performance of Polymeric Dopant-Free Hole-Transporting Materials for Perovskite Solar Cells. *Adv. Mater. Inter.* 6 (18), 1901036. doi:10.1002/admi.201901036

Zhang, H., Yang, K., Chen, C., Wang, Y., Zhang, Z., Tang, L., et al. (2018b). 1,4-Diketo-pyrrolo[3,4-c]pyrroles (DPPs) based insoluble polymer films with lactam hydrogens as renewable fluoride anion chemosensor. *Polymer* 149, 266–272. doi:10.1016/j.polymer.2018.07.011

Zhang, H., Yang, K., Chen, Y. M., Bhatta, R., Tsige, M., Cheng, S. Z. D., et al. (2017). Polymers Based on Benzodipyrrolidone and Naphthodipyrrolidone with Latent Hydrogen-Bonding on the Main Chain. *Macromol. Chem. Phys.* 218 (13), 1600617. doi:10.1002/macp.201600617

Zhang, H., Yang, K., Zhang, K., Zhang, Z., Sun, Q., and Yang, W. (2018c). Thionating iso-diketopyrrolopyrrole-based polymers: from p-type to ambipolar field effect transistors with enhanced charge mobility. *Polym. Chem.* 9 (14), 1807–1814. doi:10.1039.C1038PY00292D10.1039/c8py00292d

Zhang, H., Zeng, W., Du, H., Ma, Y., Ji, Z., Deng, Z., et al. (2020b). Comparison for color change between benzodifuranone and benzodipyrrolidone based epoxy coating. *Dyes Pigm.* 175, 108171. doi:10.1016/j.dyepig.2019.108171

Zou, X., Cui, S., Li, J., Wei, X., and Zheng, M. (2021). Diketopyrrolopyrrole Based Organic Semiconductor Materials for Field-Effect Transistors. *Front. Chem.* 9, 671294. doi:10.3389/fchem.2021.671294

Conflict of Interest: The authors declare that the research was conducted in the absence of any commercial or financial relationships that could be construed as a potential conflict of interest.

Publisher's Note: All claims expressed in this article are solely those of the authors and do not necessarily represent those of their affiliated organizations, or those of the publisher, the editors and the reviewers. Any product that may be evaluated in this article, or claim that may be made by its manufacturer, is not guaranteed or endorsed by the publisher.

Advantages of publishing in Frontiers

OPEN ACCESS
Articles are free to read for greatest visibility and readership

FAST PUBLICATION
Around 90 days from submission to decision

HIGH QUALITY PEER-REVIEW
Rigorous, collaborative, and constructive peer-review

TRANSPARENT PEER-REVIEW
Editors and reviewers acknowledged by name on published articles

Frontiers
Avenue du Tribunal-Fédéral 34
1005 Lausanne | Switzerland

Visit us: www.frontiersin.org
Contact us: frontiersin.org/about/contact

REPRODUCIBILITY OF RESEARCH
Support open data and methods to enhance research reproducibility

DIGITAL PUBLISHING
Articles designed for optimal readership across devices

FOLLOW US
@frontiersin

IMPACT METRICS
Advanced article metrics track visibility across digital media

EXTENSIVE PROMOTION
Marketing and promotion of impactful research

LOOP RESEARCH NETWORK
Our network increases your article's readership